AD-766 479

ADVANCED MODE CONTROL AND HIGH-POWER OPTICS TECHNOLOGY

VOLUME II. HALIDE WINDOW MATERIALS TECHNOLOGY

HUGHES RESEARCH LABORATORIES

PREPARED FOR
AIR FORCE WEAPONS LABORATORY

JULY 1973

DISTRIBUTED BY:

NTIS
National Technical Information Service
U. S. DEPARTMENT OF COMMERCE

AFWL-TR-72-152, Vol II

AFWL-TR-
72-152,
Vol II

AD 766479

ADVANCED MODE CONTROL AND HIGH-POWER OPTICS TECHNOLOGY

Volume II

Halide Window Materials Technology

R. C. Pastor

M. Braunstein

Hughes Research Laboratories

TECHNICAL REPORT NO. AFWL-TR-72-152, Vol II

July 1973

AIR FORCE WEAPONS LABORATORY
Air Force Systems Command
Kirtland Air Force Base
New Mexico

Approved for public release; distribution unlimited.

152

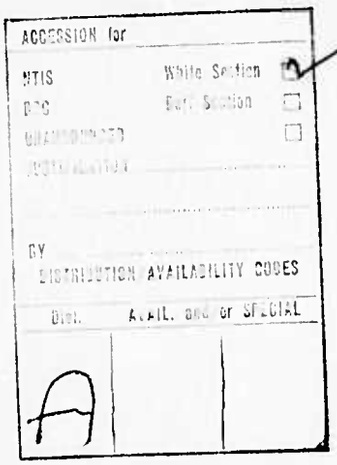

AIR FORCE WEAPONS LABORATORY
Air Force Systems Command
Kirtland Air Force Base
New Mexico 87117

UNCLASSIFIED
Security Classification

DOCUMENT CONTROL DATA - R & D

(Security classification of title, body of abstract and indexing annotation must be entered when the overall report is classified)

1 ORIGINATING ACTIVITY (Corporate author) Hughes Research Laboratories 3011 Malibu Canyon Road Malibu, California 90265	2a. REPORT SECURITY CLASSIFICATION UNCLASSIFIED 2b. GROUP

3 REPORT TITLE

ADVANCED MODE CONTROL AND HIGH-POWER OPTICS TECHNOLOGY, Vol II, Halide Window Materials Technology

4 DESCRIPTIVE NOTES (Type of report and inclusive dates)

18 October 1971-31 October 1972

5 AUTHOR(S) (First name, middle initial, last name)

R. C. Pastor; M. Braunstein

6. REPORT DATE	July 1973	7a. TOTAL NO. OF PAGES 150	7b. NO. OF REFS 30
8a. CONTRACT OR GRANT NO.	F29601-71-C-0101	9a. ORIGINATOR'S REPORT NUMBER(S) AFWL-TR-72-152, Vol II	
b. PROJECT NO.	1256 and 317J		
c. Task Nos	0 and 8	9b. OTHER REPORT NO(S) (Any other numbers that may be assigned this report)	
d.			

10. DISTRIBUTION STATEMENT

Approved for public release; distribution unlimited.

11. SUPPLEMENTARY NOTES	12. SPONSORING MILITARY ACTIVITY AFWL (LRO) Kirtland AFB, NM 87117

13. ABSTRACT

(Distribution Limitation Statement A)

The results reported here represent significant advances in the state of the art of high-power laser windows and coatings. An order-of-magnitude improvement was achieved in the material parameters of single crystal KCl over the values which characterized the best available materials at the beginning of the study. Single crystal specimens of KCl (up to 10-cm diameter) having optical absorption at 10.6 μm $\leq$ 0.0005 cm^{-1} and rupture strengths as high as 4000 psi were produced using a reactive atmosphere processing (RAP) technology which was developed during the program. The RAP technique, involving processing under an atmosphere of He + CCl_4, was used for window materials purification, crystal growth, and for surface layer exchange in KCl crystals. It led to the development of a one-step processing for KCl crystal growth, from powder to crystal, which minimizes the incorporation of OH^- in the KCl crystals. Optical, mechanical, and surface stability evaluations of various fluoride and chloride crystals are also reported. The coating program goal, which was to achieve 0.1% or less absorption per coated window surface at 10.6 μm, has been demonstrated for some of the optical coatings prepared during the program. Theoretical designs and experimental results for coatings for alkali halides, zinc selenide, and cadmium telluride are presented with emphasis placed on coatings for KCl. Rigorous control of starting material purity and substrate preparation was found to be essential for the preparation of low-absorption coatings.

DD FORM 1 NOV 65 1473

UNCLASSIFIED
Security Classification

14. KEY WORDS	LINK A		LINK B		LINK C	
	ROLE	WT	ROLE	WT	ROLE	WT
Laser window materials Laser window coatings Antireflection coatings Protective coatings Halide materials						

ADVANCED MODE CONTROL AND HIGH-POWER OPTICS TECHNOLOGY

Volume II

R. C. Pastor

M. Braunstein

Hughes Research Laboratories

TECHNICAL REPORT NO. AFWL-TR-72-152, Vol II

FOREWORD

This report was prepared by Hughes Research Laboratories, Malibu, California, under Contract F29601-71-C-0101. The research was performed under Program Elements 61101D and 63605F, Projects 1256 and 317J, Tasks 0 and 8. The research was partially funded by the Advanced Research Projects Agency under ARPA Order Number 1256.

Inclusive dates of research were 18 October 1971 through 31 October 1972. The report was submitted 18 May 1973 by the Air Force Weapons Laboratory Project Officer, Captain Harry V. Winsor (LRO).

The following personnel participated in various phases of the study: A. C. Pastor; M. Robinson; K. Arita; A. Timper; R. Turk; K. Robinson; A. I. Braunstein; J. E. Rudisill; D. H. Williams; C. E. Pilon; J. E. Kiefer; and J. H. Yoder.

This technical report has been reviewed and is approved.

Harry V. Winsor

HARRY V. WINSOR
Captain, USAF
Project Officer

Edward N. Laughlin

EDWARD N. LAUGHLIN
Lt Colonel, USAF
Chief, Optics Technology Branch

Russell K. Parsons

RUSSELL K. PARSONS
Colonel, USAF
Chief, Laser Division

ABSTRACT

(Distribution Limitation Statement A)

The results reported here represent significant advances in the state of the art of high-power laser windows and coatings. An order-of-magnitude improvement was achieved in the material parameters of single crystal KCl over the values which characterized the best available materials at the beginning of the study. Single crystal specimens of KCl (up to 10-cm diameter) having optical absorption at 10.6 μm ≤ 0.0005 cm^{-1} and rupture strengths as high as 4000 psi were produced using a reactive atmosphere processing (RAP) technology which was developed during the program. The RAP technique, involving processing under an atmosphere of He + CCl_4, was used for window materials purification, crystal growth, and for surface layer exchange in KCl crystals. It led to the development of a one-step processing for KCl crystal growth, from powder to crystal, which minimizes the incorporation of OH^- in the KCl crystals. Optical, mechanical, and surface stability evaluations of various fluoride and chloride crystals are also reported. The coating program goal, which was to achieve 0.1% or less absorption per coated window surface at 10.6 μm, has been demonstrated for some of the optical coatings prepared during the program. Theoretical designs and experimental results for coatings for alkali halides, zinc selenide, and cadmium telluride are presented with emphasis placed on coatings for KCl. Rigorous control of starting material purity and substrate preparation was found to be essential for the preparation of low-absorption coatings.

TABLE OF CONTENTS

LIST OF ILLUSTRATIONS

LIST OF TABLES

SECTION I

INTRODUCTION AND SUMMARY

The Halide Window Materials Technology Program is a continuation of work started on the Advanced Mode Control and High-Power Optics Technology (AMCHiPOT) Program. The AMCHiPOT Program is intended to advance the state of the art in high power optical components and high-power laser mode control. The AMCHiPOT Program includes: advanced mirror and grating development, windows and coatings, and mode control. The results of both the advanced mirror and grating development work were reported in final technical report Volume I, (AFWL-TR-72-152). Volume III will document mode control findings, while the present volume (Volume II) includes results on the windows and coatings studies.

The object in the study of window materials was to upgrade the technologies of purification, crystal growth, and surface preparation of halides for their use as windows for high-power lasers. The approach taken was based on our hypothesis that the values of material parameters employed in the earlier evaluation of figures of merit[1] were not intrinsic to the materials but reflected the status of halide materials technology. Our results now allow us to assert the validity of this proposition.

At the start of the program, the optical absorption at 10.6 μm, β, for KCl crystal (Harshaw, window grade) was 0.007 cm^{-1}. Currently, $\beta \leq 0.0005\ cm^{-1}$ can be obtained in a reproducible fashion. Initially, the yield point was Y = 300 psi and the rupture strength, S = 640 psi. (Ref. 1); Hughes Research Laboratories now routinely achieves Y ≈ 1000 psi and S ≈ 4000 psi. Preliminary evidence shows that further improvements in optical absorption and mechanical integrity can be expected from technological advances in surface preparation. The improvements are noteworthy in that they were realized in the purified material, and were superior to the improvements obtained earlier by bivalent metal ion doping.[2] Related to the difference in the two

approaches to upgrade (Y, S) is the observation that doping exacts a tradeoff in β.[3] Bivalent cation impurities stabilize the hydroxide ion (OH^-) and cation vacancies in alkali metal halides.[4] Also, because of the extremely limited solubility of such dopants in the pure solid, the achievement of bulk homogeneity over a large piece presents a severe constraint; an increase in optical scattering through precipitation is a constant threat.

The emphasis in materials purification by reactive atmosphere processing (RAP) (see Appendix I) is anion purity. The nonmetal impurities, being much larger than the metal ions, affect the lattice array at concentration levels of a part in 10^4 or even lower. Regarding the ion as an incompressible sphere, the halide anion accounts for a major fraction of the molar volume. Consequently, the anion determines generally the closeness and symmetry of packing; its impurities exert a greater influence on lattice vibrations and, therefore, affect the crystal's IR transmission, structural integrity, and transport parameters.

Among the anion impurities, the hydroxide ion (OH^-), a pseudohalide, is probably the most obstinate because the reactivity of the radical is very close to that of fluorine as shown in Fig. 1. From the standpoint of optical transmission, the O-H vibration is active in the 3-μm region and the O-M at the 10-μm region. The substitutional OH^- dipole couples with the dipole consisting of a bivalent metal ion impurity and a metal ion vacancy.[4,5,6] Through such couplings and the tendency to diffuse to the surface, the OH^- can effect a degradation of the mechanical behavior of the alkali halide. Our surface-stability studies indicate that the presence of OH^- on the alkali halide crystal surface renders the surface more hydrophilic and, consequently, less resistant to surface corrosion by water vapor.

Because of its reactivity and the omnipresence of its source, H_2O, in all steps of processing, the substitutional entry of OH^- by hydrolytic exchange is always a threat. To suppress the substitutional entry of OH^- in the growth of chlorides, the critical process parameter in RAP is the ratio of partial pressures, P_{H_2O}/P_{HCl} (see eq. (2),

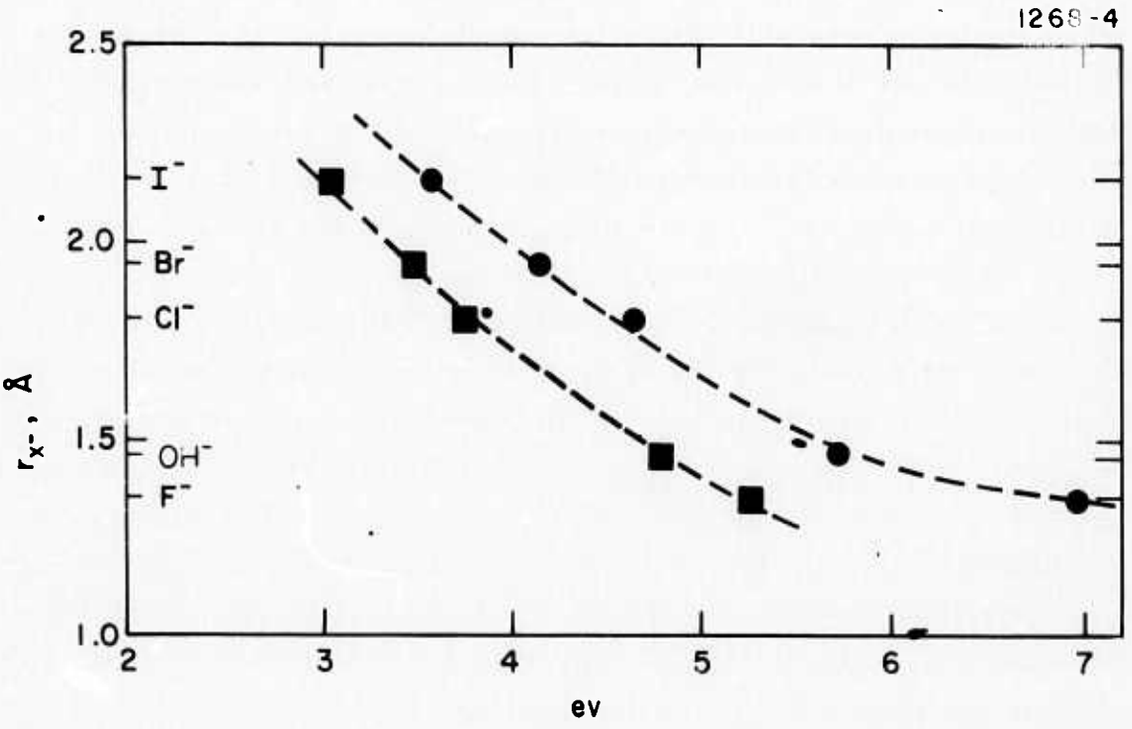

Fig. 1. Anion Size versus the Mulliken Electronegativity (●) and the Hydration Energy (■).

Appendix I), which should be taken as close to zero as is compatible with the operation. Consideration of this process parameter shows why the current popular approaches, processes based on atmosphere control, are far from achieving the effect of RAP. The use of vacuum or an inert gas is not wholly effective in excluding OH^- from the solid because P_{H_2O} is never zero while P_{HCl} is essentially zero. The same situation holds in the use of chemical getters in the condensed phase (melt), e.g., PbF_2 in fluoride melts to remove the oxide as the more volatile PbO. The latter process involves a tradeoff of a cation impurity, Pb^{2+}, for an anion impurity, O^{2-}, which may have an adverse effect on β (Ref. 3).

A reactive atmosphere process incorporates a reactive vapor phase which reduces the process parameter, P_{H_2O}/P_{HCl}, to a very low value by suppressing the concentration of H_2O and enhancing that of HCl. One approach is to live with the steady-state outgas pressure of P_{H_2O} and apply a positive P_{HCl}. Unfortunately, the weighting factor to the process parameter is the equilibrium constant of hydrolysis (see Appendix I) which can be larger than unity at the melting point. Also, aside from the problem of corrosion, bottled HCl gas has ordinarily an effective $P_{H_2O}/P_{HCl} \geq 10^{-4}$; the desired value is $\leq 10^{-7}$. Such a dew-point in the source is difficult to obtain and maintain in a flowing system. A more effective approach to reduce the pressure ratio makes use of a reactive vapor which produces HCl at the expense of H_2O. This optimization of RAP, leading to the choice of CCl_4, is presented in greater detail in Appendix I. The above problems lead one to appreciate that further optimization of all processing steps, from starting powder to the single crystal (congruent growth), into a one-step RAP was a very significant development in this program.

Optical, mechanical and surface-stability evaluations all show the advantages derived from the use of RAP. With a dynamic flow one-step RAP it became possible to start with a 99.9% pure KCl powder, priced at <1 \$/lb, and obtain the same performance as with a 99.999% pure starting material, priced at $\geq 10^2$ \$/lb. Optimizing a one-step RAP with the 99.9% powder improved β from 0.0016 cm^{-1} to $\leq$0.0005 cm^{-1}.

One need not elaborate on the obvious significance of this result for the production of large single-crystal ingots.

An earlier study by other workers reported a large surface absorption at 10.6 μm (Ref. 1). For KCl, the reported surface absorption was >80% of the total absorption for a 1-cm thickness (Ref. 1). The cause was thought to be the hygroscopic behavior. However, our RAP treatment of the crystal surface, i.e., topochemical exchange, did not improve β. In addition, we showed that neither surface hydrolysis (exchange of OH^- for Cl^-) nor hygroscopic behavior (surface uptake of H_2O) contributed to the surface absorption of a KCl crystal with $\beta = 0.0042\ cm^{-1}$, with measurements well within a precision of $\pm 0.0004\ cm^{-1}$. Instead, our study indicated that fabrication damage (surface preparation) can contribute to bulk absorption in a manner which could be mistaken for surface absorption. These results are collected in Appendix II

Mechanical evaluations (Knoop hardness and rupture strength, S) showed the benefit of a RAP treatment following fabrication of the test specimen. Evidence was obtained showing this also to be the case in a study of surface stability of KCl cleaved at (100), at humidities exceeding 100 percent. At the end of the program, we felt the need for developing a milder RAP treatment for the more refined requirements of the last stage of surface preparation; i.e., prior to coating.

In the last quarter considerable effort was devoted to the quantitative determination of the OH^- content of KCl crystals, commercial versus the RAP-grown. The primary method, acidimetry, is a more reliable alternative to the optical absorption methods. Unfortunately, the testing is destructive and does not differentiate between the surface layer OH^- and that in the bulk. At the end of the contract, the problem had not been resolved of defining a reference material where C, the mole fraction of OH^-, was zero. The measurements support the expectation that $C < 10^{-5}$ for RAP-grown KCl and, if such was the case, then $C = 2.2 \times 10^{-4}$ for the Harshaw KCl. Further background material on the subject is given in Appendices III and IV.

The study of noncongruent (solution) growth was not intended for large crystal production. Theoretically, the method is capable of producing crystals with very low OH^- content. Conceivably, crystal specimens with known OH^- content could be grown which would serve as analytical standards for melt grown materials. Although clear crystals were grown, the study showed that the probability, per unit volume, of producing a fairly occlusion-free crystal was not low enough with growth recipes which included those given in the literature. Our best solution-grown NaCl and KCl were inferior in β and in transmission from 2.5 to 25 μm to material melt-grown by a one-step RAP.

The objective in hot pressing was to press mixed metal halides from the powder to effect good bulk homogeneity and improve mechanical strength. The study began with a one-component system (KCl) to acquaint ourselves with, and solve, problems of the technology: powder preparation, compaction behavior, pressure versus temperature tradeoff, interface corrosion, etc. Our initial comparison of the pressed disc with the single crystal showed a β which was one order of magnitude higher. The problem was aggravated by marked interface corrosion resulting from the use of powder that had a preliminary RAP treatment. Towards the end of the program, chemical compatibility at the interface was achieved by pumping out the reactive gases from RAP before pressing. Considerable improvements followed in the optical transmission and in the mechanical strength of the pressed disc. The applicability of hot pressing to IR window materials for high-power lasers hinges on solving the problem of β. From the experience gained in the other technologies, we expect dramatic improvements from the development of a dynamic one-step RAP in hot pressing.

We carried out a low-level effort study on the crystal growth and evaluation of metal fluorides as window materials for the 3- to 5-μm region. Both β and the Knoop hardness proved to be useful measures of the efficacy of RAP with He + HF at a dewpoint of $P_{H_2O}/P_{HF} \approx 10^{-6}$. The use of β as an index to anion purity with respect to OH^- was based on the activity of the metal-to-oxygen vibration at the 10-μm region,

which, in turn, was a measure of the absorption at the 3-μm region arising from the oxygen-to-hydrogen vibration. The observed changes in β could have been consistent with larger changes in the optical absorption at the 3-μm region where the absorption cross section is larger. Unfortunately, this correlation was not demonstrated as there was no apparatus available to measure low-level optical absorption in the 3- to 5-μm region. The Knoop hardness was a qualitative indicator of the effect of RAP on the mechanical properties, but more direct evidence was obtained after the contract ended: The maximum strength reported for CaF_2 is 8000 psi at Raytheon (Quarterly Report December 1970, ARPA Order 1180); our RAP-grown CaF_2 gave a modulus of rupture of 12,000 psi. The study, reported in Appendix VI, shows that the advantages of RAP are best realized if the procedure is applied beginning with the conversion step to the fluoride powder and maintaining the specific surface to reverse hydrolysis prior to crystal growth.

The results of optical, mechanical, and surface-stability evaluations of metal halides at the Hughes Research Laboratories support the main thesis. The intrinsic limitations of alkali halides as windows for high-power lasers remain to be defined by the future development of materials technology.

The objective in the window coating task was to develop anti-reflecting/passivating optical coatings for candidate high-power IR laser windows. Major emphasis was placed on the goal of achieving 0.1% or less absorption per coated surface for the optical coatings. Theoretical designs and experimental results for coatings for alkali halides, cadmium telluride, and zinc selenide are reported, with the major emphasis on coatings for KCl.

The performance of the optical coatings on KCl is greatly dependent on the surface finishing operations performed on KCl prior to coating. Results of experiments on surface finishing of KCl are presented and the optical absorption in the KCl and the coatings is discussed relative to the surface finishing and handling operations.

At visible wavelengths, the availability of low optical absorption dielectric materials has made it possible to produce required window

coatings. One of the major problems that had to be overcome was optical beam losses from scattering caused by the coating texture. At 10.6 μm, low absorption dielectric materials have only recently begun to be available; however, optical beam losses due to scattering may not be a major problem and at this longer wavelength, some texture in the optical coatings may be tolerated without major contribution to scattering losses.

Window materials that show promise for use in the near infrared have refractive indices that fall in the 1.5 to 3.5 range. Antireflection coatings for the low index materials serve the dual purpose of improving the optical performance of the windows while simultaneously protecting the halide window surface from environmental degradation (since one of the promising candidates among the optical window materials for use in the infrared, KCl, has appreciable solubility in water).

For window materials that have good optical characteristics as a result of their low optical absorption losses but which have indices of refraction greater than 1.5, the lowered optical transmission due to the high reflection from the window surfaces makes the use of antireflection coatings mandatory.

The surface finishing and coating technology, established to date, has produced the following results for 10.6-μm absorption in our antireflection coatings:

KCl

Two coating designs for KCl were investigated. One design is a two layer coating of As_2S_3 and ThF_4 in which we have achieved 0.19% absorption per surface for the coating; the second design is a two layer coating of ZnTe and ZnS which has produced coatings with 0.05% absorption per surface.

CdTe

Antireflection coatings for CdTe were produced using a coating design which consists of two film layers of BaF_2 and ZnS in which we have achieved 0.06% absorption per surface.

The ambitious goal for our coating program, which was projected at the first laser window conference at AFCRL in October of 1971, was to achieve less than 0.1% absorption per surface for window coatings. The results, achieved to date, are impressive when one considers that in October of 1971 our state of the art in antireflection coatings was absorptions per surface in the 0.5% to 1% range.

Our ability to achieve the coating program goals was based on the following combination of capabilities available to us at Hughes Research Laboratories:

- Availability of high quality single crystal KCl and CdTe window materials grown at Hughes.
- Surface finishing technology for KCl and CdTe which provides minimum degradation to the intrinsic optical absorption of the bulk window materials.
- Availability of processes for preparation and purification of As_2S_3, ZnTe, and ThF_4 starting materials used for film preparation.
- 10.6-μm laser optical monitor for precise thickness control of optical film layers.
- Complete and comprehensive computer design and analysis programs, which include optical absorption in the films, so that theoretical designs and experimental results can be compared.
- 10.6-μm laser absorption calorimeter for measurement of absorption in coated windows, window substrates, and for determination of absorption indices for optical films.

The important requirement for future coating work is to continue efforts at improving window materials, window surface finishing and coating technology so that windows when subjected to 10.6-μm high power incident laser fluxes will not fail at damage thresholds far below the intrinsic damage thresholds for the bulk window material.

SECTION II

RESULTS AND EVALUATION

A. WINDOW MATERIALS

1. Crystal Growth and Evaluation of KCl

The technology of single-crystal congruent growth from the melt under RAP was studied for NaCl and KCl. Greater emphasis was given to KCl. Since the technologies for the two materials are quite alike, they will not be discussed separately.

The study began with the design and construction of a Czochralski apparatus for 1- to 2-cm diameter crystals (Fig. 2) which could be adapted to a RAP operation. The apparatus provided specimens for optical evaluation. It was also used to study interface compatibilities (corrosion) and transport problems (impurity pickup) accompanying RAP. Optical evaluation showed that radial inhomogeneity of the refractive index; i.e., lensing, was not insignificant. Consequently, a larger Czochralski apparatus with a 5-cm diameter capability was constructed (see Fig. 3).

The first few runs with the large Czochralski apparatus showed Poco graphite crucibles to be permeable to molten KCl, behavior which led to crucible failure during cooldown. Vitreous carbon crucibles from Beckwith Corp. were used to grow several 5-cm diameter boules. These boules showed elongated voids. Bubbles formed at the growth interface and nucleated these regions of negative growth. It was observed earlier that the gas atmosphere in RAP manifested a high solubility in molten KCl and lowered drastically the distribution coefficients of impurities. This feature was, of course, an asset to scrubbing in purification but, in turn, caused a larger flux of gas (bubbles) during the change of state from liquid to solid; i.e., crystal growth.

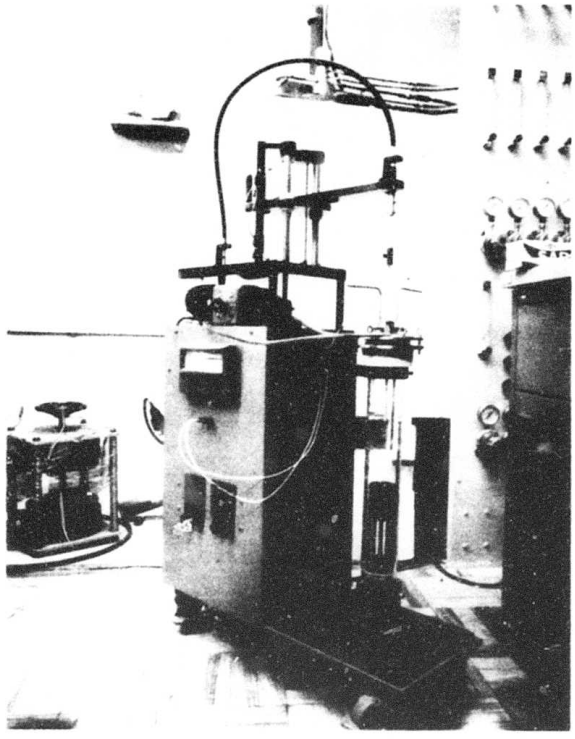

(a) Congruent growth apparatus

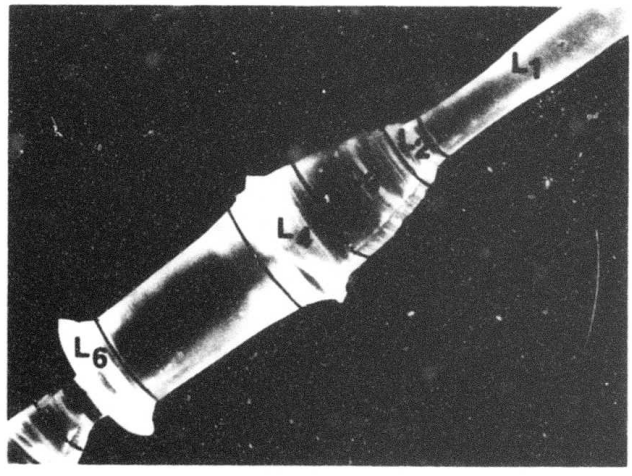

(b) Crystal of KCℓ

Fig. 2. Growth of KCℓ From the Melt.

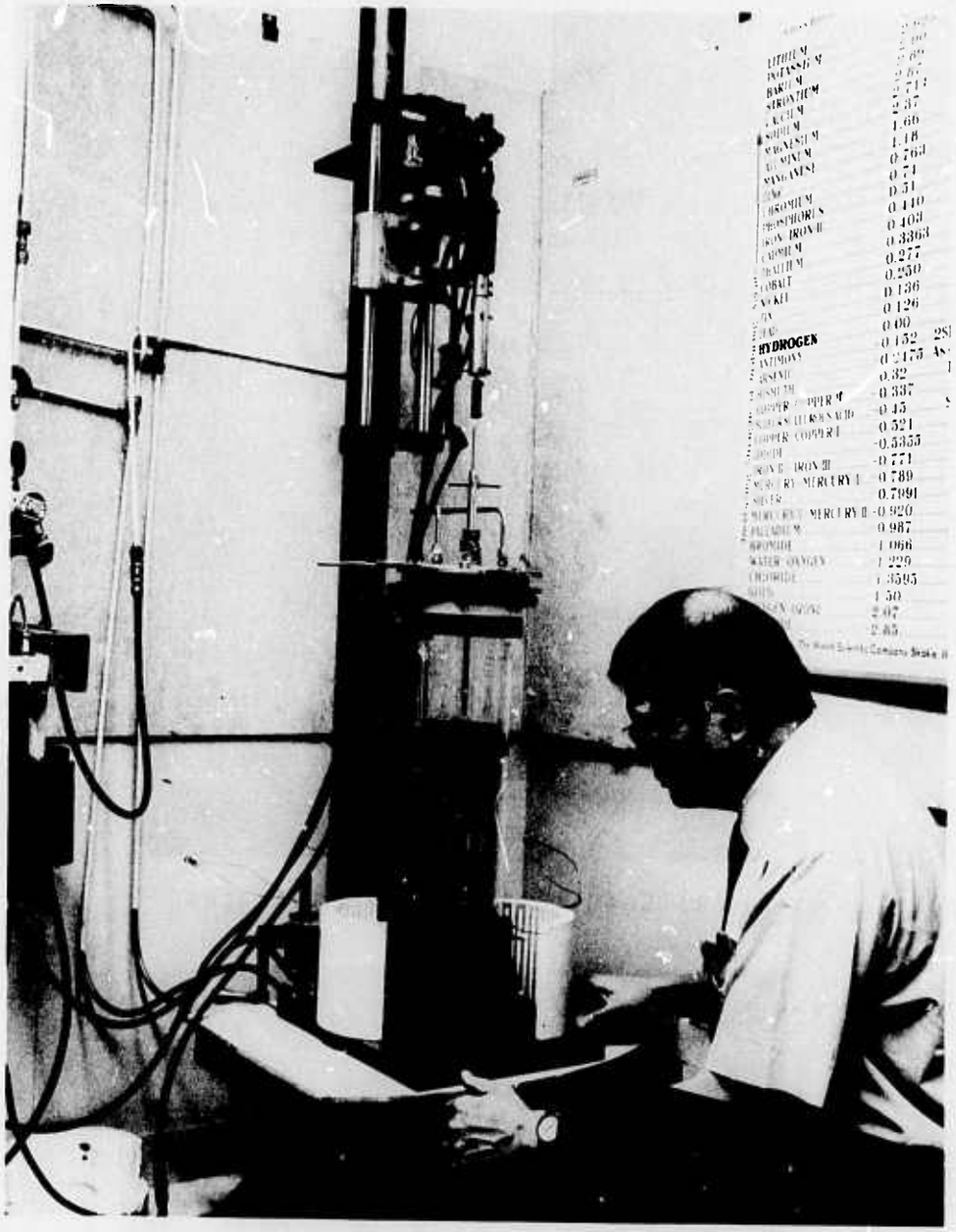

Fig. 3. Czochralski Apparatus for the Growth of KCl from a 10-cm Crucible Under Controlled Atmosphere.

An internally funded study on the technology of scale-up in RAP crystal growth paralleled this program. RAP crystal growth was developed in the vertical Bridgman mode, a geometry more favorable for coping with the problem of gas at the growth interface. The technology also allowed for the optimization of interface compatibilities, a problem accompanying the use of reactive atmospheres. Another advantage of the method was its adaptability to the growth of flat single crystals. Figure 4 shows a collection of single crystal KCl Czochralski boules ranging from 1 to 5 cm in diameter and Bridgman cylindrical ingots and flats up to 5 cm across the cross section. The elongated voids described previously are seen extending through the bulk of the large Czochralski boules. Figure 5 shows a 10-cm diameter Bridgman cylindrical ingot of single crystal KCl grown by the RAP method.

The optical absorption at 10.6 μm, β, was measured with an adiabatic calorimeter. The measurement technique and the apparatus employed are discussed in Appendix II. Surface hydrolysis and hygroscopic behavior were shown to have a negligible contribution to surface absorption; however, the contribution of fabrication damage was found to be significant. If such a contribution was not separated from the bulk absorption, the extrapolation of power absorbed to zero sample thickness gave an intercept which could be misinterpreted as a contribution from the surface. Also, a consequence of the apparent surface absorption was an exaggeratedly low bulk absorption derived from the slope of the plot of power absorbed against sample thickness*. However, legitimate contributions to surface absorption exist. An instance such as this was shown to arise from the ingredients employed in surface polishing. These earlier developments are collected in Appendix II.

Using KCl crystals of different purity grades, no correlation of β with the metal ion impurities was established. Table I lists the results of emission spectrograph analysis, modulus of rupture (S),

*The ambiguity in the value of the slope arises from the scatter in the experimental values of (x, y). The least-square fit to $y = mx + b$ yields a smaller value of m than the fit to $y = mx$ (cf. Fig. 35, Appendix II). When there is no surface absorption, the observed absorption must all be accounted for in the bulk.

Fig. 4. Czochralski Boules and Bridgman Cylinders and Flat Ingots of Single-Crystal KCl.

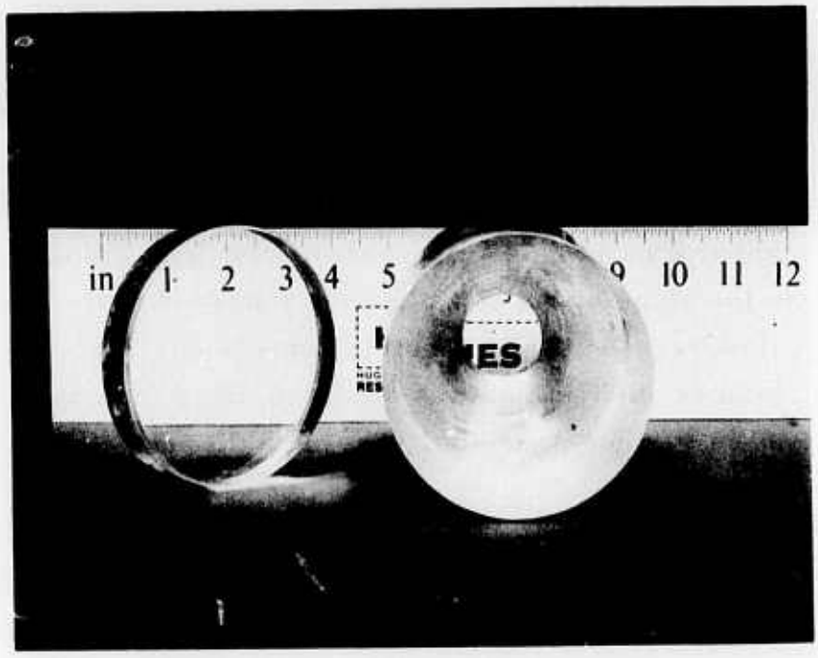

Fig. 5. A 10-cm Diameter Bridgman Cylindrical Ingot of Single-Crystal KCl Grown by the RAP Method.

TABLE I

Analysis of KCl Crystals, Modulus of Rupture S, and Absorption Coefficient at 10.6 μm (β)

	MCB (99.9%)	JM (99.999%)	HRL Zone Refined*	Harshaw Heel	Harshaw Cone
Cu	0.00079	0.000049	0.00019	ND < 0.00004	ND < 0.00004
Ag	ND < 0.0001	ND < 0.0001	ND < 0.0001	ND < 0.0001	0.0011
Mg	0.00032	0.00039	0.00033	0.00046	0.00054
Ca	0.00039	0.00032	0.00086	0.00066	0.00090
Fe	ND < 0.001	ND < 0.001	ND < 0.001	ND < 0.001	0.0012
Ni	ND < 0.0007	TR < 0.0007	ND < 0.0007	ND < 0.0007	ND < 0.0007
Si	0.0030	ND < 0.003	0.0094	ND < 0.003	ND < 0.003
α, cm^{-1}	0.0015 ±0.0000	0.00082 ±0.00005(3)	0.00050 ±0.00001(3)	0.0017	0.0058
S, psi	930 ±240(4)	---	---	600 ±300(4)	1020 ±870

*Three-pass, zone refined MCB (99.9%).

T565

and β. The first three samples from the left, identified by the source material in the column heading, give the analysis of the tips of Czochralski crystals grown at Hughes Research Laboratories (HRL). The other two are Harshaw specimens sampled from two different regions of a Stockbarger crystal. The metal ion impurities are grouped according to the most likely valence assumed: +1, +2, and +4.

No correlation of S and β with groups I and IV impurities can be drawn. However, with bivalent impurities, the Harshaw cone material is a factor of two to three larger in total content (~30 ppm), which may account for the higher S compared to the heel section (Ref. 2). Yet, according to the results with MCB specimens,* an increase in the level of bivalent impurities is not necessary to attain $S \approx 10^3$ psi.

Bivalent impurities can lead to a higher β through the stabilizing effect of the impurity on OH^- (Ref. 7). The effect could account for the increase in β of KCl with Pb^{2+} doping, (Ref. 3) although $PbCl_2$ itself has a low β(0.0020 cm^{-1}). On the assumption that OH^- was not excluded in the Pb^{2+} doping of KCl (Ref. 3), the model leads to an absorption cross-section at 10.6 μm of, $\sigma < 10^{-19}$ cm^2. The model would also explain the tradeoff between β and S in the heel and cone sections of the Stockbarger ingot of the Harshaw specimens.

The MCB result shows that there need be no tradeoff in β for a high S. Although the three HRL specimens show the lower β, no correlation with impurity levels can be drawn. The molar sum of the bivalent impurities is constant for the three, corresponding to a mole fraction, $x = (2.66 \pm 0.03) \times 10^{-5}$. These results are consistent with the interpretation that: $C < 10^{-5}$ and 10^{-21} $cm^2 < \sigma < 10^{-19}$ cm^2. If β is not metal-ion impurity limited and RAP growth is capable of achieving $C \approx 10^{-7}$, then from $\sigma \approx 10^{-20}$ cm^2 the value of β limited by OH^-(s) is $10^{-7} \times 10^{22} \times 10^{-20} = 10^{-5}$ cm^{-1}, where 10^{22} cm^{-3} is the anion density in KCl.

*Supplier code of KCl source powder: MCB = Matheson, Coleman, and Bell and JM = Johnson Mathey.

The value of β, OH^-(s) limited only, is two orders of magnitude smaller than the average for the three HRL specimens, which show a standard deviation of $\Delta\beta = 5 \times 10^{-4}$ cm^{-1}. It is necessary to locate the source of $\Delta\beta$ as β is at most 3 $\Delta\beta$. Annealing experiments show that a source of $\Delta\beta$ is the bulk damage brought about in surface polishing (see Appendix II). These results indicate that β is now limited by the technique of surface finishing instead of materials processing.

The above conclusion is supported by the results of evaluation of 3-cm diameter Bridgman ingots. Thin disks, ~ 5-mm thick, were taken from each end of the cylindrical section: $\beta = 0.00082$ cm^{-1} at the region which crystallized first and $\beta = 0.0014$ cm^{-1} at the later stage of growth. The intervening cylinder, L = 11.2 cm, gave 93.0% transmission uniformly over the face within 1% variation. With no absorption and scattering losses, the theoretical transmission is 93.35%. Thus, the value of β over the cylinder is 0.0035/11.2 = 0.00031 cm^{-1}. The end faces of the cylinder were wedged to avoid interference effects.

Similar results occur in the case of NaCl. Our best value on melt grown Harshaw NaCl is $\beta = 0.005$ cm^{-1}. A nonoptimum RAP on a Czochralski boule (sample NA-9) yielded $\beta = 0.0018$ cm^{-1} for L = 2.69 cm. When this sample was sectioned further with a wire saw, the limiting effect of surface polishing is seen as follows: $\beta = 0.0016$ cm^{-1} for L = 0.85 cm, $\beta = 0.0023$ cm^{-1} for L = 0.80 cm, $\beta = 0.0025$ cm^{-1} for L = 0.52 cm, and $\beta = 0.0037$ cm^{-1} at L = 0.47 cm. However, with an optimum RAP Bridgman ingot, a cylinder with L = 12.0 cm showed a uniform transmission of 92.0% which was the theoretical value for no absorption and scattering losses. Yet, at the region which crystallized first, $\beta = 0.0028 \pm 0.0005$ (3) cm^{-1}, and that which was last, $\beta = 0.0030 \pm 0.0005$ (5) cm^{-1}. Obviously, these two measurements do not reflect the intrinsic value of the material but the limiting effect of fabrication. Otherwise, $\beta = 0.003$ cm^{-1} over L = 12.0 cm would have shown a 3.6% discrepancy below the theoretical transmission. Again, the end faces of the cylinder were wedged.

For the measurement of yield (Y) and the modulus of rupture (S), Instron equipment was employed to carry out the flexure test to failure. The crystal, in the form of a parallelepiped, was mounted as a simple beam resting on end supports with force applied as two equal concentrated loads at the one-third points (four-point loading). A slow loading rate (0.005 or 0.002 in. min^{-1}) was used to give reproducible readings of S. At the beginning of the study, the parameters of commercial KCl crystal were: Y = 300 psi and S = 640 psi (Ref. 1). As seen in Table I, S $\approx 10^3$ psi can be achieved with no tradeoff in β in the undoped material.

Parallelepiped specimens were prepared by cleaving at (100); either Harshaw or Optovac KCl gave Y = 300 psi and S = 700 psi, values in agreement with the parameters given above. With a nonoptimum RAP procedure and the same method of preparation of the test specimens, the HRL specimens yielded, Y = 400 psi and S = 930 psi.

The preparation of the surface of the test specimen (Harshaw and Optovac KCl) was also shown to play a significant role in the results of mechanical testing. Using cleaved specimens at (100), the measured average (S_{av}) and the standard deviation (ΔS) showed that uniformity in test performance improved with polishing (Linde A in alcohol) but the average strength decreased; i.e., ΔS and S_{av} were lower. The lower value of ΔS indicated that polishing removed the shallow microcracks; the lower value of S_{av} suggested that polishing may have caused some of the cracks to propagate into the interior faster than the surface material was removed, and/or surface recrystallization occurred after polishing.[8] Thus, without polishing, Optovac specimens prepared by cleaving yielded S = 430 ± 50 (2) psi and, if followed by water etching, S = 850 ± 360 (11) psi.*

---

*Water etching removes an ~ 0.5-mm layer of the material. The sample is swished for 1 to 2 sec in water, followed by a rapid alcohol rinse and hot air drying to avoid surface recrystallization.

The above results suggested an examination of annealing procedures as a means of repairing the damage on the surface and in the interior caused by cleaving. Harshaw KCl specimens were used and the following results were obtained:

When cleaved only,	S_{av} = 640 psi
When cleaved and He-annealed,	S_{av} = 450 psi
When cleaved and RAP-annealed,	S_{av} = 970 psi

Annealing consisted of a 20-hour exposure at 670°C to a pressure of 100 to 200-mm Hg of either He or CCL_4.

The effects on the yield point (Y) of the generation and treatment of (100) surfaces of test specimens were studied. Since damage from the surface into the interior followed cleaving (Appendix II), cutting with an 8-mil diamond-impregnated copper-clad steel wire was examined as an alternative. Cleaved and polished Optovac KCl gave Y = 450 ± 50 (3) psi, while the same material cut and polished yielded Y = 580 ± 40 (4) psi. When polishing was replaced by water etching, the difference was even less, Y = 400 ± 50 (11) psi versus Y = 410 ± 60 (3) psi, cleaved versus cut, respectively. The lower value in the Y_{av} suggests that water etching removes a work-hardened surface. This proposition also implies that a cut surface work-hardens in polishing better than a cleaved surface. The opposing effects of cleaving followed by water etching should be noted: A dramatic increase in S_{av} and a decrease of Y_{av} from the work-hardened value to what may be intrinsic; i.e., a widening of the plastic region.

Test specimens were fabricated from single-crystal RAP Bridgman KCl and NaCl and polycrystalline KCl (Polytran) by cutting with the wire saw and polishing with Linde A in alcohol. The Polytran specimens showed a yield of Y = 580 ± 20 (3) psi and the HRL specimens gave Y = 660 ± 120 (7) psi. A summary of the results of the (Y,S) measurements is shown in Fig. 6. It is seen that in the case of

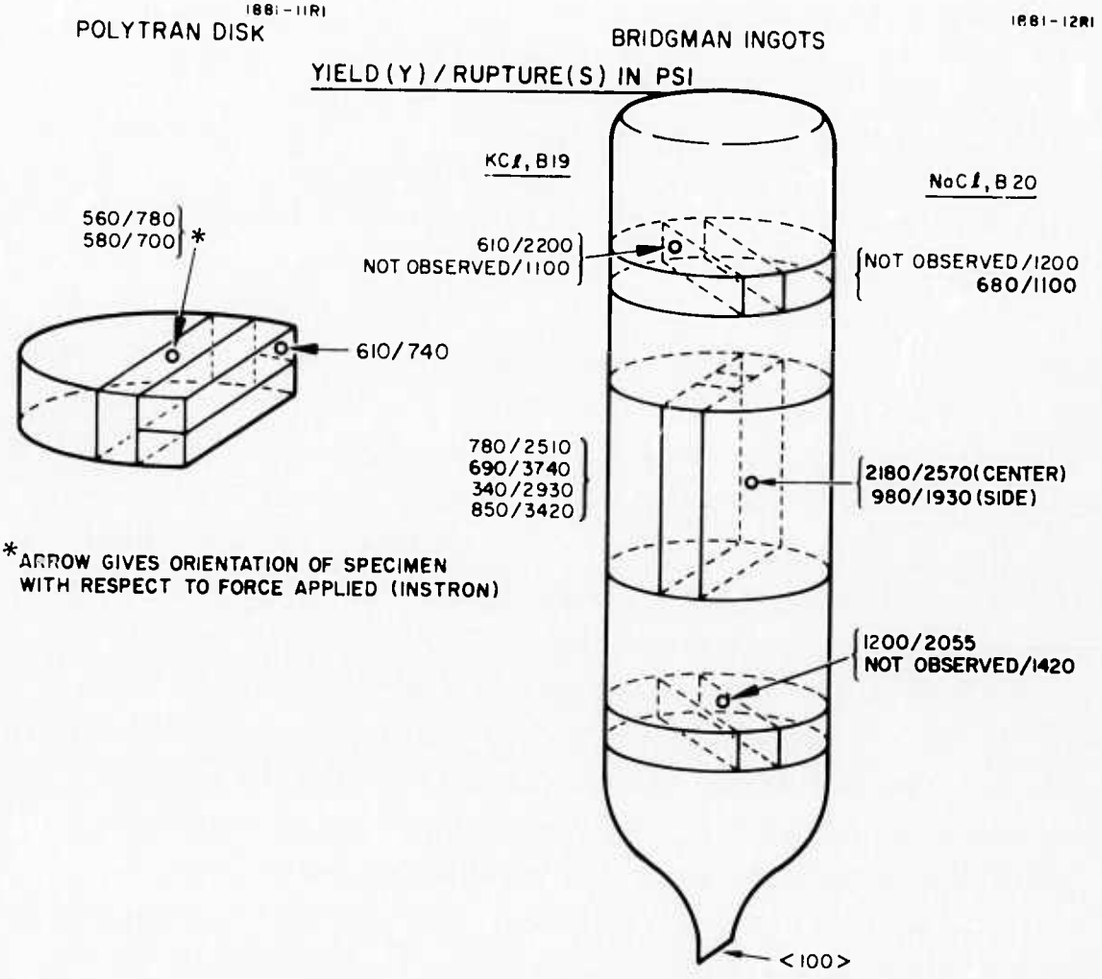

Fig. 6. Mechanical Evaluation of RAP Single Crystal of NaCl (B20) and KCl (B19) and Polycrystalline KCl.

polycrystalline KCl, Y_{av} increased slightly while S_{av} remained the same as the earlier value; therefore, the plastic region was narrower. In the case of single-crystal KCl, Y_{av} increased by more than 100% and S_{av} increased by as much as 500% above the earlier values. The net effect was a wider plastic region, without the use of water etching. In fact, the S_{av} values in this case exceed the S_{av} obtained in the earlier specimens (Czochralski, nonoptimum RAP) by the use of water etching.

Similar increases also occurred in the case of single-crystal NaCl (early value of S = 570 psi) but, as seen in Fig. 6, the plastic region is narrower than in the case of single-crystal KCl. At times, no yield is observed up to failure.

The growth direction of KCl ingot B 19 was found to be close to <111>. The observation suggested a search for an optimum direction in (Y, S). For window application to high-power lasers, the optimum in Y was preferred over that of S if the optimization could not be effected simultaneously. Consequently, water etching of the wire-saw cut specimens was employed. The results which follow give the test specimen axis along the long direction, the test direction, and Y:

<100>, <100>, and Y = 390 ± 30 (7) psi

<110>, <111>, and Y = 500 ± 50 (4) psi.

<111>, <111>, and Y = 530 ± 50 (4) psi

From these results in Y and those of S (Fig. 6), it is quite likely that the growth direction along <111> provides the optimum in Y and S (Appendix V).* This growth direction is realized in spontaneous nucleation.

---

*Although the program had ended, it was felt necessary to check out this feature with a commercial crystal. Optovac KCl specimens were prepared by the same procedure, i.e., wire-saw cut followed by water etching. With the long bar axis at <100> and test direction at <100>, Y = 410 ± 60 (3) psi; with the long bar axis at <111> and test direction at <111>, Y = 600 ± 150 (7) psi.

Figure 7 shows the different failure patterns revealed by polarized light. Figure 7(a) shows KCl specimens with the (100) surfaces generated by cleaving and tested at <100>. Starting from the left, the first seven are Harshaw crystals, the next five are Optovac, and the last four are HRL. With either Harshaw or Optovac, Y = 300 psi and S = 700 psi; the HRL specimens, Y = 400 psi and S = 930 psi. The test direction was applied from right to left; the density of slip planes at (110) reveal the load points, and the failure occurs at (100).

Figure 7(b) shows the wire-saw cut specimens (polished) from B 19. The test direction, from right to left, is <111>. The long bar axis of the two at the left and the two at the right are perpendicular to <111> while the three at the center are parallel. The specimens store a larger amount of strain energy in the testing and break with a louder report than the specimens of Fig. 7(a). The failure region, where the strain pattern is washed out, when observed in the test direction shows a wedge of two (100) planes.

Early in the program, compressive strength tests on Optovac KCl revealed yield strengths of 225 to 230 psi and a rupture strength of 2410 psi. Plastic flow occurred only in one of the <100> directions, while the other <100> directions remained constant.

2. Topochemical Exchange (Scrubbing)

In this study we established a RAP procedure for the surface-layer treatment of KCl crystals at temperatures below the melting point. The arguments given in Appendix I for the choice of CCl_4 as the exchange agent to reverse hydrolysis apply to the present case. The apparatus employed He as the carrier gas or was operated as a closed system under a vapor pressure of CCl_4, as shown in Fig. 8. It was observed that surface hardness (Knoop) increased after scrubbing with He + CCl_4(g) but not with He alone. Hence, Knoop measurements were used to study the depth of penetration of scrubbing at various temperatures and dwell times.

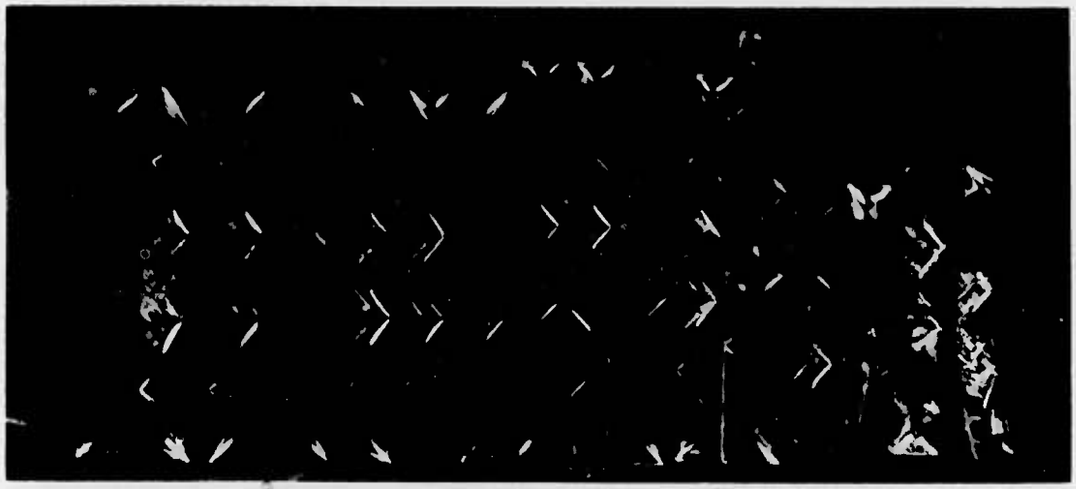

(a) (100) surfaces tested at <100>

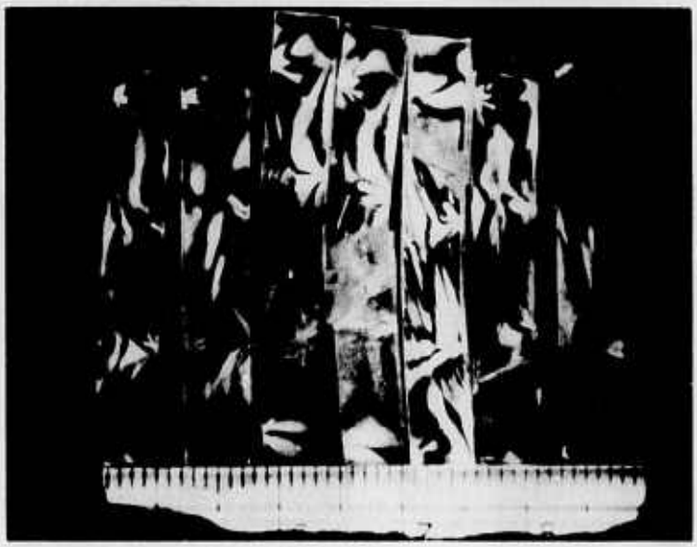

(b) (111) surfaces tested at <111>

Fig. 7. Test Specimens of KCl, Flexed to Failure, Viewed in Polarized Light.

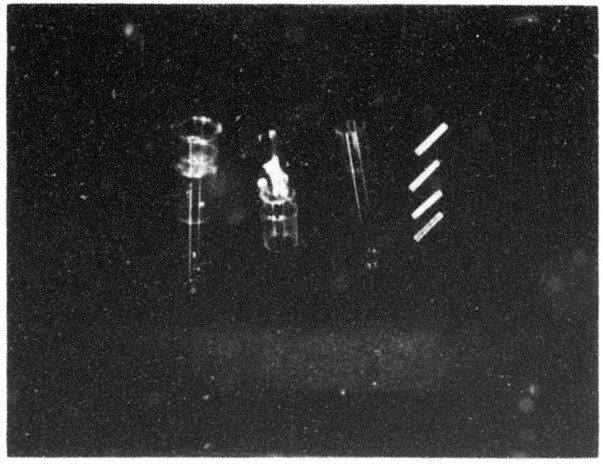

(a) Scrub apparatus showing four parallelepiped crystals

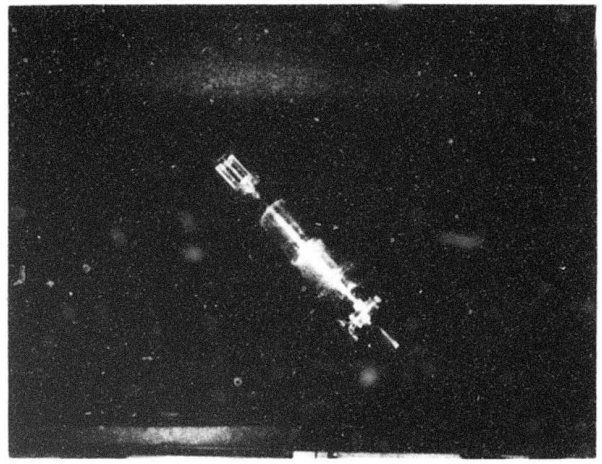

(b) Scrub apparatus assembled

1379-1

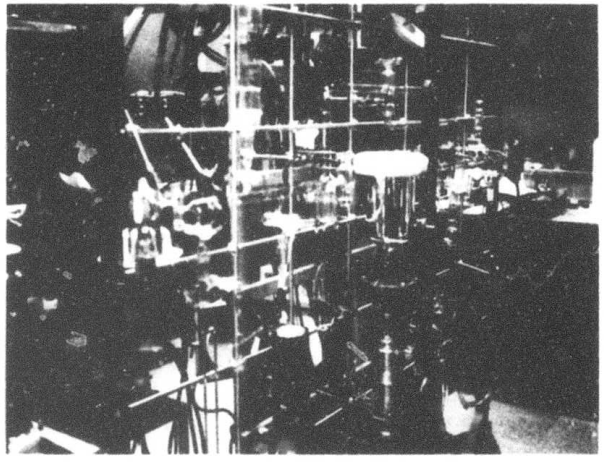

(c) Evacuation and introduction of CCl_4

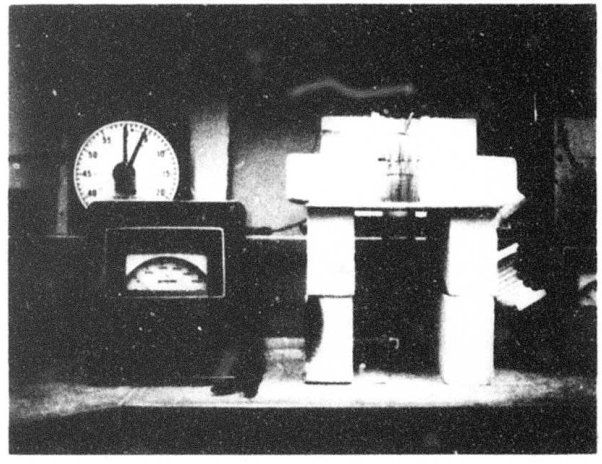

(d) Furnace and timer

Fig. 8. Scrubbing of Metal Chloride Crystals.

Specimens were obtained by cleaving at (100). The hardness at depth zero was taken on the as-scrubbed material. Then the scrubbed material was cleaved from the opposite side. The depth of penetration was measured away from the region where contact was made with the cleaving tool. At 450 °C, no penetration could be established up to a 35-hour dwell time for KCl. A 300-μm depth was achieved with 500 °C and 15-hour dwell time for KCl. A comparable penetration was achieved for KBr at 350 °C and 90-hour dwell time using CBr_4.

A greater depth of penetration was achieved with an 8-mm thick KCl crystal, by a 20-hour exposure to 100 to 200-mm Hg of $CCl_4(g)$, in a closed system at 670 °C. This is shown in Fig. 9. These conditions of exposure were also found to be adequate for the removal of slip lines in KCl crystals, as shown in Fig. 10. These slip lines are at (110) and are generated by cleaving and can be seen to a few millimeters depth by polarized light.

Table II shows the effect of annealing and the atmosphere employed in the process on the mechanical properties of KCl crystals (Harshaw). The best improvements in mechanical properties are seen to be associated with the RAP surface treatment of a 20-hour exposure at 670 °C under 100 to 200 mm Hg of CCl_4.

3. Crystal Surface Evaluation

The object of this study is to establish fabrication and surface preparation procedures (in particular, optical finishing) which avoid surface features that limit the material's optical transmission at 10.6 μm, resistance to corrosion by water vapor, and mechanical strength.

The first attempts to cut KCl made use of a steel wire using 320-grit silicon carbide (SiC). The use of glycerine as a vehicle was found to be unsuitable. Because of solvent action on KCl, the saw tends to bind and break. Solvent action varied with exposure time and cutting rate. The region close to the source of the glycerine-grit suspension, introduced by gravity, was badly etched. The resulting cut was quite jagged.

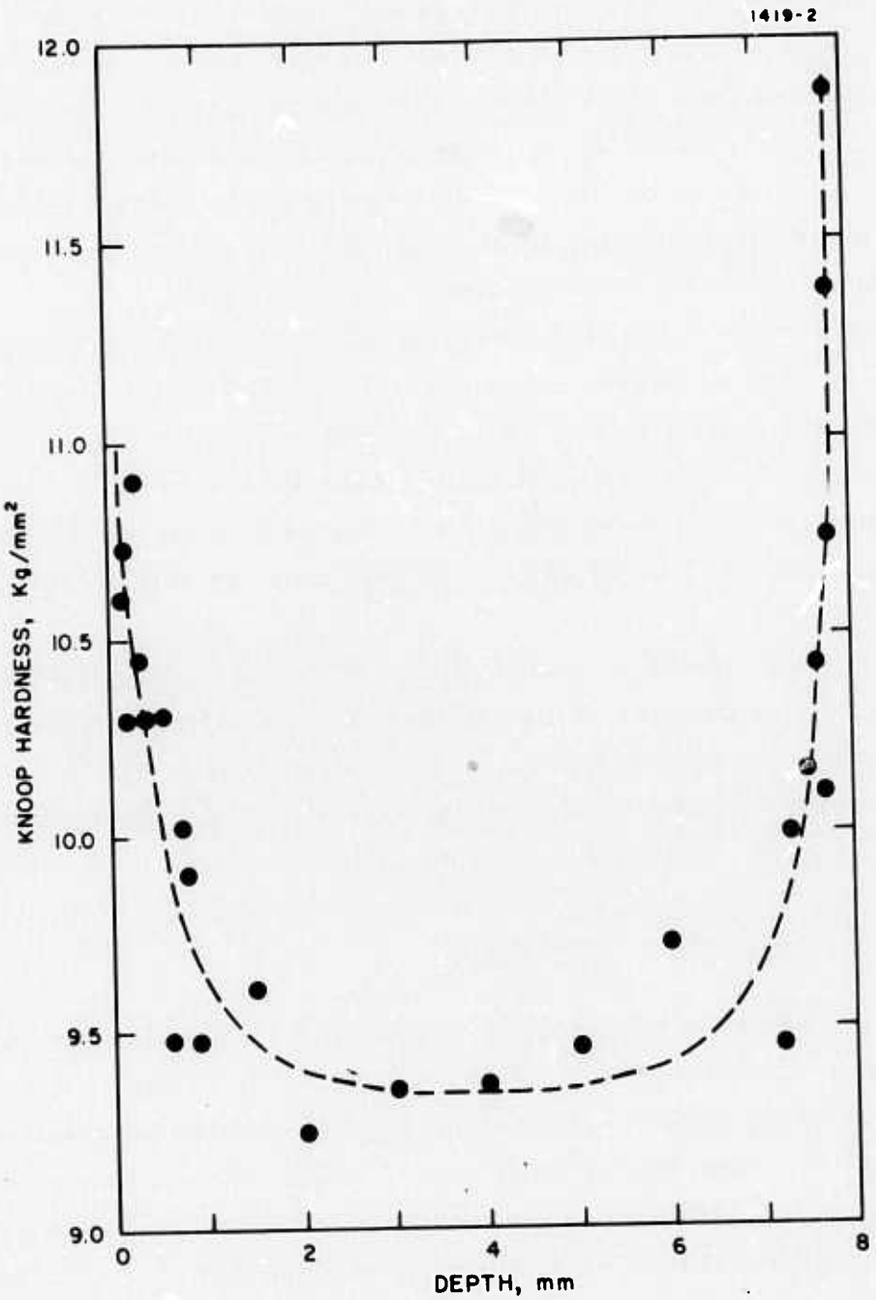

Fig. 9. Harshaw KCl Scrubbed (20 Hours, 670°C) with CCl_4 Vapor (~100 mm Hg). Penetration Curve Across Cleaved Surface (8-mm Thick Crystal).

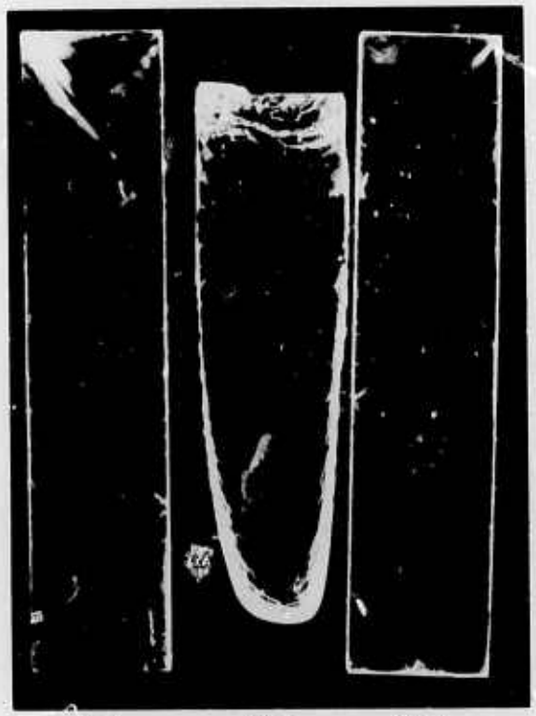

(a) (b) (c)

(a) KCl surface as cleaved in (100). (b) A similar surface after 20 hours at 670°C under a low pressure of helium. (c) A similar surface after 20 hours at 670°C under CCl_4 vapor..

Fig. 10. Behavior of Slip Lines (110) in KCl With Thermal Treatment (Viewed in Polarized Light).

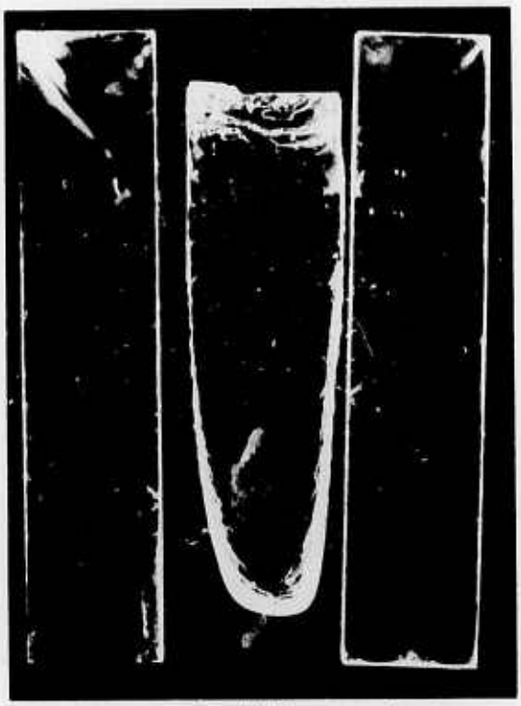

(a) (b) (c)

(a) KCl surface as cleaved in (100). (b) A similar surface after 20 hours at 670°C under a low pressure of helium. (c) A similar surface after 20 hours at 670°C under CCl_4 vapor..

Fig. 10. Behavior of Slip Lines (110) in KCl With Thermal Treatment (Viewed in Polarized Light).

TABLE II

Effect of Annealing and RAP on the Mechanical Properties of KCl Crystals

Specimen Preparation *	Knoop value, kg/mm^2 **		S, psi
	At d = 0	Penetration	
Cleaved only	9.5	9.5	640 ± 290 (5)
Cleaved + 20-hour at 670 °C in He	10.3 ± 0.3 (4)	10.0 ± 0.2 (7). 0.1 mm ≤ d ≤ 2 mm	450 ± 230 (2)
Cleaved + 20-hour at 670 °C in He + H_2O	10.5 ± 0.4 (8)	9.8 ± 0.1 (7), 0.15 mm ≤ d ≤ 5 mm	– ***
Cleaved + 20-hour at 670 °C in CCl_4	12 to 13	9.4 to 9.5,† 1 mm ≤ d ≤ 7 mm	970 ± 450 (4)

* The gas pressure is 100 to 200 mm Hg.

** The numbers in parentheses following the standard deviation refer to the number of measurements. The crystal surface corresponds to a depth, d = 0. Penetration depth is taken right after cleaving.

*** This measurement was not warranted as the specimens were extensively etched. There is no doubt that hydrolysis occurred; upon opening the apparatus, the sharp smell of acid vapor (HCl) was unmistakable.

† These are the values plotted in Fig. 9. The effect of the annealing atmosphere on the volatility of KCl crystal can be appreciated in Fig. 10.

T885

A much smoother cut was effected with the use of a nonsolvent vehicle. The nonsolvent chosen was a heavy hydrocarbon,* since OH-derivative liquids of low volatility (such as glycol or glycerine) increased the surface absorption in the 3- and 10-μm regions. However, hydrocarbons are not completely inactive in these regions (C-H at the 3-μm and C-C at the 10-μm regions) and should be removed after cutting. These results are discussed in Appendix II. A comparison of the cuts obtained with the two liquid vehicles is shown in Fig. 11.

The next comparison study dealt with the combination of abrasive and cutting wire. Bridgman KCl and NaCl ingots were used for this purpose. The previous procedure, (slurry of 320-grit SiC in light mineral oil) took 30 to 50 minutes to cut across 3-cm diameter ingots; the cut was not very uniform. An 0.008 in. wire impregnated with 45-μm diamond, lubricated with the same mineral oil, effected a uniform cut across in 4 to 7 minutes. The latter apparatus** was also shown to be applicable without the use of the hydrocarbon.

We have already considered the effect on the mechanical strength of the bulk material (KCl) of the method of generating the surface. The results showed that wire-saw cutting was preferable to cleaving. The relevance of the annealing procedure following the primary step of generating the surface has been shown. In addition, data showing the pertinence of the extent of surface rework and the nature of the materials used in the last step (optical finishing) to surface absorption at 10.6 μm is given in Appendix II.

The effect of cleaving and polishing damage on β was studied in three sections cleaved from a Czochralski KCl boule (sample C-58) which was grown from scrub-cast JM (99.999%) source powder. The

---

* Convoil-20 from Consolidated Vacuum Corp. of Rochester, New York.

** Lastec No. 2005-C from Laser Technology Inc., North Hollywood California.

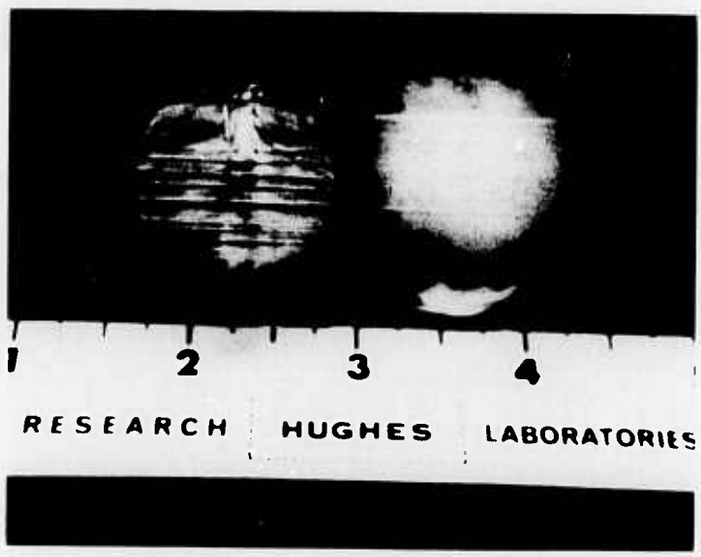

Fig. 11. Wire Saw Cut KCl Using 320 Grit Silicon Carbide. The Specimen to the Left Made Use of Glycerine as the Vehicle and That on the Right, a Heavy Hydrocarbon.

three sections were identified as L2 with L = 1.90 cm, L1A with L = 1.22 cm, and B2 with L = 0.57 cm. Figure 12 shows the batch between crossed Polaroids. The sequence (a) to (d) is given in chronological order. Figure 12(a) shows the sections just after they were cleaved and polished (linde A in alcohol). Figure 12(b) is the batch in 12(a) after a 20 hour heat treatment; 12(c) is the batch after an additional 30 hour treatment. Surface etchings in 12(b) and 12(c) are seen in these unpolished pieces. These surface irregularities were removed by polishing prior to the measurement of β. Figure 12(d) shows the polished batch in 12(c) after β was measured. The amount of damage reintroduced by polishing is clearly revealed by 12(d). As shown in Table III of Appendix II, β increases with repeated surface polishing.

In the calorimetric determination of β, the slip lines may account for a significant fraction of the laser beam being scattered directly to the thermocouple. The surfaces shown in Fig. 12 are parallel to (100) and the slip planes are (110). That the damage occurs over the bulk is easily appreciated by observing in another $<100>$ direction under crossed Polaroids. The slip lines are seen to propagate under light squeezing to a stress value easily achieved in conventional handling in polishing or packaging and mounting for shipping and storage.

The results of the measurements in β on the specimens, shown in Fig. 12, are collected in Table III. Within the accuracy of the measurements, the results for the 20 hour and the 50 hour treatments for section L1A are the same. In spite of some damage being reintroduced in polishing, Fig. 12(d), Table III shows that the heat treatment achieved a factor of two reduction in β over the value for 0-hour treatment. The polished section B2 after the 50-hour treatment was damaged accidentally while positioning the laser beam. A crack developed at the edge which propagated internally (Fig. 12(d)).

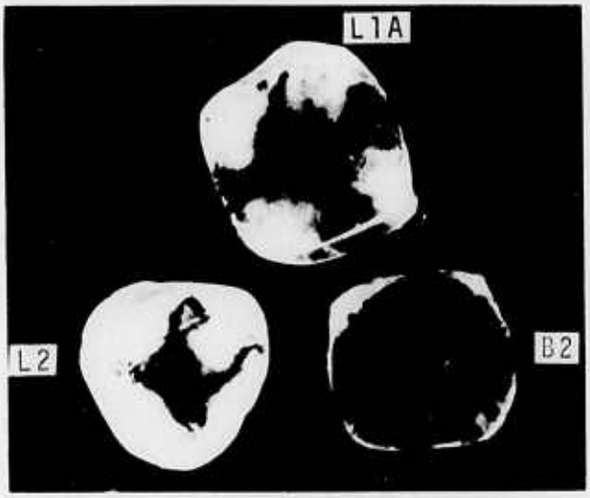

(a) Cleaved and polished, no heat treatment, (1.7x)

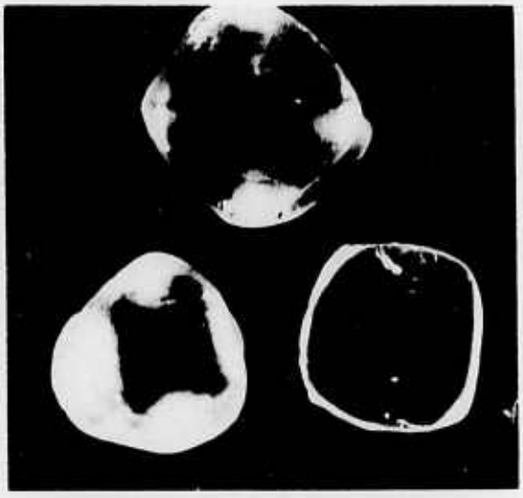

(b) Batch (a) after 20 hour heat treatment, unpolished, (1.7x)

(c) Batch (b) plus 30 hour heat treatment, unpolished, (2.0x)

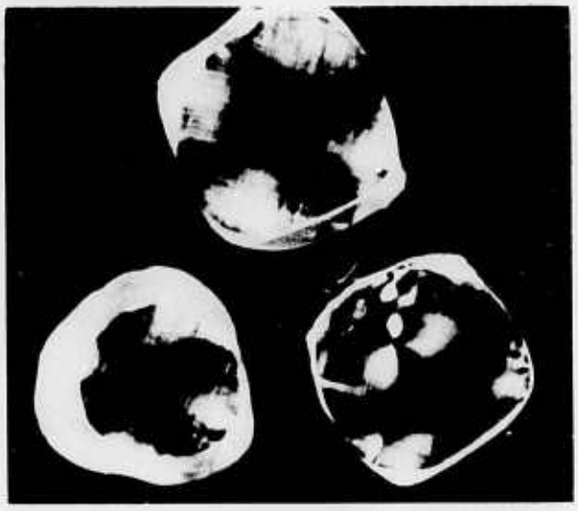

(d) Batch (c) polished, (2.0x)

Fig. 12. KCl Boule Sections Seen Under Crossed Polaroids. Each Batch Photographed Shows L2, L1A, and B2.

TABLE III

The Value of β in KCl Sections versus Cumulative Time in Heat Treatment*

Section Identification	L, cm	Calorimetric Absorption Coefficient β, cm^{-1}		
		0 Hour†	20 Hours**	50 Hours††
L2	1.90	0.0012	----	0.00063
L1A	1.22	0.0012	0.00050	0.00053
B2	0.57	0.0015	0.0010	---***

*Exposure to 100 to 200 mm Hg of CCl_4 vapor at 700°C.

† Sections obtained by cleaving and then polished. No heat treatment.

** Sections from † after a 20 hour treatment and polished.

†† Sections from ** after another 30 hour treatment and polished.

*** Section accidentally damaged by laser beam.

T594

For the study of surface resistance to water vapor corrosion, (isothermal case) there are three vapor pressure regions of interest. Representing P_{H_2O} as the ambient vapor pressure, the regions are defined with respect to the vapor pressure of the saturated solution, $P^{*}_{H_2O}$, and the solvent, $P^{o}_{H_2O}$. The more common situation is where $P_{H_2O} \leq P^{*}_{H_2O}$. The stability in this vapor pressure region was studied with respect to β. It was shown that hygroscopic behavior was negligible in single crystal KCl (Appendix II).

As the ambient vapor pressure, P_{H_2O}, increases, the intermediate region is reached where $P_{H_2O} < P_{H_2O} < P^{o}_{H_2O}$. In this

region, an unstable crystal will not only mar its surface by hygroscopic behavior but can cause water to condense from the atmosphere because $P_{H_2O} > P^{\circ}_{H_2O}$, and, therefore, deliquesce. The extreme region is, of course, the dewpoint region and above (i.e., $P_{H_2O} \geq P^{\circ}_{H_2O}$). Transient residence of the KCl single-crystal surface at this extreme region was studied.

The surfaces were generated by cleaving and subjected to various treatments to assess their effect on corrosion stability. Fleeting residence above the dewpoint was achieved by careful breathing on the surface of the crystal which was observed under a microscope. The breath effects a dense decoration of the surface with microscopic droplets. In a room held at 23°C and 40% relative humidity, the layer evaporates off in ~5 sec. After repeating the cycle a few times, the surface appears unmarred to the unaided eye. Examination was made on a microscopic scale of such a response in KCl after one cycle using surfaces which have been prepared by cleaving (see Fig. 13); cleaving followed by annealing in He at 670°C for 20 hours (see Fig. 14); and cleaving followed by annealing in CCl_4 at 670°C for 20 hours (see Fig. 15). These three photo sequences illustrate that the surface free energy is consistently different for the three methods of preparation and decreases from Fig. 13 to Fig. 15.

Typical cleavage steps are seen in Fig. 13(a). After one breath cycle of condensation and evaporation, Fig. 13(b) shows the irregular outline of the condensate pattern. Etching action by what was once a droplet occurred at a cleavage step. A higher magnification of the central region, Fig. 13(c), reveals square pits as large as 4 μm to the edge, with a hopper pattern extending to a depth of 1 to 2 μm. Such a pit corresponds to the etching out of 10^{-12} mole. Initial volume of the droplet is 10^{-6} cm^3. The volume of the saturated solution is three orders of magnitude smaller if one considers the fast dissolving region (i.e., the etched region) as the main source of solute (total dissolved: 10^{-11} mole). The maximum area of the etched region (10^{-5} cm^2) is

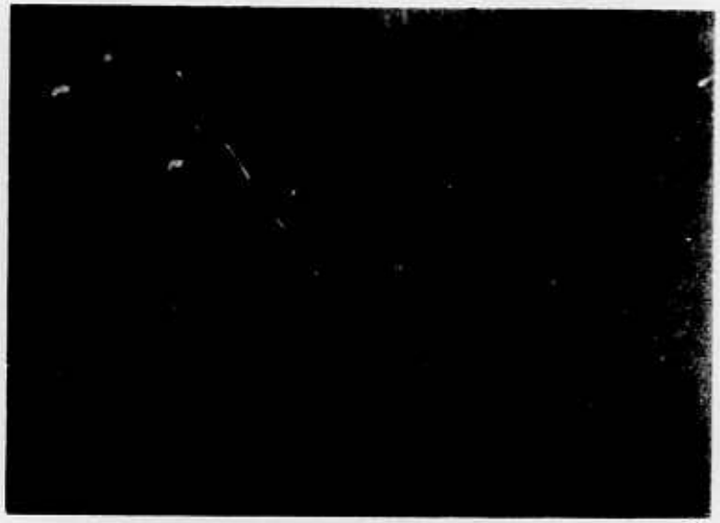

(a) Initial surface (200x) prepared by cleaving at (100). Note cleavage steps

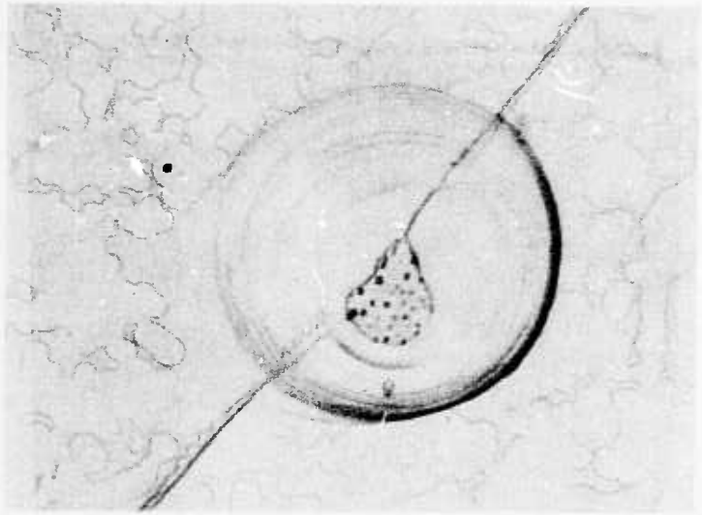

(b) Surface (200x) after completion of cycle, showing the irregular outline of the initial condensate and what was once a droplet

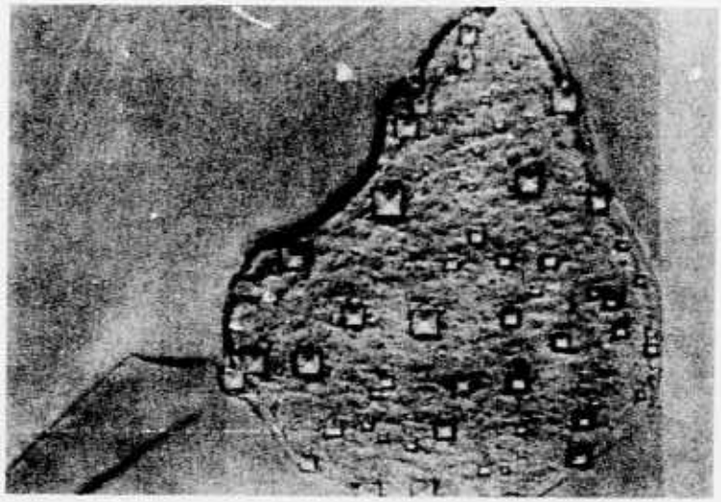

(c)
Etched region within droplet in (b) magnified (1000x) showing square pits with edges parallel to (100) and a hopper-shaped face

Fig. 13. Photo Sequence Showing the Effect of One Breath Cycle Leading to Condensation and Evaporation of a Film of Moisture.

(a) Initial surface (200x) prepared by cleaving at (100) and followed by a heat treatment at 670°C for 20 hours under He. Cleavage steps almost gone and surface is decorated by vapor deposited material.

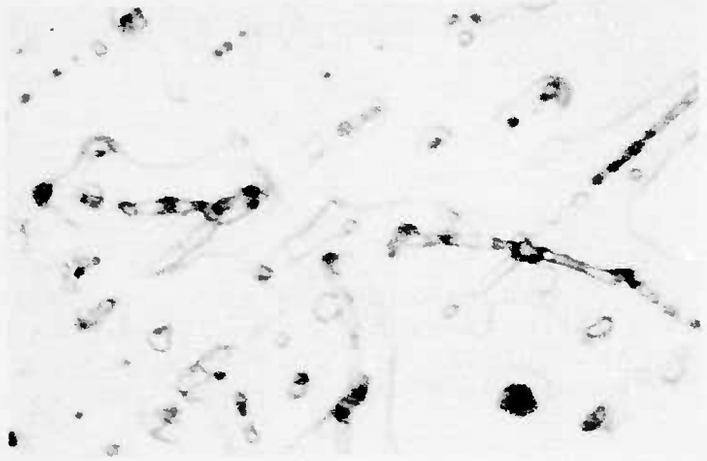

(b) Same region in (a) after the cycle (200x). Irregular outline of the initial condensate can be seen at the expense of the very fine vapor-deposited material. The layer regions, although not completely dissolved, are rounded off.

(c) The center of (b) at 1000x showing no etch pits.

Fig. 14. Photo Sequence Showing the Effect of One Breath Cycle Leading to Condensation and Evaporation of a Film of Moisture.

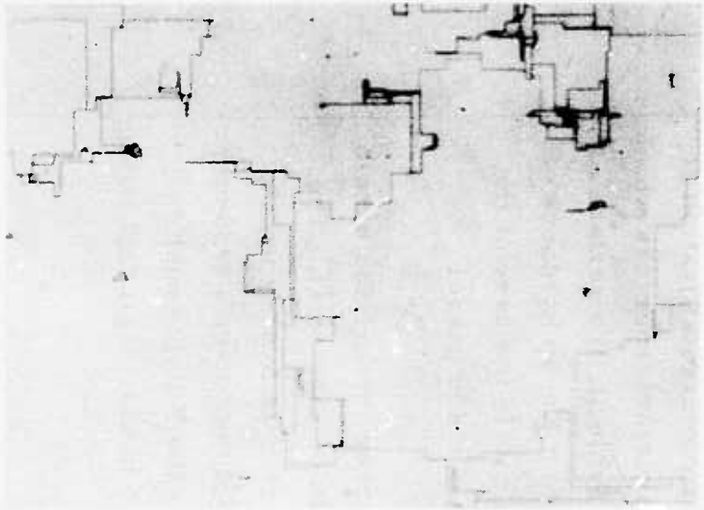

(a) Initial surface (200x) prepared by cleaving at (100) and followed by a heat treatment at 670°C for 20 hours under CCl_4(g). Cleavage steps are gone. Surface shows new steps bounded by (100) and very scanty decoration by vapor deposited material.

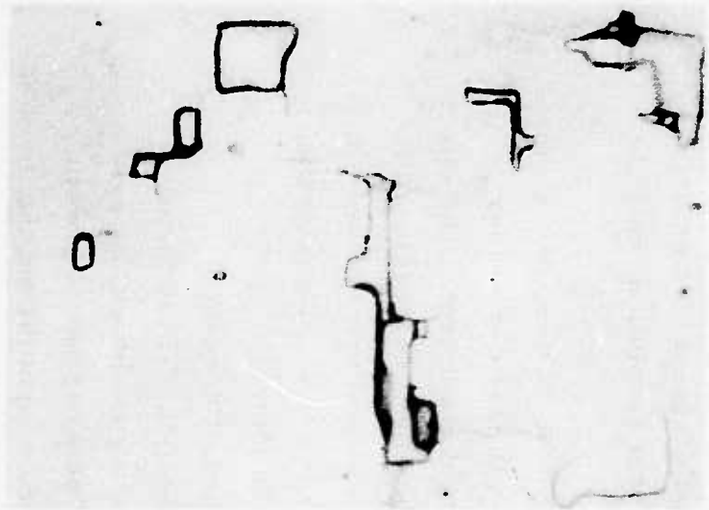

(b) Same region in (a) after the cycle (200x). The irregular outline shown in Figs. 13(b) and 14(b) is not seen, just a rounding off of the edges and corners of the steps in (a).

(c) The center of (b) at 1000x, showing no pits. Except for the rounded off steps, the surface is devoid of structures seen in Figs. 13(c) and 14(c).

Fig. 15. Water Vapor Effects on RAP Annealed KCl Surfaces.

assumed to correspond to the crossover from the undersaturated to the saturated condition. Redeposition of solute would account for an average depth of $\lesssim 10^{-1}$ μm. Hence, under the present resolution, only the effect of etching can be seen.

In Fig. 14(a), the cleavage steps are almost obliterated. Cohering to the substrate are isolated regions of growth that were vapor deposited during the slow cooldown of the thermal treatment. The effect of one breath cycle is shown in Fig. 14(b). The small new regions of growth have been removed (dissolved) and the sharp edges rounded off. The irregular outline of the condensate pattern is seen. Magnification of the central portion, Fig. 14(c), shows no etch pits.

In Fig. 15(a), the cleavage steps are gone, the surface rearranged to give prominent steps bounded by (100). These steps accommodated growth from the vapor phase during cooldown, as evidenced by the low substrate density of isolated new regions of growth. The effect of one breath cycle, Fig. 15(b), merely smooths out the sharp edges; no irregular outline of a condensate pattern is seen. High magnification of the central portion, Fig. 15(c), shows no etch pits.

The interface of small crystals formed by recrystallization at the surface has been shown to be a source of initial microcracks which cause premature failure (Ref. 8). As seen in Table II, the surface conditions of Figs. 13(a) and 14(a) correspond to a Knoop hardness of 10 kg mm^{-2}, while Fig. 15(a) yields 12 kg mm^{-2}. In the case of the modulus of rupture, S = 640 psi for Fig. 13(a), S = 450 psi for Fig. 14(a), and S = 970 psi for Fig. 15(a).

Wetting and evaporation behaviors observed through the breath cycle provide additional evidence of the stability of Fig. 15(a). The free energy per unit area at the solid-gas interface is lower than that at the solid-liquid. The microscopic dewdrops do not have a tendency to spread (i. e., no coalescence). According to the Kelvin equation, these drops are unstable even at 100% humidity; hence, a gradual fading away of the film.

The opposite inequality holds for Figs. 13 and 14. Coalescence of the small droplets leads to larger droplets or irregular contours as suggested by the irregular outlines left. Solvent action and evaporation are mutually governing factors, but both lead to the attainment of droplet saturation. In the fraction of the residence time (~5 sec) that the solution is under-saturated, its etching action depends upon solubility rate which, in turn, depends on the free energy of the locale. In Figs. 13(b) and 13(c), etching action is evident only on the stressed or high free-energy (defect) region. No etch pits are seen in Figs. 14(b) and 14(c), presumably due to the thermal treatment under He which partially relieved the stressed condition brought about by cleaving.

The above experiments indicate that considerable surface stabilization followed from the RAP treatment, perhaps to a stability approaching that of a natural crystal face.

In the last quarter of the study, Polytran specimens were received for surface evaluation. Photographs were taken of an as-received Polytran disc, identified on the Lucite holder as #77. Photomicrographs at 83x and 166x show polishing scratches in the as-received surface. Photomacrographs at 2x show the grain size to be 10 to 40 mm^2. The grains developed readily by exposure at 23°C and 40 percent relative humidity. Photomacrographs taken at 2x between crossed polarizers show a correlation between the grains and the strain pattern of slip lines. This comparison is seen in Fig. 16. Sections were sliced from the disc. A piece was kept for control and another was scrubbed in CCl_4(g) at 670°C for 20 hours. Figure 17(a) shows the control and the scrubbed pieces at 2x magnification. Figure 17(b) is an 83x magnification showing the surface texture across the grains before scrub and Fig. 17(c), also at 83x magnification, is after scrub. In the latter case very prominent (100) surfaces developed in each grain.

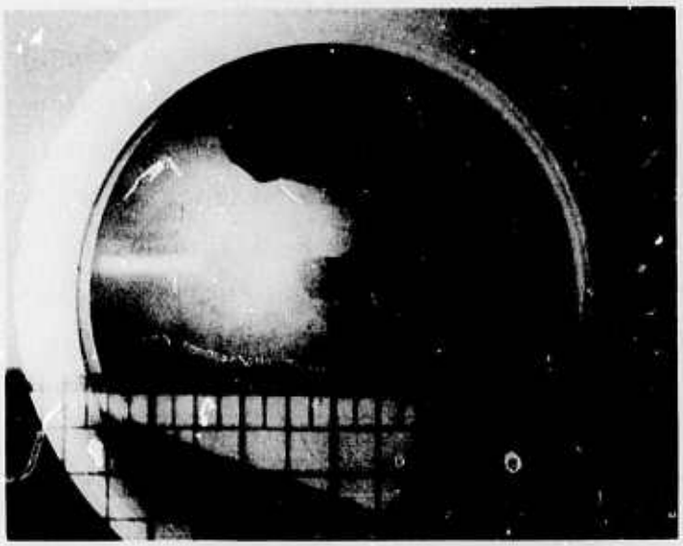

(a) Polytran disk No. 77 as received (2x magnification)

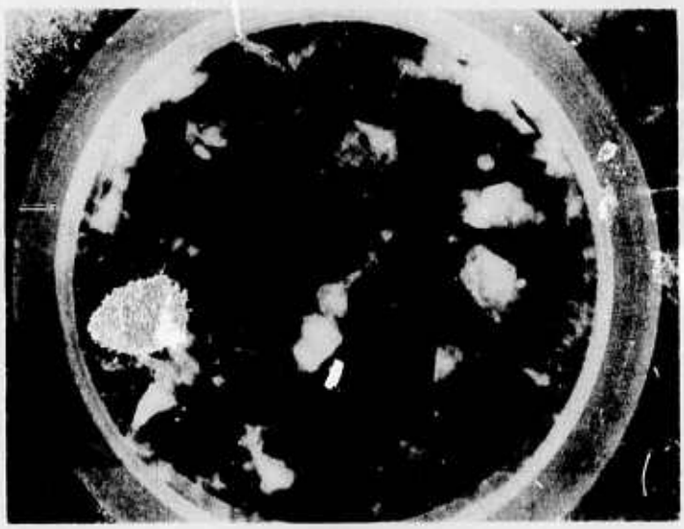

(b) Same as (a) but viewed in polarized light (2x magnification)

Fig. 16. Surface of Polytran Disk No. 77.

(a) Polytran sections (2x magnification)

(b) Control piece
(83x magnification)

(c) Scrubbed piece
(83x magnification)

Fig. 17. Polytran Surface Before and After Scrub.

4. Purification and Analysis

Powdered KCl five-nines pure in the metal ion is easily available. However, the anion purity may not be any better than three-nines pure. Before this study began, we had demonstrated that various anions; e.g., NO_3^-, HCO_3^-, $CO_3^=$, $C_2O_4^=$, etc., of the alkali metals can be converted quantitatively to the chloride by treatment with CCl_4 (Ref. 9, 10). It was also known that the chlorides of many heavy metals are quite volatile. It was, therefore, possible that CCl_4 vapor could be used to effect simultaneous cation and anion purifications of molten KCl.

With purification as the objective, the casting and zone refining of KCl ingots under RAP, He + CCl_4, was developed as shown in Fig. 18. The analyses of the starting powder and the RAP treated specimens are shown in Table IV. Emission spectrograph analysis turned out to be inadequate to differentiate between the two powders, MCB (99.9%) and JM (99.999%). The method was also unable to distinguish the purity level of the MCB powder from the various sections of the zone refined ingot derived from it.* However, beyond a doubt, the volatilized material, or scrub deposit (sixth column, Table IV), showed that various impurities had been transported through the vapor phase.

The study was complicated by the fact that the boat (vitreous carbon) used in zone refining was a source of impurities. Table V shows that under CCl_4 vapor, Ca and Mg, unlike Si and Cu, have a high escaping tendency (fugacity) from the vitreous carbon matrix. The fugacity across the solid-vapor interface is a measure of leachability by the halide melt. While Poco graphite is more suitable in purity, it is inapplicable because it is fairly permeable to the melt.

---

*Zone refining conditions: The molten zone was ~2 in. wide and was moved at the rate of 5 in./hr. Three unidirectional passes were taken.

(a) Scrub-cast ingot, 3 x 14 cm

(b) Scrub-zone refining

Fig. 18. Alkali Metal Chloride (KCl) Technology.

TABLE IV

Emission Spectrograph Analysis of KCl Powders and Crystal Specimens

Impurities	Zone Refined Ingot			MCB Powder	Scrub Deposit	JM Powder
	Nose	Center	Tail			
K	52%	52%	52%	52%	50%	52%
Si	TR < 0.002	ND < 0.002	0.0031	ND < 0.002	1.5	ND < 0.002
Ca	0.0013	0.0012	0.011	0.0012	0.040	0.00045
Fe	ND < 0.001	ND < 0.001	ND < 0.001	ND < 0.001	0.15	ND < 0.001
B	ND < 0.004	ND < 0.004	ND < 0.004	ND < 0.004	0.019	ND < 0.004
Mg	0.00014	0.00010	0.0017	0.00032	0.0039	0.000085
Pb	ND < 0.005	ND < 0.005	ND < 0.005	ND < 0.005	0.026	ND < 0.005
Cr	ND < 0.0001	ND < 0.0001	0.00019	ND < 0.0001	0.017	ND < 0.0001
Bi	ND < 0.001	ND < 0.001	ND < 0.001	ND < 0.001	0.0067	ND < 0.001
Al	ND < 0.0004	ND < 0.0004	ND < 0.0004	ND < 0.0004	0.015	ND < 0.0004
Cu	ND < 0.00005	ND < 0.00005	0.000074	ND < 0.00005	0.0024	ND < 0.00005
Li	ND < 0.001	ND < 0.001	ND < 0.001	ND < 0.001	0.0031	ND < 0.001
Ag	ND < 0.00007	ND < 0.00007	ND < 0.00007	ND < 0.00007	TR < 0.00007	ND < 0.00007
Na	ND < 0.005	TR < 0.005	0.015	TR < 0.005	0.057	ND < 0.005
Ti	ND < 0.001	ND < 0.001	ND < 0.001	ND < 0.001	0.0019	ND < 0.001
Ni	ND < 0.0005	ND < 0.0005	ND < 0.0005	ND < 0.0005	0.0015	ND < 0.0005

T390

TABLE V

Impurity Content of Vitreous Carbon and Poco Graphite

Impurity	Vitreous Carbon		Poco Graphite	
	As Received	After Scrub*	As Received	After ZR**
	%		%	
Ca	0.0026	0.0016	TR<0.0002	0.00065
Mg	0.00086	ND<0.0003	0.0023	0.00060
Si	0.0048	0.0041	ND<0.001	0.060
Cu	0.00026	0.00032	0.00021	0.00075
Other Elements	Nil	Nil	Nil	Nil

* Exposed to CCl_4 vapor at 700°C for 21 hours.

** Exposed to three zone refining passes on molten KCl (~800°C under CCl_4 vapor) for 21 hours.

T593

Impurity cleanup in molten KCl under CCl_4 was demonstrated directly by employing concentration levels of the impurities above the sensitivity limits of the emission spectrograph. The results are shown in Table VI. The vapor pressure of molten KCl is ~1 mm. An approximate measure of the order of the relative fugacity of the dopants is the temperature of the pure form at its vapor pressure of 1 mm: $FeCl_3$, 194°C; $PbCl_2$, 547°C; $NiCl_2$, 671°C; and $MgCl_2$, 778°C. To correlate the order to the relative cleanup achieved in molten KCl, the evaporation flux of the solvent needs to be determined.

TABLE VI

Impurity Cleanup in Molten KCl Under CCl_4

Impurity	Exposure Time of Melt to CCl_4		
	0 Hour*	5 Hours	20 Hours
	Weight Percentage		
Mg	0.0050	0.0016	0.0014
Pb	0.22	0.039	0.041
Ni	0.032	0.020	0.035
Fe	0.023	0.0010	ND < 0.001

*Averaged over the ingot obtained from melting under He and freezing the melt rapidly.

T592

Consider first that, for a given impurity, a conservation relation holds,

$$\frac{\bar{x}_f}{x_i} = \frac{\left(1 - \frac{x_s}{x_i} \cdot \frac{m}{M}\right)}{\left(1 - \frac{m}{M}\right)} \qquad (1)$$

where x_i is the initial concentration in the melt (weight M), x_s is the concentration in the sublimate (weight m), and $\bar{x}_f$ is the final concentration averaged over the residue (weight M-m). In terms of measurable parameters,

$$\frac{m}{M} = ft\,\sigma \qquad (2)$$

where f is the evaporation flux (g cm^{-2} hr^{-1}) at constant temperature ($T \geq T_{mp}$), t is the soak duration (hr), and σ is the specific evaporation surface of the melt (cm^2 g^{-1}). For the process to be practical, the first constraint is

$$\frac{m}{M} << 1 \tag{3}$$

i.e., the evaporation loss of the host material should be low.

Two runs were carried out with KCl in a quartz boat held at 840°C, at a gas (He + CCl_4) flow rate of 2.5×10^3 cm^3 hr^{-1} and a mole ratio of He:CCl_4 = 7. The results are as follows (a = evaporation surface):

Run 1: M = 7.36 g, a = 10.3 cm^2, t = 5.0 hr, m = 0.169 g

Run 2: M = 7.72 g, a = 11.2 cm^2, t = 20.0 hr, m = 0.560 g

The value of m was obtained by the difference in weight before and after soak. The average of the two runs yields $\sigma = 1.43 \pm 0.04$ cm^2 g^{-1} and $f = (2.9 \pm 0.6) \times 10^{-3}$ g cm^{-2} hr^{-1}. For these values of f and σ, an overnight scrub (t = 15 hr) is a practical processing time because m/M = 0.062 according to eq. (2), which meets the constraint shown in inequality (3).

The second constraint is seen in eq. (1) in terms of x_s/x_i, the relative volatility factor.* Impurities with

$$\frac{x_s}{x_i} \geq \frac{M}{m} \tag{4}$$

*In ideal-solution behavior where the host (solvent) follows Raoult's law, $P_1 = (1 - x_i) P_1^o$, and consequently, the impurity (solute) obeys Henry's law, $P_2 = x_i P_2^o$. It can be shown that $x_s/x_i \sim P_2^o/P_1^o$ when $(x_i, x_s) << 1$.

would have been stripped out of the melt at $t < 15$ hr. Only those with

$$\frac{x_s}{x_i} < \frac{M}{m} \tag{5}$$

would still be detectable in the residue (i.e., x_f measurable). For the given case, $M/m = 16$. A relative volatility factor of 10 would strip out only 60% of the impurity (i.e., $\bar{x}_f/x_i = 0.40$).

For the impurity cleanup work reported in Table VI, $\sigma = 0.5\ cm^2\ g^{-1}$. From the value of f, it follows that $m/M = 0.0073$, satisfying constraint (1). Using the 5 and 0 hour values to calculate $\bar{x}_f/x_i$, where x_f is the final concentration averaged over the residue, the $x_s m/x_i M$ value for each impurity in decreasing order of volatility from the melt is as follows: Fe^{3+}, 1.0; Pb^{2+}, 0.8; Mg^{2+}, 0.7; and Ni^{2+}, 0.4. The actual volatility order shows that $NiCl_2$ has a relatively low fugacity in the melt (KCl).

In the zone refining experiment whose analysis is reported in Table IV, $M = 450$ g and $a = 170\ cm^2$; therefore, $\sigma = 0.38\ cm^2\ g^{-1}$. The molten zone had a residence time of 0.4 hr. With three passes, $t = 1.2$ hr. It follows from eq. (2) that $M/m = 760$. It is seen that Si has $x_s/x_i > 750$ and satisfies eq. (4); i.e., $(x_s/x_i) \cdot (m/M) \gtrsim 1$. To this class belongs the volatile chlorides of B, Al, Fe, Cr, Bi and Ti. The latter group, taken collectively, is characterized by $x_s/x_i > 200$. The others belong to the class characterized by eq. (5), i.e., $(x_s/x_i) \cdot (m/M) < 1$. Because of leaching of the vitreous carbon boat (Table V), Ca, Mg and Cu account for $x_s/x_i = 30$, while the rest amount to $x_s/x_i > 8$. Using the impurity-class content of the original powder as the weighting factor, the average for three zone passes under RAP is $x_s/x_i > 100$. The purification effected is even better if we include the effect of segregation in the condensed phase. The results of these calculations lead us to believe that RAP purification is capable of converting KCl from 99.9% to 99.999% purity in both metal ion and anion species.

Our initial emphasis was on the development of a procedure for purification; it was convenient to begin the study by eliminating OH^- as completely as possible and comparing the resulting physical properties of ordinary material containing an unknown quantity of OH^-. Of course, the most convincing evidence that $OH^-(s)$ is the culprit would be a determination of the physical properties as functions of directly measured $[OH^-(s)]$.* In keeping with this objective, the last quarter was spent comparing analytical methods, destructive and nondestructive for the quantitative determination of $[OH^-(s)]$ in KCl crystals — acidimetry appears to be the most reliable.

As pointed out in Appendix I, one needs to attain $P_{H_2O}/P_{HCl} \leq 10^{-7}$ in RAP to suppress hydrolysis. At the melting point, the equilibrium constant of hydrolysis may be as large as 10^2. Consequently, $C \leq 10^{-5}$ is the requirement on the sensitivity of applicable analytical methods.

In the nondestructive category, there are two direct spectrophotometric methods,[11] one indirect method based on color center formation,[12] and a method based on the measurement of ionic conductivity.[12,13] The latter two have been utilized most extensively as analytical methods to assess general purity of the crystal.

In the conductivity method, the plot of the logarithm of conductivity against reciprocal temperature yields a knee temperature which divides the region into two modes of conduction, the extrinsic and intrinsic (high-temperature region). The position of the knee temperature is sensitive to both $[OH^-(s)]$ and total heterovalent cation impurities.[13] The inapplicability of the method for determining $[OH^-(s)]$ lies directly in this feature of nonspecificity.

The potential usefulness of the method based on color center formation is demonstrated in the observation that X-irradiation decreases the uv absorption of $OH^-(s)$ as well as the IR absorption of the free substitutional $OH^-(s)$ and the narrow line spectrum of the

*The use of (s) in $OH^-(s)$ specifies the phase, i.e., solid, and the bracket refers to the concentration.

complexes (Ref. 6). Further, it has been shown that the F band produced in NaCl and KCl by ionizing radiation is proportional to the initial $OH^-(s)$ absorption band.[7] However, such colorability is also dependent on background impurities; e.g., great enhancement by Ca^{2+} or Sr^{2+} (Ref. 12). In the case of the impurity Pb^{2+} in KCl crystal, enhancement is observed in early-stage coloration (gamma irradiation) and the reverse in the late-stage; i.e., a dependence on the energy absorbed by the crystal from the gamma-ray field. For the direct determination of $[OH^-(s)]$, the drawbacks of the method are obvious.

The two useful regions of the spectrum are: The IR region at 2.75 μm for the O-H vibration and the uv region for its electronic excitation, 0.185 μm for NaCl and 0.205 μm for KCl. The absorption cross-sections are: $\sigma(NaCl) \leq 3.4 \times 10^{-21}$ cm^2 and $\sigma(KCl) = 2.8 \times 10^{-20}$ cm^2 for the IR; $\sigma(NaCl) = 4.0 \times 10^{-17}$ cm^2 and $\sigma(KCl) = 2.5 \times 10^{-17}$ cm^2 for the uv.[14] In the case of KCl, it follows that $C_{min} \sim 10^{-5}$ for the IR and $\sim 10^{-8}$ for the uv.* These limits may be pushed one more order of magnitude lower by improved sensitivity in detection (D_{min}) and the use of thicker samples (L). Therefore, these two methods are capable of providing enough sensitivity.

However, results are reported in the literature which show the difficulty of rendering these methods quantitative for $[OH^-(s)]$ at $C \leq 10^{-5}$ because of a nonspecificity resulting from the presence of heterovalent cation impurities. The experiments with KCl have shown two classes of $OH^-(s)$ in alkali halide lattices (Ref. 4). With certain bivalent impurities present in the crystal, $OH^-(s)$ reacts with the impurity metal ions to form $OH^-(s)$-impurity complexes. Not until all of the appropriate complexes have been formed will $OH^-(s)$ incorporate

*It is shown in Appendix III that for a sample thickness of L = 1 cm and a minimum optical density of $D_{min} = 10^{-2}$, the minimum mole fraction of $OH^-(s)$ is $C_{min} = 4.48 \times 10^{-25}/\sigma$ for NaCl and $6.24 \times 10^{-25}/\sigma$ for KCl.

into the lattice as the free substitutional ion. From 2.6 to 2.9 μm, a sharp line spectrum is produced by the impurity complexes and a broad line from free substitutional $OH^-(s)$. These features have also been shown in LiF crystal containing the impurities Mg^{2+} and OH^- (Ref. 5) and also in OH^- doped NaF crystal (Ref. 6). For these reasons, we require more than one σ value in the IR region (Ref. 14) for total $OH^-(s)$ at $C \leq 10^{-5}$ when the total mole fraction of heterovalent impurities is $\sim 10^{-5}$.

In the case of uv absorption of $OH^-(s)$, it is found that SiO_2 in the molten halide and Ca^{2+} or Sr^{2+} in the crystal remove the absorption at 0.185 μm in NaCl and 0.204 μm in KCl (Ref. 11). Hence, the method, like the IR method, suffers similar drawbacks for quantitative application at $C \leq 10^{-5}$.

In summary, the results in the literature indicate that the above nondestructive analytical methods cannot be relied upon for the quantitative determination of $OH^-(s)$ at $C \leq 10^{-5}$ due to interactions with heterovalent impurities.

We do not know whether the impurity-concentration inequalities were satisfied in determining the σ values in the IR and uv (Ref. 14). We assume that they were determined at $[OH^-(s)]$ much larger than the total concentration of interfering impurity ions. However, these σ values cannot be applied at $C \leq 10^{-5}$ unless the total mole fraction of interfering ions is $<< 10^{-5}$, which is not generally the case.

The next question which must be raised concerns the primary method, i.e., the procedure used to establish $[OH^-(s)]$ independently for the calculation of σ from the optical density measured at the given peak wavelength of the absorption band. This issue was not taken up in sufficient detail in reference 14. The issue needs to be resolved as the σ values are used by various workers to calculate $[OH^-(s)]$. For instance, an $[OH^-(s)] < 10^{-8}$ in KCl, using the absorption at 0.204 μm, has been reported.[12] A study of reference 12 indicates possible contradictions because, assuming that σ is correct, the value of $[OH^-(s)]$ is meaningful only if it can be shown that the total mole fraction of

interfering impurities is $<< 10^{-8}$, a limit beyond the present analytical methods in use. In the case of Group IIA, alkaline-earth impurities, the detection limit for Ca^{2+} corresponds to a mole fraction of $\sim 10^{-6}$; with Group IIB, for Zn^{2+} or Cd^{2+}, $\sim 10^{-8}$; with 3d transition ions, say Fe^{2+}, $\sim 10^{-7}$; etc., (refer to Table I, Ref. 12).

The popular resort of employing the initial value of OH^- doping of the melt in place of a primary method of determining $[OH^-(s)]$ is unsatisfactory. Usually, the concentration range employed in the doping is between 10^{-3} and 10^{-4} mole fraction. The practice assumes that the melt-crystal interface has a distribution coefficient close to unity and that there are no other sinks for OH^- in the melt-vapor and melt-crucible interfaces – the assumptions are open to question. Comparing the vapor pressures over the bulk material, say at the melting point of KCl, it is easily shown that KOH is about an order of magnitude more volatile. At the given doping range, the melt is very reactive. Platinum, carbon, and silica crucibles are subject to chemical attack.* Indeed, these corrosion reactions serve as qualitative indicators for the melt concentration of OH^-; the transition from wetting to nonwetting being observed at $< 10^{-5}$.

The failure of nondestructive methods to yield a reliable and practical procedure to measure $[OH^-(s)]$ led to a feasibility study of converting a primary method (acidimetry) into a practical procedure; i. e., capable of operating at $C \leq 10^{-5}$. Unfortunately, this meant the use of a destructive method, acidimetry.

Two solution methods are available: pH measurement and absorption spectrophotometry in solution based on the acid-base equilibrium of a dye (indicator). In terms of sensitivity, it is shown in Appendix IV that a pH-shift measurement precision of ±0.01 is satisfactory for the measurement of C down to 10^{-7}. It is also shown

*In reference 9, the authors employed mullite (alumina-silica) crucibles which are known to be corroded by molten alkali hydroxides.

(refer to Appendix IV) that operating parameters in acid-base dye colorimetry can yield an absorbance-shift measurement with a precision matching the requirements for pH-shift to measure C down to 10^{-7}. Hence, both methods are sensitive enough, and should be applicable to the range, $10^{-7} \leq C \leq 10^{-5}$.

An earlier study, on the alkalinity of NaCl crystals, was carried out by D. Otterson using p-nitrophenol (p-NP) as the dye indicator (Ref. 6). He measured the change in absorbance at 0.415 μm of the dye at a concentration, $c = 1.5 \times 10^{-3}$ M (M = molar), and electrolyte (NaCl) concentration of 0.3 M. A calibration curve was given for the change of absorbance in terms of NaOH added to the dye solution and a correction curve for the dependence of absorbance on salt concentration, i.e., ionic strength.

Our spectrophotometric characterization of p-NP solution* gave very different results, indicating the necessity of modifying the procedure. Using pH buffered solutions, our measurements which are seen in Fig. 19 show two absorption bands which peak at $\lambda_1 = 0.319$ μm and $\lambda_2 = 0.402$ μm. The λ_2-band grows at the expense of the λ_1-band with increasing pH, showing an isosbestic at 0.348 μm.** At $[H^+] = K$ (or pH = pK), where K is the ionization constant of the dye, equal amounts of the absorbing species exist. Then, the ratio of the absorption peaks equals that of the extinction coefficients. We have determined the values of the extinction coefficients and as seen below the ratio is 1.94. Consequently, from pK = pH, Fig. 19 predicts pK = 7.2 in agreement with the literature.

---

*The powder p-NP was the indicator grade of Eastman.

**At the isosbestic wavelength, the absorbance is constant and independent of the concentration displacement of equilibrium between the two absorbing species.

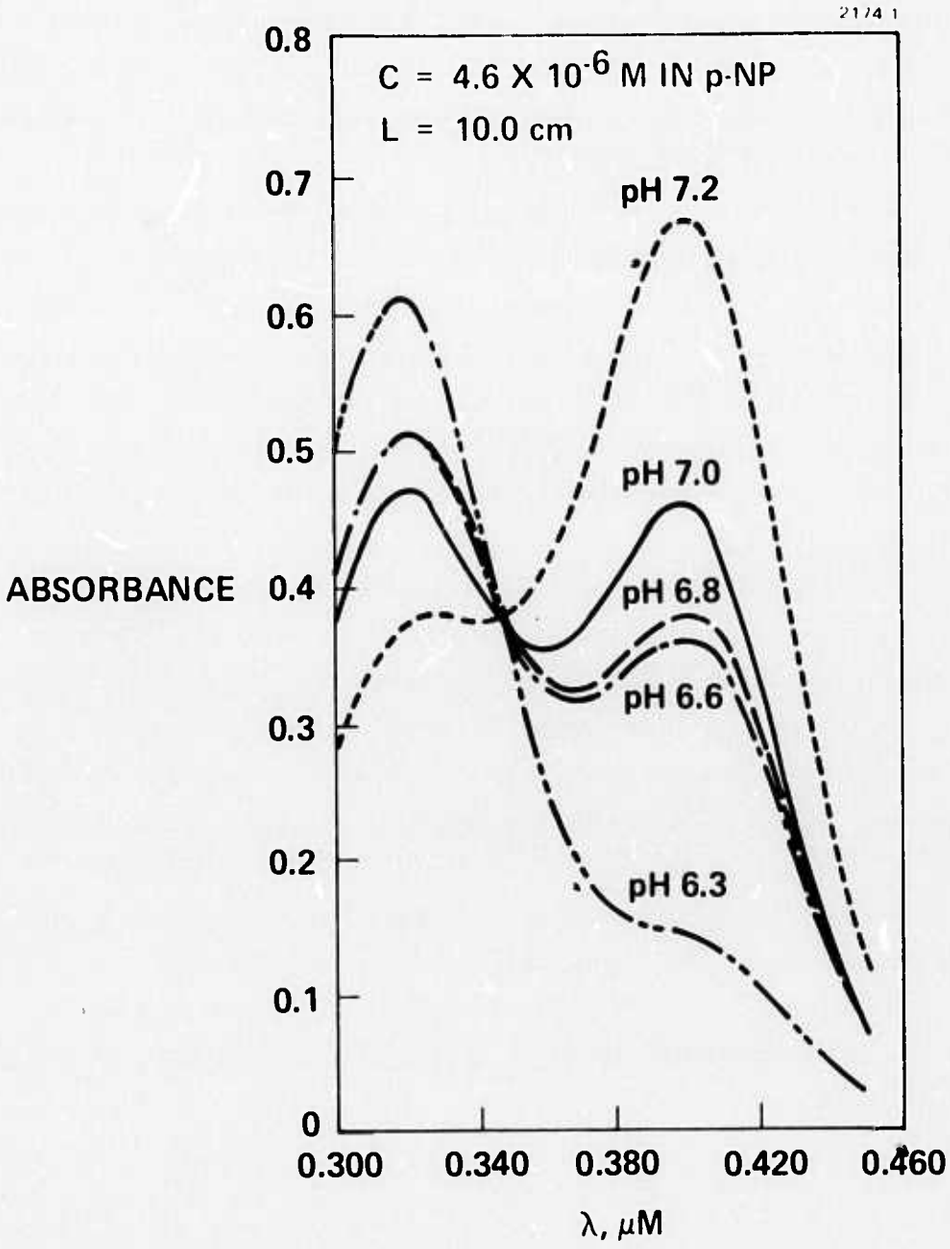

Fig. 19. Optical Absorption of p-Nitrophenol Dye in Buffered Aqueous Solutions. Note the Isosbestic at 0.348 μm.

In the ionization of the dye,

$$HI \rightleftharpoons H^+ + I^- \quad , \tag{6}$$

the HI species gives rise to the λ_1-band and I^- to the λ_2-band. From a pK = 7.1, the value for zero ionic strength,[15] we can show that Otterson's choice of operating parameters is far from optimum. It follows from eq. (6) that the degree of dissociation is $\alpha \approx (K/c)^{1/2}$ and from $K = 10^{-7.1}$ and $c = 1.5 \times 10^{-3}$ M, the dissociation corresponds to $\alpha = 0.0073$. As shown in Appendix IV, the optimum operating point is $\alpha = 1/2$. Note also that $[H^+] \approx \sqrt{Kc}$ corresponds to the indicator solution having pH = 5.0. Figure 19 shows there will be very small absorption at $\lambda_2 = 0.402$ μm. A further loss in sensitivity is exacted by choosing to measure the absorbance at 0.415 μm.

In working with p-NP, we first carried out Beer's law measurements (refer to eq. (11), Appendix IV). The concentration range of p-NP solutions was 2.32×10^{-6} M ≤ c ≤ 1.86×10^{-5} M. The optical cell had L = 10.0 cm. The cell was filled and capped with solutions mixed in 50.0 cm^3 volumetric flasks. With the solution 1.00 M in KCl and 0.010 M in HCl, there was essentially no absorption at the λ_2-band and $\epsilon_1 = 0.98 \times 10^4$ M^{-1} cm^{-1}. Similarly, using 1.00 M in KCl and 0.010 M in KOH, $\epsilon_2 = 1.92 \times 10^4$ M^{-1} cm^{-1}.

For comparing the alkalinity of KCl crystals, interaction with the atmospheric constituents (especially CO_2) had to be avoided. Unfortunately, cells with L = 1.00 cm were the only ones available at the time which could be used for vacuum processing.* The stock of water employed for all these measurements was deionized water distilled twice in vacuum over $KMnO_4$. A constant amount of p-NP was introduced into the cell, using a CH_3OH-solution. The solvent was evaporated. Then a weighed amount of KCl crystal was introduced into

*A thicker cell would have been preferable as this allows lower values of c.

the cell. Grinding the crystal was avoided as this operation has been reported to increase the alkalinity.[16] The cell was provided with a stopcock which allowed evacuation to $\sim 10^{-5}$-mm Hg, after which water is distilled up to a fiducial mark in the cell. The stopcock was then closed, the contents shaken for thorough mixing, and the spectra recorded with a Cary double-beam spectrophotometer. Water in a matched cell was used as the reference. The weight of the solution was obtained and this yielded the concentrations of p-NP and KCl with a reproducibility to within ±5%.

According to the mass-action expression for eq. (6), the measurement of the concentration ratio, $[H\mathscr{I}]/[\mathscr{I}^-]$, yields $[H^+]/K$. The latter quantity can be obtained from the measurement of the absorbancies in λ_1 and λ_2. If only one band is available, the value $[H^+]/K$ can still be calculated because of the conservation relation, $[H\mathscr{I}] + [\mathscr{I}^-] = c$. Representing the absorbance by y,

$$\frac{[H^+]}{K} = \frac{\epsilon_2}{\epsilon_1} \cdot \frac{y_1}{y_2} \text{ , (refer to eq. (14), Appendix IV)} \qquad (7)$$

for the two-band method, and

$$\frac{[H^+]}{K} = \frac{\epsilon_2 Lc}{y_2} - 1 \text{ , (refer to eq. (15), Appendix IV)} \qquad (8)$$

or, a similar expression making use of the λ_1-band.

Our first attempt to compare Harshaw KCl with RAP-grown KCl was based on 1.00 M KCl and $c = 8.3 \times 10^{-5}$ M in p-NP. Because of the high concentration of KCl, the one-band method at λ_1, was used. Two measurements with Harshaw KCl crystal gave,

$$\frac{[H^+]}{K} = 15.2 \pm 0.3 \text{ ,}$$

and one measurement on IIRL B-29 KCl crystal yielded,

$$\frac{[H^+]}{K} = 18.5 \ .$$

All we can say at this point is that IIRL B 29 is 3.3 K units more acidic.* At the concentration of KCl employed, only one absorption band dominated (λ_1-band); hence, K could not be determined.

The two-band method was employed using more dilute KCl solutions. The p-NP concentration was $c = 12.0 \times 10^{-5}$M. With no KCl, $[H^+]/K = 18.29$. From $[H^+]/K = (1-\alpha)/\alpha$, it follows that $\alpha = 0.052$ and $[H^+] = \alpha c = 6.2 \times 10^{-6}$; therefore, pH = 5.21 and pK = 6.47. The value of pK is unexpected; however, it was reproducible in the vacuum set up. The value of pK = 7.2 as suggested in Fig. 19, and which agrees with the literature is obtained in buffered solutions. Thus, for vacuum-prepared solutions, we adopted pK = 6.47 for dilute KCl, say 0.02 M.

The two-band method for 0.020 M of Harshaw KCl yielded $[H^+]/K = 22.87$. From pK = 6.47, pH = 5.11. Similarly, for 0.022 M of RAP-KCl (HRL, C-4), $[H^+]/K = 36.05$, or pH = 4.91.** If we let $[H^+]_o$ represent the case of C = 0, mole fraction of OH^- in the crystal, it follows that,

$$7.78 \times 10^{-6} = [H^+]_o - 0.020 \, C_H$$

$$12.26 \times 10^{-6} = [H^+]_o - 0.022 \, C_R$$

---

* This is also C for $[OH^-(s)]$ since the solution is 1.00 M in KCl.

** The low values in pH will be discussed later.

where C_H and C_R are the mole fraction of OH^-(s) in the Harshaw and RAP specimens, respectively. These two relations yield,

$$C_H - 1.1\, C_R = 2.24 \times 10^{-4} \quad .$$

We believe that RAP growth can easily achieve a $C_R < 10^{-5}$; therefore,

$$C_H = 2.2 \times 10^{-4} \quad .$$

At the end of the contract we realized that there were still problems remaining. How would one define $[H^+]_o$ as a basis to calculate C? Is the low value of C_R due to RAP constituents dissolved in the crystal? Obviously, the method needs to be optimized; e. g., choice of the dye.

The low pH values seen in this work surprised us as we expected solutions of KCl (or NaCl) to be close to pH = 7. This was not the case. Our pH meter, calibrated against standard buffered solutions, registered a pH of 5. 8 to 5. 6 for 0. 3 M KCl (or NaCl), independent of the source of reagent powders examined. The water employed to make the solutions was deionized; when boiled and cooled under N_2 it measured to pH = 7. 0.

5. Other Preparative Approaches

a. Hot Pressing

Hot pressing produces a uniform size distribution of fine grain material and, therefore, better uniformity in mechanical behavior. Further gain in mechanical strength results from the use of mixed halides. The object of the study was to establish the feasibility of applying the technology to mixed halides for high-power laser windows.

The anticipation of technological problems in hot-pressing determined that the study of a one-component system should precede that of the mixed halides. Potassium chloride was adopted as the working material with (99.9%) powder as the source. Pressing was carried out with an 0.5-in. diameter double-action tungsten-carbide die under Ar.

Purity control was not considered initially. The temperature-pressure-time dependence of compaction under Ar, expressed as percent density, %d, of the crystal was established at 25°C. It was found that %d does not vary for dwell times exceeding 15 min. Figure 20 shows KCl powder at 25°C in the pressure range of 7.5×10^3 to 3.5×10^4 psi, under a 15-min interval, compacts to a %d which ranges from 89.0 to 99.6.

For the purpose of suppressing hydrolysis, a brief study of the tradeoff between temperature and pressure was made. At 10^4 psi, %d = 94.0 at 25°C (refer to Fig. 20) while at the same pressure at 200°C, %d = 99.2. To obtain a %d = 99.2 at 25°C, a pressure of 2.7×10^4 psi is necessary (refer to Fig. 20). With this tradeoff, pressing at ambient temperature is feasible, which is an important feature for the suppression of hydrolysis.

Hydrolysis is favored by an increase in temperature of the material. The equilibrium constant for the ionization of water (K_w), which process yields OH^- (and H^+), increases 100% for every 13°C rise in temperature. Thus, the factor of three increases in pressure at constant %d avoided a 10^2 increase in the concentration of OH^-. This follows from, $[OH^-] = K_w^{1/2}$, in the ionization of water. The increase

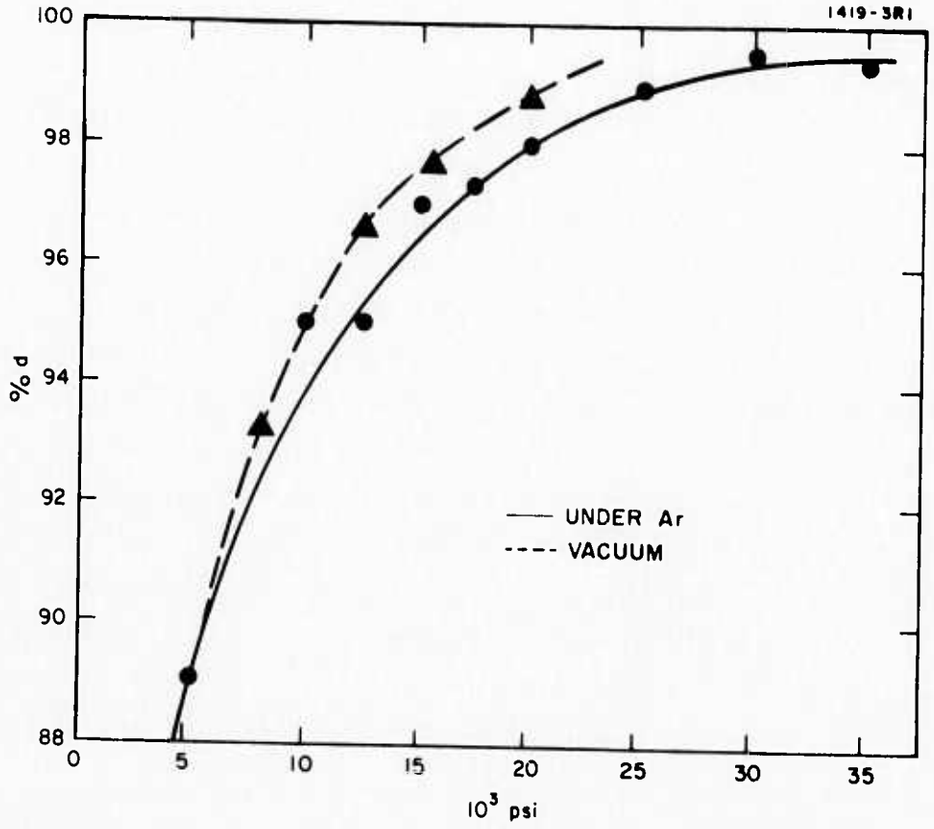

Fig. 20. Dependence of Percent Density of KCl Disc on Pressure at 25°C (Pressing Time = 15 min).

in K_w from 25 to 200°C is, $2^{175/13}$; therefore, for $[OH^-]$, the increase is $10^{0.30(175/26)}$, or 10^2. Also, the same increase in $[H^+]$, in the presence of Cl^-, favors the formation of HCl, a gas. Hence, the Le Chatelier effect operates to favor further hydrolysis.

When KCl powder was pressed under Ar at 25°C, fogging of the disc was observed. The phenomenon appeared different from that commonly observed in the fogging of pressed KBr. In the latter case, fogging is rapid, (within an hour or so) and is observed to be a surface-layer process with minute cracks developing and propagating. In the present case, it took about a day for the same degree of fogging (visual rating) to develop. This observation led to the hypothesis that the pieces were metastable solutions of a gas (Ar) in the solid (KCl) with slow kinetics of exsolution.

The thin samples which were pressed under Ar at 25°C and 5.0×10^4 psi for long periods of time, achieved %d = 100. The pieces were clear and gave an excellent transmission under the infrared microscope (1.06 μm). One such disc, weighing 0.38 g and with a thickness of L = 0.15 cm, gave $\beta = 0.058\ cm^{-1}$ and $\beta = 0.057\ cm^{-1}$ at two different beam locations (≤2 mm apart). While these observations make a good case for homogeneity, it should be pointed out that the source powder employed is capable of achieving $\beta \leq 0.0005\ cm^{-1}$ in the single crystal form grown by RAP. The above specimens eventually fogged under storage. No control or exclusion of water vapor from the air was exercised.

In line with the hypothesis of gas, fogging should not occur in the disc obtained by pressing in vacuum. Hence, a 1-in. diameter vacuum-pressing die was designed and fabricated. Subjecting the same material to a 15 min evacuation, a curve of %d against pressure at 25°C and a dwell time of 15 min was established. The resulting compaction was significantly better than that carried out under Ar (refer to Fig. 20).

Using the same source powder, the discs from vacuum pressing were found to be already fogged as they came out of the die. Obviously, this was not the gas exsolution behavior observed earlier but a bulk

precipitation phenomenon. With a ≤ 0.1-mm Hg pressure maintained during pressing, it seemed unlikely that precipitation was caused by anions formed from atmospheric constituents but rather absorbed or incorporated constituents, as in hydrolysis (OH^-). It had been shown previously that the extent of hydrolysis increased with the specific surface of the material.[Ref. 16] Also, such fogging may have been present but not appreciated in the pressing under Ar because the pieces were a factor of four thinner. On the other hand, Ar may be acting or reacting in some manner which is yet to be understood. To check out the effect of hydrolysis, a comparison of the unscrubbed and scrubbed powder in vacuum pressing was pursued.

Thus far, hydrolysis has served as a heuristic model which has worked out consistently as a guide to material processing approaches. Consequently, the use of scrubbed powder (Section II. A. 2) was preferred over a further study of pressing under Ar.

Vacuum pressing of the unscrubbed powder ranged from 25 to 150°C, 7.85×10^3 to 7.64×10^4 psi, and 5 to 90 min in dwell time. These were 1-in. diameter discs. In all cases, the disc was already fogged as it came out of the die. This was not the case for the scrubbed powder. Figure 21 shows a comparison of the transparency between the unscrubbed (L = 0.621 cm) and the scrubbed (L = 0.626 cm), at 150°C, 7.64×10^4 psi and 60 min dwell time.

Three determinations of the ultimate strength (rupture) for each, yielded 1780 ± 200 (3) psi for the unscrubbed and 2560 ± 310 (3) psi for the scrubbed. Whereas the microhardness (Knoop) of the unscrubbed, 10 kg mm^{-2}, was just about the value for the single crystal, the scrubbed specimen gave 18 kg mm^{-2}, which value approximated that of the press-forged material.*

---

* Our measurement of microhardness on press-forged KCl crystal grown by an earlier RAP procedure was 19 kg mm^{-2}. (Procedure has been optimized since then.) This was a specimen provided by R. W. Rice who obtained a yield strength of 5500 psi. See Semiannual Report No. 1 (30 June 1972), ARPA Order 2031, Naval Research Laboratory, Wash., D. C.

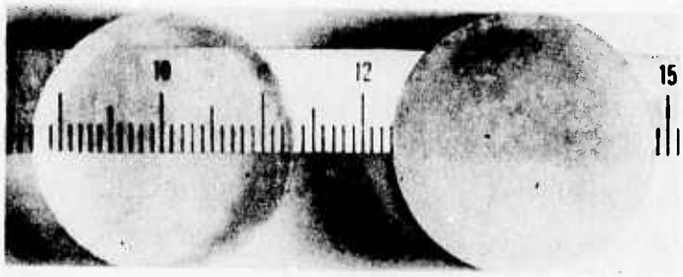

Scrubbed Unscrubbed

Fig. 21. Hot Pressed KCl, 2.54 cm Diameter and 0.62 cm Thick, From Scrubbed and Unscrubbed MCB (99.9%) Granules.

For comparison, in the same Instron equipment, Polytran gave a yield point of 600 psi and an ultimate strength of 800 psi.

The optical transmission and absorption coefficient at 10.6 μm were: 46% and $\beta = 0.55\ cm^{-1}$ for the unscrubbed (weight = 6.22 g and L = 0.62 cm) and 84% and $\beta = 0.077\ cm^{-1}$ for the scrubbed (weight = 6.24 g and L = 0.63 cm). The one-order-of-magnitude improvement in β attests to the importance of the initial surface state of the starting powder. The pressing parameters still need to be optimized. For instance, the dependence of β on thickness is appreciated, using the scrubbed powder. For L = 0.15 cm, both long and short dwell times, 18 hr at 25°C and 1.5 hr at 110°C, gave similar results, $\beta = 0.050 \pm 0.001\ cm^{-1}$, which is significantly lower than the case of L = 0.63 cm.

A mixed halide mechanical mixture of equimolar NaCl and KCl granules, from MCB (99.9%), was scrubbed with CCl_4. A sample was hot pressed in vacuum using the 1-in. diameter die at 150°C, 5.1×10^4 psi, and 60 min dwell time. The resulting disc was opaque.

Another mixed halide mechanical mixture, KCl and KBr, 1:2 molar ratio, was scrubbed with CBr_4 and $CHBr_3$. A sample was hot pressed in vacuum using the 1-in. diameter die, at 170°C, 5.1×10^4 psi, and 60 min dwell time. The resulting disc was opaque. However, KCl·2KBr single crystals grown under an internally-funded program, press-forged under Ar, produced repeatedly clear discs. The 1/2-in. diameter die was used at 650°C, 2.66×10^3 to 7.64×10^3 psi, and 60 min dwell time. Powder scrubbing and solid-solution crystal growth are far from being an optimum RAP because one deals in this case with a mixed halogen solution.*

---

* With the crystal, $\beta = 0.002\ cm^{-1}$, which is a factor of two lower than the value reported by AFCRL. The crystal shows no yield point. However, there is more than a factor of four variation in the modulus of rupture. Our measurement yields 5400 psi while the AFCRL reported value is 1345 psi. It is not known at this point in time whether these differences are real and attributable to RAP. For the AFCRL results quoted, see Table 3 on page 6 of "High Power Infrared Laser Window Materials (LQ-10 Program)," Quarterly Progress Report No. 5 (1 Jan to 31 Mar 1972), Air Force Cambridge Research Laboratories, Bedford, Mass.

The results of our studies on materials purification, topochemical exchange, and crystal growth from the congruent melt lead us to believe that significant advances in the technology of hot pressing will come from the development of a one-step RAP operation from scrubbing to pressing. It is conceivable that such a development can be easily realized with mixed halides based on a common halogen (chlorine in particular). The case of mixed halides based on mixed halogens will require more extensive background studies.

b. Crystal Growth From Solution

The object in this study was to obtain high quality single crystals of high purity NaCl and KCl with an $OH^-(s)$ mole fraction of $C < 10^{-7}$. The exchange reaction of interest is,

$$Cl^-(c) + OH^-(aq) \rightleftharpoons OH^-(c) + Cl^-(aq), \tag{9}$$

where (c) is the crystal and (aq) is the saturated solution. It follows from the mass-action expression for eq. (9) that,

$$C = K \frac{[OH^-(aq)]}{[Cl^-(aq)]} \tag{10}$$

If it is assumed that the ionization constant of water is $pK_w = 14$ even for the saturated solution, then

$$[OH^-(aq)] = 10^{-14 + pH} . \tag{11}$$

The saturated solution of KCl or NaCl is approximately five molar, or

$$[Cl^-(aq)] = 10^{0.7} \tag{12}$$

It follows from eqs. (10) to (12) that,

$$C = 10^{-14.7 - (pK - pH)} \qquad (13)$$

From eq (13) it is easily demonstrated that, in principle, $C < 10^{-7}$ is quite feasible. Besides, $OH^-(s)$ can be controlled via the pH of the solution: e. g., adding HCl. Depending on the value of K, there may be very little $OH^-(s)$ even without intentional pH control.

Solution-grown specimens would provide standards for the behavior of the melt-grown counterparts as these achieve low $OH^-(s)$ content, for instance, F-band coloration susceptibility and transition temperature from extrinsic to intrinsic dc conductivity.[17] These expectations are justified to the extent that occlusion can be avoided during growth. The main concern in obtaining high quality single crystals from solution is control of the growth behavior. However, this feature may not be independent of purity because of the effect of traces of growth poisons.[18]

A very low concentration of $PbCl_2$ was employed as a growth habit modifier for NaCl and KCl. Figure 22 indicates that there is an optimum concentration of $PbCl_2$ required in solution growth. Figure 23 shows the crystal quality obtained with NaCl and Fig. 24 for KCl.

The transmission at 10. 6 μm of specimen (a) of Fig. 23 with thickness L = 0. 41 cm was 93%, specimen (b) ranged from 53 to 74%, and specimen (c) from 0 to 15%. Specimen (a) was repolished and its transmission from 2. 5 μm to 20 μm (Beckman IR 12) was compared with the melt-grown materials, as shown in Fig. 25. It is quite obvious that the IR transmission of the solution-grown material is inferior to that of the melt grown. Of the melt-grown materials, the RAP crystal is the better transmitting material. A comparison between the two extremes, the solution-grown versus the RAP melt-grown NaCl, was also made in terms of the optical absorption coefficient at 10. 6 μm, β, using an adiabatic calorimeter apparatus (refer to Appendix II). The solution-grown NaCl gave $\beta = 0.013\ cm^{-1}$ while the RAP melt grown yielded, $\beta = 0.0018\ cm^{-1}$. Most likely, the higher β in solution grown

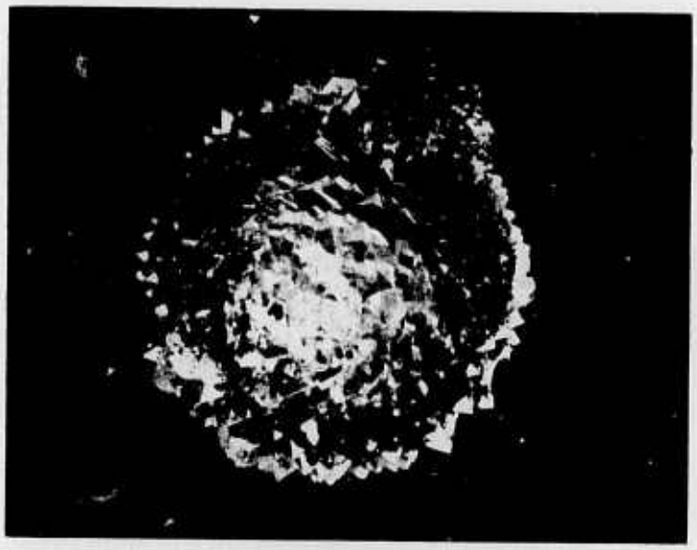

(a) Spherical growth of KCl from solution 1% wt $PbCl_2$

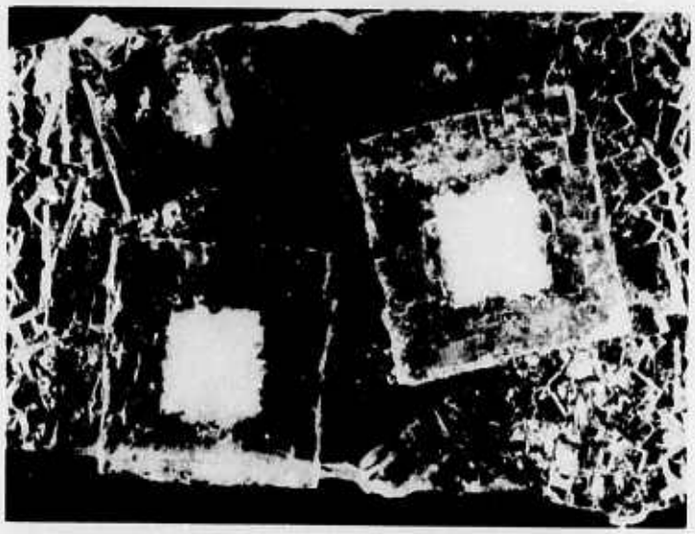

(b) Crystals of NaCl showing high opacity in the center, which was the initial growth with no $PbCl_2$. The clear growth was effected with 0.25% wt $PbCl_2$

Fig. 22. Influence of $PbCl_2$ on Growth From Solution (Magnification 1.6x).

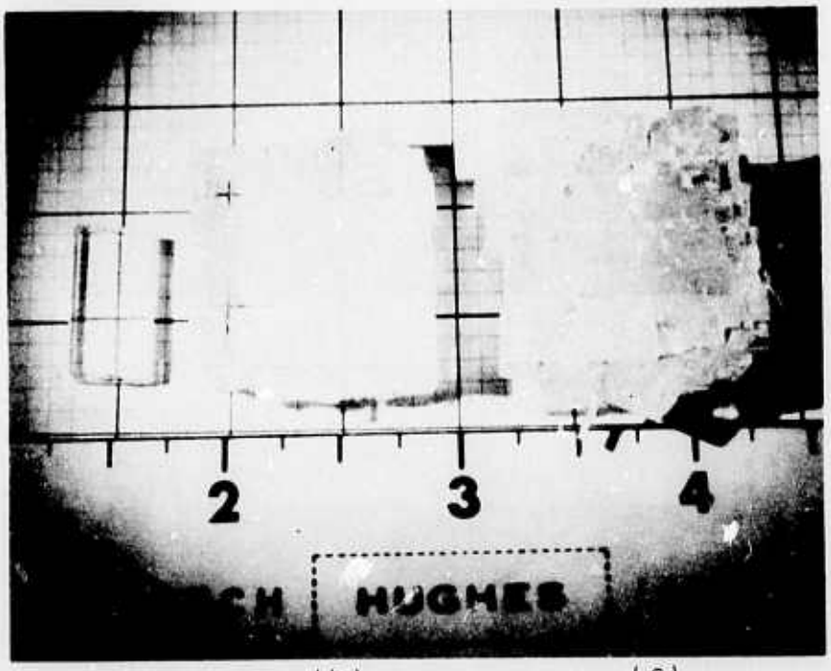

From left to right, the crystals were grown as follows: (a) Convection cell, $x(PbCl_2) = 2.3 \times 10^{-3}$, and pH 1. (b) Convection cell, $x(PbCl_2) = 1.0 \times 10^{-4}$ and pH 2. (c) Beaker at 70°C with $x(Pb(NO_3)_2) = 1.8 \times 10^{-4}$.

Fig. 23. Solution Grown NaCl Crystals (scale unit: inch).

Clear outer layer was grown in a solution with $x(PbCl_2) = 1.8 \times 10^{-4}$ and pH 2.

Fig. 24. Solution Grown KCl Crystal (scale unit: inch).

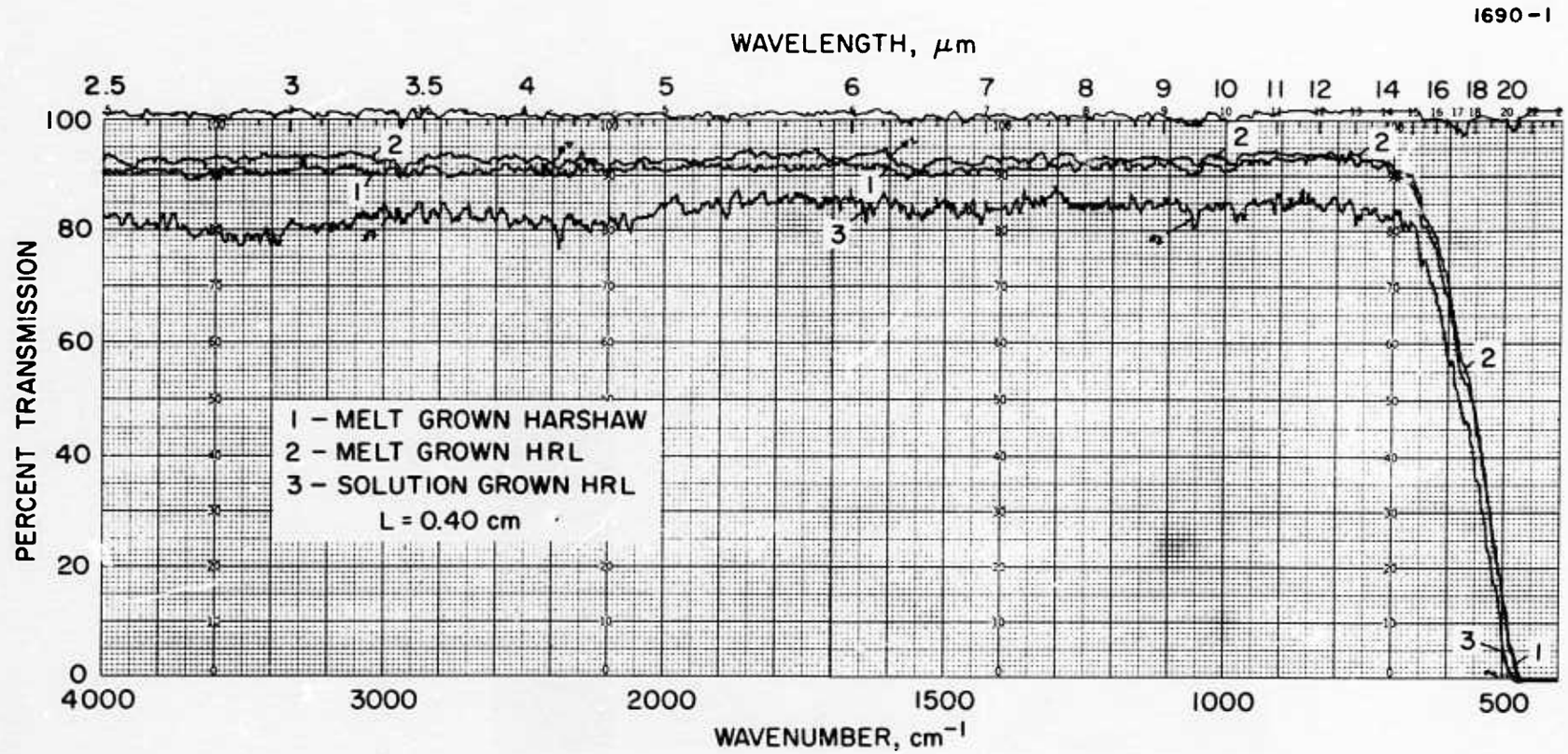

Fig. 25. Infrared Transmission of Solution and Melt Grown NaCl.

NaCl is due to occlusion and other growth defects that plague solution growth. These drawbacks were not rectified by scrubbing with $CCl_4(g)$ at 670°C for 20 hours, which yielded $\beta = 0.010\ cm^{-1}$.

In the case of the solution-grown KCl specimen (refer to Fig. 24), the internal region of the crystal was cloudy. The polished specimen yielded an 85% transmission at 10.6 μm. A thin section (L = 0.27 cm) was sliced off, polished, and gave a 93% transmission. The larger section (L = 1.25 cm) gave an 87% transmission. In view of the results obtained with NaCl, and the slightly better quality of solution-grown NaCl over KCl, further comparison of solution-grown KCl with melt-grown KCl was not warranted.

B. WINDOW COATINGS

1. Theoretical Considerations

a. Design of Antireflection Coatings

Antireflection coatings can range from a simple single layer having virtually zero reflectance at one wavelength to a multilayer system of twenty or more layers having virtually zero reflectance over a wavelength range of several octaves. The type used in any particular application will depend on a variety of factors including the substrate material, the wavelength region, the required performance, and the cost.

For design of coatings and for tutorial purposes, most reference works assume that the substrates and materials used for coating are completely transparent (i.e., k = 0, where k = absorption index or extinction coefficient of the material) in the spectral region in which the reduction of surface reflectance is to be obtained. Cox and Hass [19] and H.A. Macleod,[20] using this assumption, have presented detailed designs and discussions of antireflection coatings for optical surfaces using a single layer, double layer, and multilayer coatings. Therefore, this section will not include any detailed discussion of the derivation of these designs since they are treated in an excellent manner in the above works, although material and design information for 10.6 μm is not included in those references. However, design data incorporated in this section does consider the factor of absorption in film materials, because at the present technological stage of coating application methods, the high power 10.6 μm laser flux to which the coatings will be subjected makes the inclusion of absorption considerations in the designs mandatory.

Practical coatings are generally restricted to one- or two-layer designs with an occasional use of a three-layer coating. This is particularly true at 10.6 μm where the large physical thicknesses required in the layers cause problems in the realization of a given design. Single layer coatings are limited in usefulness since one obtains a zero

of reflectance only when the refractive index of the coating material is equal to the square root of the substrate index. When this condition cannot be met, two or more layers must be used to obtain a true zero of reflectance using available materials.

When two layers are used in the coating design, the added freedom permits one to choose many different combinations of refractive indices and layer thicknesses to produce a zero of reflectance at a prescribed wavelength. The basis for choice of a particular design to pursue experimentally then becomes criteria such as the minimization of absorption and the minimization of differential strains which might lead to poor adherence. In the work reported here, minimization of absorption has been the prime criterion in making the choice of designs.

An important aid to designing two-layer antireflection coatings is a diagram such as that shown in Fig. 26 for ZnSe (see Ref. 19). Every point in the shaded regions of the diagram represents a pair of refractive index values for the coating materials which will produce a zero of reflectance on the given substrate. Points outside the shaded regions, but close to them, will yield low reflectance but not zero. The corresponding thicknesses are then calculated from a pair of design equations. The final step is to calculate the 10.6 μm absorption expected for each coating design based on either measured absorption indices for the individual film materials or best guesses where no measurements are available.

The remainder of this section contains some illustrative coating design information for KCl, CdTe, and ZnSe. This information is strictly theoretical in nature, and there are many factors that contribute to the actual performance of a coating that are not included in the theory leading to the design thicknesses and absorption values. Therefore, the optimum experimental thicknesses need not be the same as the theoretical ones (although they are usually expected to be close) and the absorptions need not be as low as the theoretical predictions. Some of these problems are discussed further in the section on experimental results.

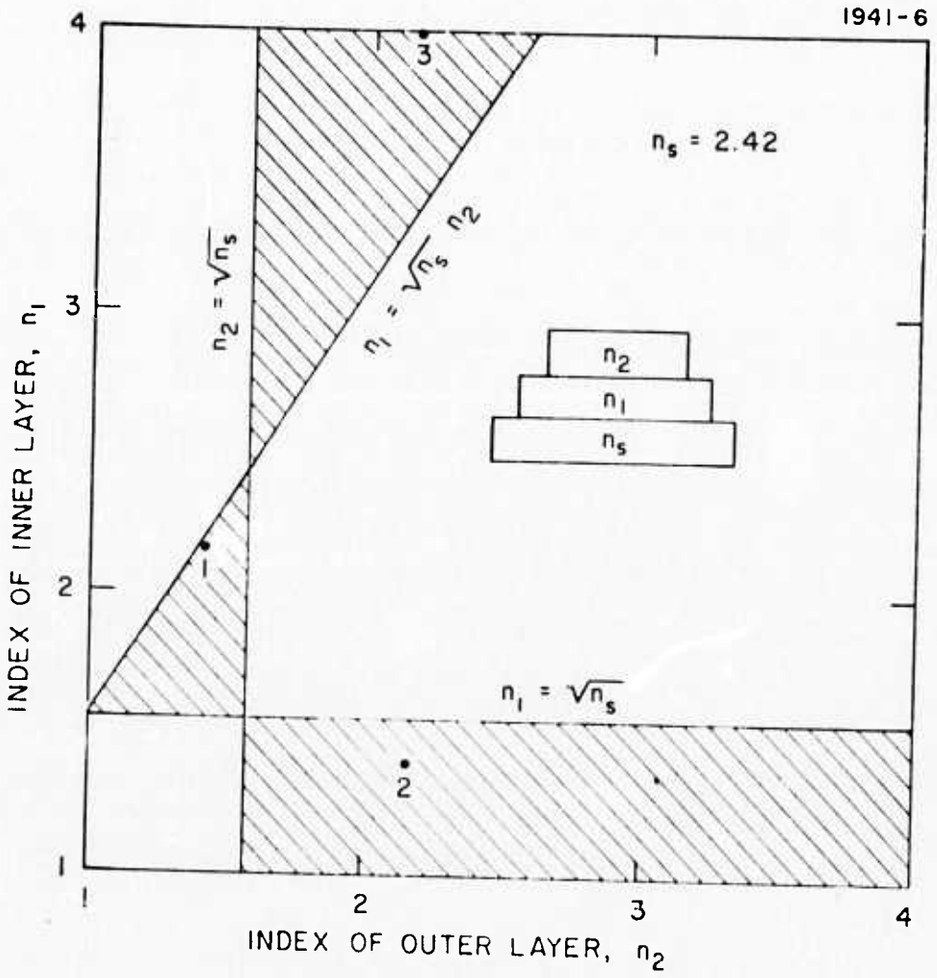

Fig. 26. Double-Layer Antireflection Coating Design Diagram for ZnSe.

b. Antireflection Coatings for KCl

In the case of a low index halide, like KCl, there are no available coating materials with refractive index equal to or less than the substrate index. This means that single layer coatings and double layer coatings from the rectangular region or the lower triangular region of a diagram for KCl similar to that of Fig. 26 are not feasible. The possible two layer coatings come from the region where the refractive index n_1, of the first deposited layer is greater than the substrate index n_s, and the index of the second deposited layer is greater than n_s and less than $n_1/\sqrt{n_s}$.

Table VII contains layer optical thicknesses as a fraction of the 10.6 μm design wavelength and predicted absorptions per coated surface for a variety of designs in which the second (outer) layer is chosen from among the low index fluorides ThF_4, BaF_2 and SrF_2 which have low absorption at 10.6 μm and low water solubility. The As_2S_3/ThF_4 combination has been extensively studied experimentally and results for it will be reported. A detailed picture of the dependence of total absorption per surface in this coating on the absorption in the individual layers is given in Fig. 27. The point labeled 1971 in the figure was shown at the 1971 Laser Window Conference as the expected best absorption in such a coating based on the best absorption indices which had been measured in As_2S_3 and ThF_4 to that time. The point labeled 1972 is based on improvements in the two materials during the intervening year.

If the refractive index of the first coating layer is high enough, the potential range of the second layer index can be increased to include ZnS as the second (outer) layer. This occurs for the combinations ZnTe/ZnS and CdTe/ZnS as shown in Table VIII. These coatings incorporate no low index fluorides and, therefore, should be less water sensitive than those in Table VII. Table VIII also illustrates another important point in the design of two-layer antireflection coatings. This is that, in general, there are two independent solutions for each pair of refractive index values (optical thickness values for one may be subtracted from one-half wavelength to find those for the other). The two

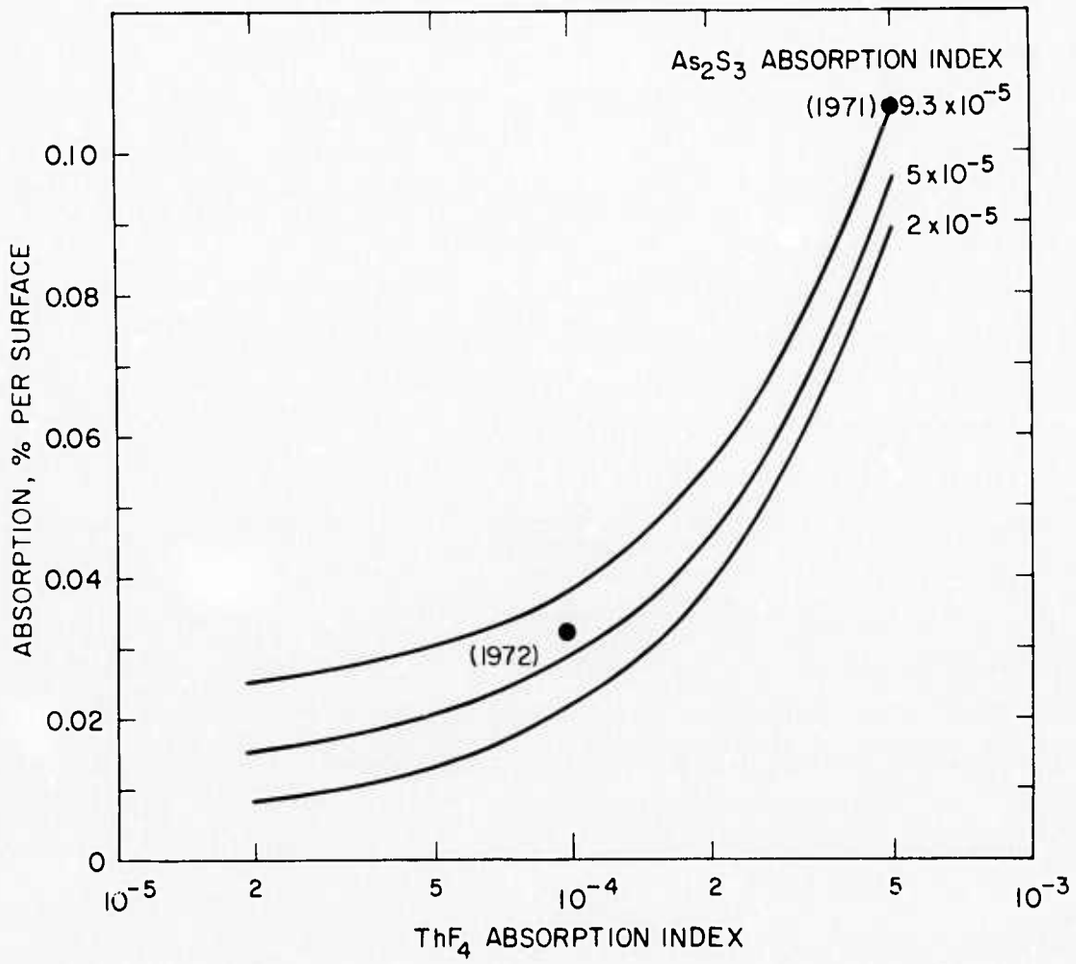

Fig. 27. Absorption per Surface in As_2S_3/ThF_4 Antireflection Coatings on KCl Versus Material Properties.

TABLE VII

Theoretical Designs for Antireflection Coatings on KCl

Layer 1 \ Layer 2	ThF_4 n = 1.5, k = 1 x 10^{-4}			BaF_2 n = 1.395, k = 5 x 10^{-4}			SrF_2 n = 1.36, k = 2 x 10^{-3}		
	L_1	L_2	A*(%)	L_1	L_2	A*(%)	L_1	L_2	A*(%)
ZnS n = 2.16 k = 2 x 10^{-4}	0.412	0.166	0.066	0.437	0.168	0.142	0.445	0.172	0.423
As_2S_3 n = 2.377 k = 6.5 x 10^{-5}	0.432	0.157	0.032	0.450	0.163	0.105	0.456	0.167	0.378
In_2S_3 n = 2.474 k = 6.5 x 10^{-5}	0.438	0.154	0.172	0.454	0.161	0.251	0.459	0.166	0.526
CdTe n = 2.67 k = 1 x 10^{-4}	0.447	0.150	0.040	0.460	0.158	0.111	0.465	0.163	0.379
ZnTe n = 3.0 k = 1 x 10^{-4}	0.457	0.146	0.039	0.467	0.156	0.109	0.471	0.161	0.376

*Absorption per coated surface.

T728

TABLE VIII

Antireflection Coatings Without Low Index Fluorides for KCl

	Layer 1	Layer 2	Absorption, % (Per Surface)
	High Index Thickness, Wavelengths	ZnS Thickness, Wavelengths	
ZnTe/ZnS n = 3.0, k = 1 x 10^{-4}, n = 2.16, k = 2 x 10^{-4}	0.116	0.343	0.054
	0.384	0.157	0.049
CdTe/ZnS n = 2.67, k = 1 x 10^{-4}, n = 2.16, k = 2 x 10^{-4}	0.185	0.297	0.053
	0.315	0.203	0.051

T520-1

solutions each will produce a zero of reflectance at the design wavelength but differ at other wavelengths, and they need not have the same absorption. In the case of the designs of Table VIII the predicted absorptions for the two solutions of each set are nearly equal so a choice between them could be made on other grounds, such as minimization of differential strains. For the coatings of Table VII the choice of solutions has been made to minimize predicted absorption where BaF_2 or SrF_2 is the outer layer. In the case of ThF_4 outer layers the predicted absorption for the two solutions was almost the same – the choice was made to limit the ThF_4 thickness.

The ZnTe/ZnS coating with optical thicknesses 0.116 and 0.343 wavelengths was chosen for experimental study, and results will be reported in the Section on coating results achieved.

Figure 28 shows more extensive theoretical predictions of the 10.6 μm absorption per surface for this coating as a function of the absorption in the individual layers. The point on the figure represents the current best guess values for the two absorption indices in the absence of firm experimental numbers (taken as equal to that achieved for CdTe films for ZnTe, ten times bulk value for ZnS).

A novel coating design, which is a modification of a basic double layer antireflection coating of possible use where the outermost layer is sensitive to moisture in the environment, consists of adding a thin third layer of a film material having low optical absorption at 10.6 μm and good resistance to moisture. Such a design, for example, is to add a thin third layer of CdTe to a basic two-layer $CdTe/BaF_2$ design. The properties of such a three-layer coating in theory are as follows.

$CdTe/BaF_2$ on KCl where the thickness of the CdTe and BaF_2 films are 0.46 wavelengths and 0.153 wavelengths at 10.6 μm, respectively, will theoretically have reflection = 0 and absorption in percent per surface of 0.111% as shown in Table VII. If the two-layer design above is modified by adding a thin layer of CdTe, the $CdTe/BaF_2/CdTe$ design with film thicknesses of 0.46/0.10/0.017 wavelengths at 10.6 μm will have a reflection of 0.074% and an absorption per surface = 0.077%. The CdTe outer layer physical thickness = 675 Å.

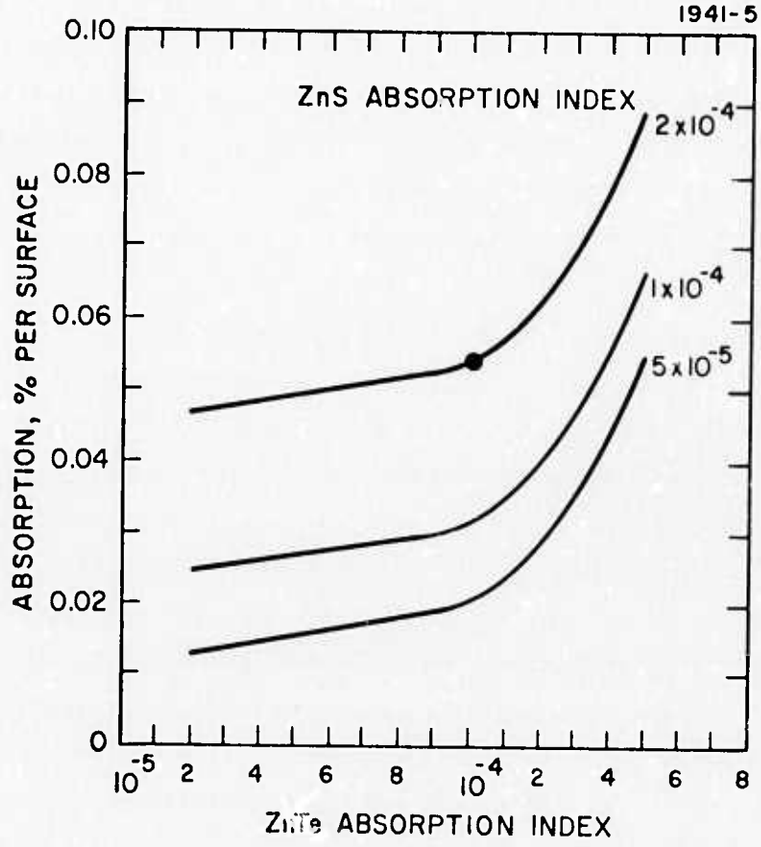

Fig. 28. Theoretical Absorption per Surface in ZnTe/ZnS Antireflection Coatings on KCl Versus Material Properties.

c. Antireflection Coatings for CdTe and ZnSe

In the case of these semiconductor window materials their high refractive indices relative to that of the low index halides provide new options in coating design. Single layers are theoretically feasible if zero reflectance is not required. Also, double layer coatings are possible with refractive index values in all three regions of the design diagram. In particular, one may now choose double layer coatings from the rectangular region of the diagram where the index of the first layer is less than the square root of the substrate index and the index of the second layer is greater than the square root of the substrate index. These coatings have important properties which are illustrated below.

The design diagram for ZnSe is shown in Fig. 26; the diagram for CdTe would be similar. The three numbered points on the diagram correspond to the identifying numbers in Table IX, which contains design data for these three coatings as well as for a ThF_4 single layer. At each point the two-layer solution which minimizes absorption and coating thickness has been chosen for inclusion in the table.

A comparison of the solutions labeled 1 and 2 illustrates the advantages of the solution in the rectangular region of the design diagram (No. 2). They both utilize the same materials to produce a zero of reflectance at 10.6 μm – but in opposite order. For solution 2, which has the order BaF_2/ZnS, the required coating thicknesses are much less than for solution 1 (which is important at long wavelengths), and the predicted absorption is less than half that for solution 1. Another important advantage of solution 2 is that the water-sensitive low index fluoride is not exposed to the environment; the outer semiconductor layer protects it.

Solution 3 in Fig. 26 and Table IX (Ge/ZnS) is included because the Ge/ZnS combination represents an important pair of materials which is widely used in commercial infrared optical coatings. The use of germanium may be prohibited at high power levels because of the danger of thermal runaway, but a Ge/ZnS antireflection coating for ZnSe may still be usable for low power applications.

TABLE IX

Theoretical Designs for Antireflection Coatings on ZnSe

No. On Design Diagram	Coating Materials		Layer Optical Thicknesses, Wavelengths		Absorption Per Coated Surface, %
	Layer 1	Layer 2	Layer 1	Layer 2	
-	ThF_4	-	0.250	-	0.023 (R = 0.13%)
1	ZnS	BaF_2	0.222	0.241	0.142
2	BaF_2	ZnS	0.138	0.059	0.066
3	Ge	ZnS	0.116	0.303	0.043

10.6 μm Optical Constants

	ZnSe	ThF_4	BaF_2	ZnS	Ge
n	2.42	1.5	1.395	2.16	4.0
k	-	1×10^{-4}	5×10^{-4}	2×10^{-4}	2.5×10^{-5}

T729

Table X contains design information for some typical coatings on CdTe. Again one sees the striking improvement in performance and reduction in layer thicknesses that can be obtained with coating designs from the rectangular region of the design diagram (compare ZnS/BaF_2 with BaF_2/ZnS). The ThF_4 single layer and the ZnS/ThF_4 and BaF_2/ZnS double layers have been studied experimentally; results will be reported below.

2. Coating Results Achieved

A general introduction and background to optical coating technology that included a number of theoretical designs and predicted performance levels for coatings on KCl and CdTe windows were presented in previous sections. It is appropriate at this point to summarize what has been accomplished to date experimentally in efforts to prepare optical coatings for these materials. The primary goal was to try to minimize the 10.6 μm absorption in the coatings. In order to assist in achieving this goal, measurements were made of the 10.6 μm absorption in the substrates, and of the coated substrates so that the coating absorption per surface, as well as the absorption index of the film, could be calculated. The film absorption index values were important to obtain so that experimental results could be compared with theoretical designs.

a. Passivation and Antireflection Coatings on KCl

Substrates for our coating work have included KCl single crystal substrates grown by Optovac and Harshaw, as well as HRL grown single crystals. In addition, coating studies were performed on Harshaw polytran substrates received from AFWL. The halide coating work placed emphasis on the development of single layer passivation coatings and two-layer antireflection coatings.

The passivation coating results are summarized in Table XI. To date, the single layer As_2S_3 passivation coatings have shown the lowest coating absorption per surface, if they are prepared on KCl

TABLE X

Theoretical Designs for Antireflection Coatings on CdTe

Coating Materials		Layer Optical Thicknesses, Wavelengths		Absorption Per Coated Surface, %
Layer 1	Layer 2	Layer 1	Layer 2	
ThF_4	-	0.250	-	0.024 (R = 0.73%)
ZnS	ThF_4	0.133	0.207	0.034
ZnS	BaF_2	0.185	0.212	0.127
BaF_2	ZnS	0.119	0.076	0.058
Note: 10.6 μm optical constants: same as Table III for coating materials, n = 2.67 for CdTe				

T730

TABLE XI

Properties of Passivating Coatings on KCl Windows

Material	Index	Thickness, Wavelengths	T, %	A, % Per Surface
ThF_4	1.5	λ/4	94 ± 1	0.52
ZnS	2.16	λ/2	94 ± 1	0.13
CdTe	2.67	λ/2	96 ± 1	0.13
As_2S_3	2.377	λ/2	94 ± 1	0.02

T731

substrates that have good surface quality and are not hazed or fogged as a result of reaction with moisture in the air. For example, where the substrate absorption was high (because of poor surface quality $0.0123\ cm^{-1}$), $\lambda/2$ As_2S_3 was 0.22% per surface. With substrate absorption of $0.00125\ cm^{-1}$ a $\lambda/2$ As_2S_3 coating absorption of 0.02% per surface resulted. It should be pointed out that in using ThF_4 that its thickness is not limited to $\lambda/2$ for passivation but can be deposited much thinner (thereby reducing absorption). This is because of the close match in the refractive index of ThF_4 with KCl which are 1.5 and 1.455, respectively.

Antireflection coatings prepared in our work, which to date have emphasized As_2S_3/ThF_4 two-layer coatings, have continued to yield percent absorption per surface greater than the desired goal of 0.1% or less (see Table XII). The As_2S_3 was deposited by e-gun evaporation and the ThF_4 by resistance heating of tungsten filaments. The thickness of both layers was optically monitored by a He-Ne laser. Figure 29 shows the spectral transmittance measured on a Beckman IR-12 spectrophotometer of one such sample, in comparison with a theoretical plot which utilizes the same parameters of index and thickness for each layer as the experimental data. However, the increase in absorption associated with ThF_4 above 10.6 μm is not included in the theoretical plot which produces high transmission values as seen in Figure 29. The dip observed between 1600 to 1700 cm^{-1} in the experimental data is also attributed to ThF_4. It is believed to be caused by OH in the ThF_4 and can be reduced by substrate heating during deposition. Calorimetric absorption measurements point out the necessity for this reduction for it has been found that increases in absorption at 10.6 μm can be correlated to the depth of this dip.

Because of the problems which seem to beset ThF_4, some nonfluoride antireflection coatings were tried. The most successful has been a two-layer ZnTe/ZnS coating which to date has yielded absorption values of 0.05% per surface (less than the desired goal of 0.1%). Both layers were deposited by resistance heating and optically monitored at a wavelength of 1 μm. Preliminary investigation of this coating design

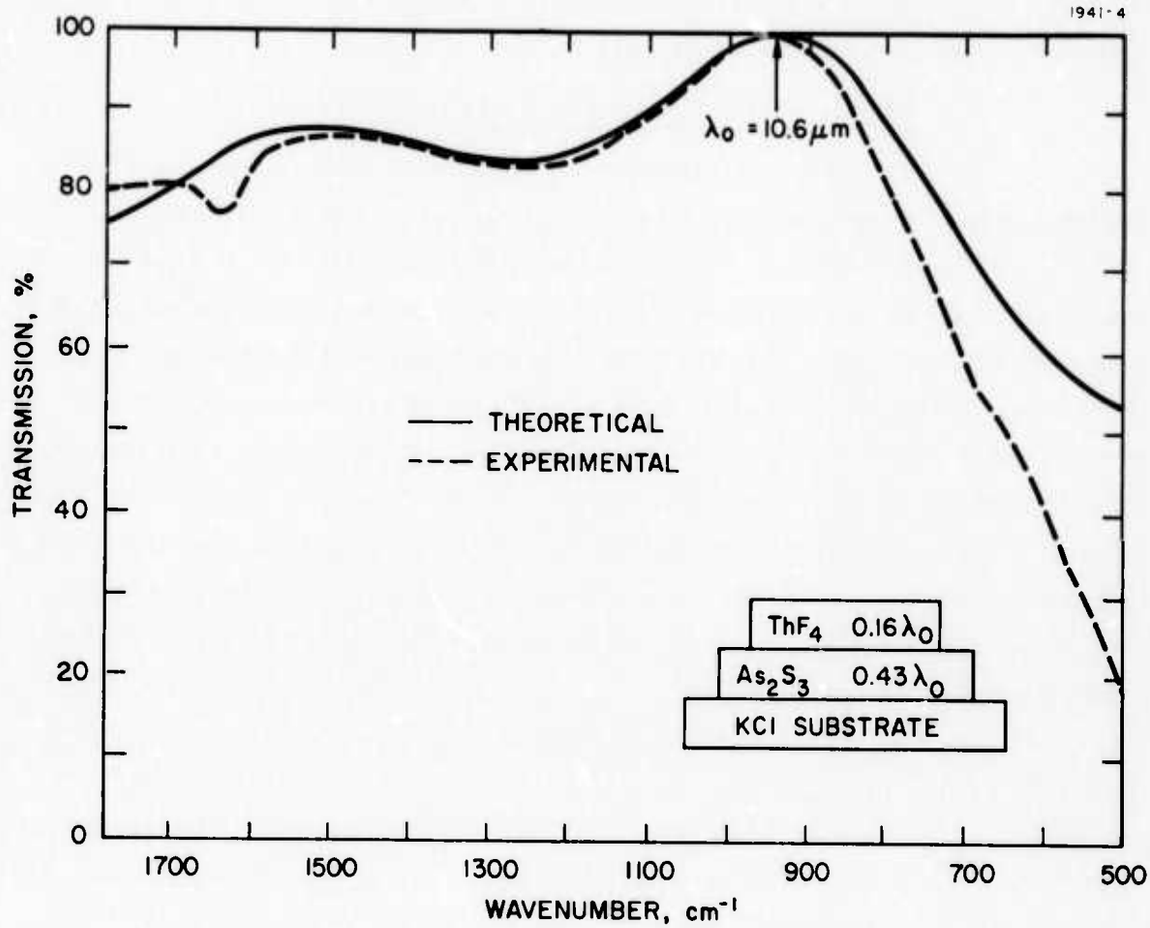

Fig. 29. Spectral Response of As_2S_3/ThF_4 Antireflection Coated KCl.

led to a value of 3.0 for the refractive index of ZnTe, compared with the value of 2.71 reported by S. O. Smith and J. S. Seeley[21]. The coating design for the ZnTe/ZnS data shown in Table XII utilized the original index value of 2.71, resulting in a peak transmission from the Beckman spectrophotometer of only 95%.

b. Experimental Coating Results for CdTe

The three different antireflection coatings that have been studied on CdTe windows are ThF_4 single layers, and ZnS/ThF_4 and BaF_2/ZnS double layers. The dominant experimental fact is that for all three of these coatings the theoretical design data does not match the experimental results. For the ThF_4 single layer of 1/4 wavelength thickness, reflectances below 4.5% could not be achieved (theoretical prediction 0.73%) whereas, for the double layers minimum reflectance is realized for layer thicknesses relatively far from the theoretical ones. The reasons for these discrepancies are not known, but they are believed to be a result of surface effects on the CdTe. Similar effects should be watched for on ZnSe, which might be expected to have surface properties like those of CdTe.

Table XIII shows results to date for the three coatings studied on CdTe. The coatings were deposited in a conventional diffusion pumped vacuum system with liquid nitrogen trapping onto CdTe surfaces heated to 150°C. The ZnS source was a vitreous carbon crucible with a tungsten pancake filament, the BaF_2 source was a heavy Mo boat, ThF_4 was deposited, using both types of source, with no apparent difference in performance.

The ThF_4 single layers were monitored with a 10.6 μm CO_2 laser so the optical thickness is known to be 1/4 wavelength at 10.6 μm in all cases. Physical thicknesses were measured interferometically to confirm the assumed value of 1.50 for the ThF_4 refractive index at 10.6 μm. The minimum reflectance achieved for these 1/4 wavelength layers was consistently in the range from 4.5 to 5.0% in conflict with the theoretical prediction of 0.73%.

TABLE XII

Coating Results on KCl

Multilayer Coating	Beckman Spectrophotometer		Absorption Per Surface Percent		
	Peak Trans.	Percent	Predicted	Goal	Achieved
As_2S_3/ThF_4	10.6 μm	99 ± 1	0.03	≤ 0.10	0.19
ZnTe/ZnS	10.5 μm	95 ± 1	0.05	≤ 0.10	0.05
Window - HRL's RAP Grown KCl Single Crystal					

T732

TABLE XIII

Experimental Antireflection Coating Results on CdTe Windows

Coating Design	Theoretical Optical Thicknesses (Wavelengths)	Theoretical Reflectance ( )	Experimental Reflectance ( )	Theoretical 10.6 μm absorption per surface ( )	Experimental 10.6 μm absorption per surface ( )
ThF_4	0.250	0.73	4.5-5	0.024	not measured
ZnS/ThF_4	0.133/0.207	0	0.15-0.25	0.034	0.25-0.50
BaF_2/ZnS	0.119/0.076	0	0.15-0.30	0.058	0.06-0.25

T733

The ZnS/ThF_4 double layers were also monitored with a CO_2 laser. In this case it was found that using the theoretical design thicknesses the reflectance at the minimum was between 1 and 1.5%. The thicknesses were then adjusted empirically to obtain minimum values in the range of 0.15 to 0.25%. The final prescription arrived at for the deposition was as follows: deposit ZnS until the original CdTe reflectance of 20.7% is reduced to 10.3%, deposit ThF_4 until a minimum is reached. The theoretical stopping point for the first layer is 13.9%.

The BaF_2/ZnS double layers were monitored with a He-Ne laser at 6328 Å. The theoretical design thicknesses require deposition of 2.1 wavelengths of BaF_2 and 1.4 wavelengths of ZnS at 6328 Å taking account of the known dispersion in the two materials. The use of these thicknesses produced a reflectance of 1.1% on the CdTe windows. When the thicknesses were empirically adjusted to 1.75 wavelengths at 6328 Å for both layers, reflectances in the range of 0.15 to 0.3% were consistently obtained. Translated to 10.6 μm, these results imply that minimum reflectance is occurring at optical thicknesses of 0.100 wavelengths and 0.090 wavelengths for BaF_2 and ZnS, respectively; whereas, the theoretical values are 0.119 and 0.076 wavelengths. Figure 30 shows the spectral response measured from 2.5 to 22 μm for a 2-in. diameter CdTe window antireflection coated with the empirically adjusted BaF_2/ZnS design along with a theoretical curve calculated from the data shown on the figure. The reflectance at 10.6 μm was also measured with a CO_2 laser; it was found to be quite uniform with an average of 0.73% (two coated surfaces) across the face of the window. The 10.6 μm absorption measured calorimetrically at the center of the window was 0.25% per coated surface.

3. Pulsed Laser Damage

Some preliminary data have been obtained for the behavior of coated and uncoated alkali halide windows when subjected to high power CO_2 laser pulses. The test results are shown in Table XIV. All tests

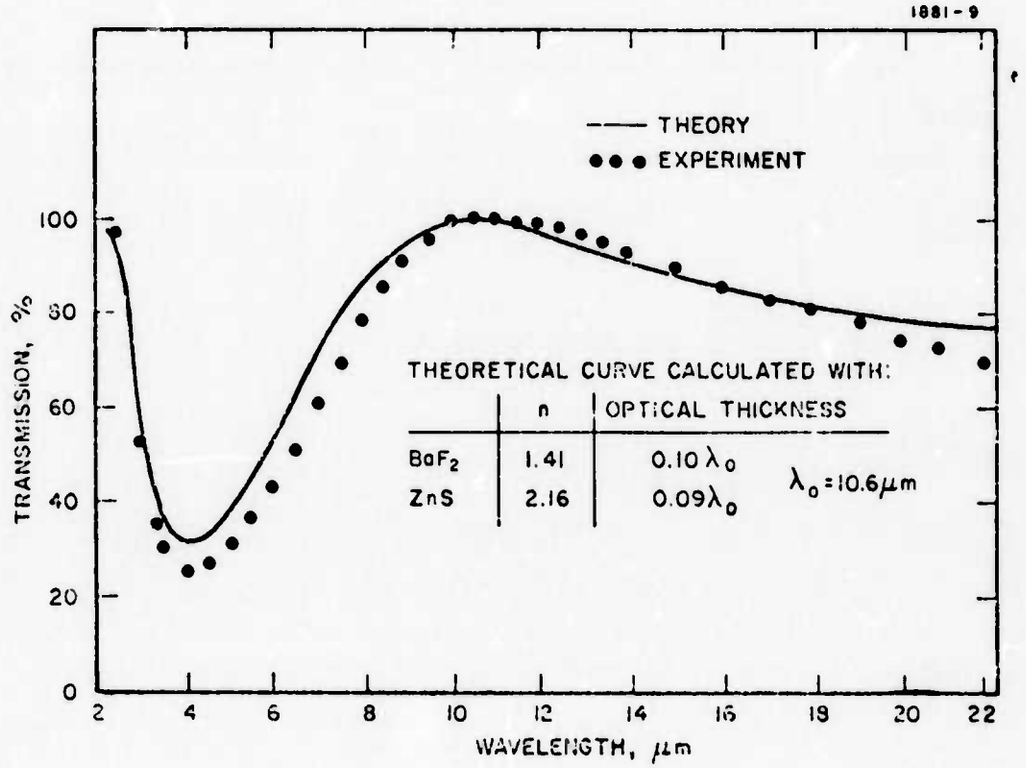

Fig. 30. Spectral Response of BaF_2/ZnS Antireflection Coating on CdTe.

TABLE XIV

Pulsed Laser Damage Results

Window Substrate	Coating	Absorption	Measured Damage[+] Threshold (J/cm^2)
NaCl (Harshaw)	None	*	40-50
KCl #87-21 (Polytran) polycrystalline	None	0.0016 cm^{-1}	14
	$\lambda/2$ As_2S_3	0.02%/Surface	6-9
KCl #69 (Optovac) single crystal	AR type As_2S_3/ThF_4	0.8%/Surface	5
KCl #B-24-6 (HRL) Bridgman grown	None	0.00076-0.00080 cm^{-1}	46-57

*not measured

[+] 30%

1734

were performed on the HRL fast-flow test bed using a multimode stable resonator with a pulse length of 2.2 μsec. The power output of the laser was adjusted below the threshold for clean air breakdown using a 6.4 cm Ge lens. The sample was located in a converging portion of the beam with the highest intensity upon the exit face. Since the spot size is determined by the lens to sample distance, corrections are included for the effect of the index of refraction of the sample upon the exit spot size. The test results are based upon a single pulse damage threshold, performed upon unstressed windows.

4. Surface Finishing

To date, no single material has been developed to the point where it exhibits both the low optical absorption and the high tensile yield stress necessary to fulfill the requirements for a window in a high-power laser system. However, since the required optical performance has been achieved in single crystal KCl grown by reactive atmosphere process (RAP) at HRL the discussion on surface finishing will be limited to this material with a few remarks on the polishing procedure for CdTe.

a. KCl Finish

Grinding and finishing relatively soft, water soluble materials, such as the alkali halide to a finish that does not degrade the intrinsic optical absorption of the window material, requires special techniques. The two most significant problems encountered in polishing halide materials are caused by their relative softness and their solubility in water. Therefore, they are difficult to clean, and the finished surfaces are unstable in normally encountered environments. Attaining surfaces of high grade optical finish is very difficult on such soft materials because of the strong tendency to develop sleeks and "orange peel" during the polishing process.

The technique utilized in this work to achieve a high quality finish on KCl consisted of a two-step process. Samples were initially

ground on a cast iron lap with SiC emery paper (No. 600) to remove gross surface roughness. They were then finished dry on cloth using the abrasive Linde A (Al_2O_3) and a small amount of ethyl alcohol.

With this technique, two types of surface finish were given to KCl samples. They are designated as optical finish and window finish. Optical finish samples are worked until flat and parallel within one fringe of visible light. Window finish samples are flat within a few fringes, with no attempt made to achieve parallelism.

Prior to coating, slices from various locations in an HRL single crystal boule of KCl were polished and subjected to calorimetric absorption measurements. These results are shown in Table XV. Although a correlation with sample length or position in a boule is not apparent, a strong dependence on the type of surface finish exists. The optical finish samples showed a strong tendency to fog during the few minutes that they were exposed to the 50% relative humidity laboratory environment before placement in the desiccated calorimeter, even though placed in desiccators immediately after polishing was completed.

The most striking example of the effect of a fogged surface on the measured absorption is slice No. 3, which was measured with both surface finishes. It was first found to have an absorption coefficient of 0.00048 cm^{-1} with a window finish. After return to the optical shop for application of an optical finish, the absorption coefficient was found to be 0.00185 cm^{-1}. The higher absorptions measured in the fogged optical finish samples may be a result of surface absorption caused by the fogging, but they are also partially due to the high scattering of these surfaces. Light scattered directly to the thermocouple in the calorimeter causes a temperature rise in the thermocouple which is then attributed to absorption in the sample. This phenomenon can be detected by examination of raw data. It is manifested as a component of the temperature signal, which does not have the normal time lag due to heat conduction when the laser is turned on or off.

To determine the nature of, and reasons for, fogged surfaces, two slices with window finish were coated with approximately 100 Å of evaporated gold to prevent surface charging and then examined for

TABLE XV

Absorption Measurements on KCl Samples

Slice No.	Length, cm	Finish	Absorption Coefficient, cm^{-1}	Comments
3	0.97	Window	0.00048	Not fogged.
		Optical	0.00185	Fogged while exposed for placement in calorimeter.
4	0.97	Optical	0.0014	Slightly fogged while exposed for placement in calorimeter.
7	0.89	Window	0.00050	Not fogged.
9	1.00	Optical	0.00145	Slightly fogged while exposed for placement in calorimeter.
12	0.83	Window	0.00115	Near Boule heel possible-Impurity contamination

T691-1

structural differences in the scanning electron microscope (SEM). Figure 31(b) shows a fogged surface. It is evident that the fogging of the surface is caused by recrystallization of the surface region of the crystal; the upward growing crystallites scatter light and thus produce the fogged appearance. Figure 31a shows an unfogged surface. This may be compared with the underlying surface of Figure 31b which appears at approximately the same magnification.

From other examinations, it appears that the surfaces of optical finish and window finish samples are very similar in structure. The optical finish is, however, smoother and more uniform, with a characteristic size of the features a few tenths of a micrometer, similar to that of the Linde A abrasive used to prepare it. The window finished surface has some regions with the same characteristic size as the optical finish but also has some features greater than 1 μm in size. The number and depth of scratches is also greater on the window finish surface.

Aside from indicating the need for further work on the reduction of surface roughness, the scanning electron microscope examination has not yielded any clue as to why the optical finish fogs so rapidly.

Efforts to improve the quality of the surface finish for single crystal KCl windows have been emphasized, because as we have previously reported, nearly all of the KCl samples polished at HRL had fogged surfaces shortly after polishing. Recently, this problem was brought under control by heating the KCl windows to ≈50° with an IR lamp immediately after polishing. Though it is believed this process removes water that was present on the surface as a result of the alcohol polish, it is not clear that this is the only process which leads to the increase in surface stability. The window can then be placed in a vacuum deposition chamber for coating or potted in carboline plastic for future use. Because of the hygroscopic nature of these halides, we find it is advisable to remove the carboline from the potted windows in a heated environment to avoid any reabsorption of water.

Investigation of surface roughness has also been emphasized. Scanning electron microscope studies on polished KCl windows show

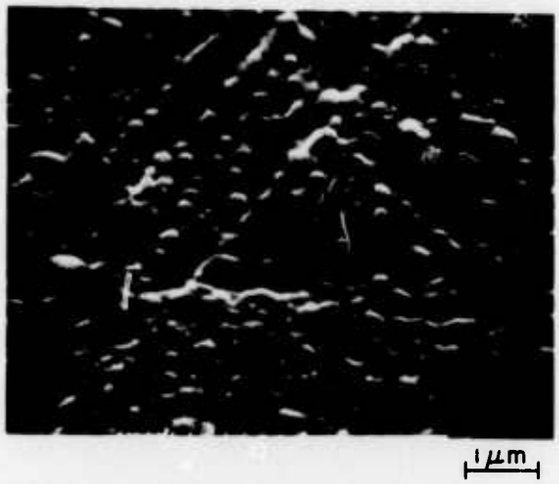

(a) Unfogged window finish

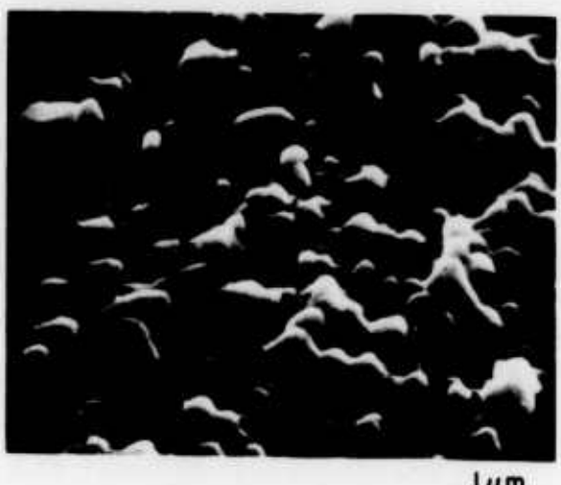

(b) Fogged window finish

Fig. 31. Scanning Electron Micrographs of Polished KCl Surfaces.

surface features of a few tenths of a micron, which is characteristic of the particle size of the polishing abrasive, Linde A. Unfortunately, dielectric coatings not only reproduce surface features, but amplify variation in the surface contour, making it even more desirable to reduce roughness to a minimum. In an attempt to reduce the roughness, Linde B, whose particle size is a few hundredths of a micron, was used as the polishing abrasive. This resulted in a smoother surface finish (see Figure 32). With these improvements, very consistent results have been obtained with absorption coefficients of 0.0015 cm^{-1} for optical finished and 0.0005 cm^{-1} for window finished samples. As indicated, the optical finish (flat within one fringe in the visible with parallel surfaces) results in a much higher absorption coefficient than the window finish (flat within a few fringes with no attempt at surface parallelism).

b. CdTe Finish

Because no major effort was placed on the study of surface roughness, cleaning and absorption as a function of surface finish, only the polishing procedure to achieve a high quality finish on CdTe windows will be discussed.

The windows are initially ground with Al_2O_3 (20 μm and 9.5 μm particle size) and then polished on a pitch lap using water as the vehicle, Linde A as the starting abrasive, and completing the procedure with Linde B. Typical calorimetric absorption values ranging from α = 0.002-0.005 cm^{-1} were obtained for these windows.

The results achieved in window coating technology to date do not reflect a limitation based only on the coating state of the art itself. The performance of the coating is greatly limited by the substrate surface finish quality prior to application of the optical coating. The KCl surface finish quality is limited by the present status of optical finishing technology and the pronounced tendency for KCl to haze and fog upon exposure to the environment prior to coating.

However, as the progress reported in this report indicates, further improvements in surface finish technology should continue with

the use of polishing agents with small grain size (10^{-3} μm or less) along with a surface cleaning procedure prior to the application of optical coatings. These improved finishing techniques will result in less surface damage, smoother surfaces, and minimum optical absorption at 10.6 μm for high power laser windows.

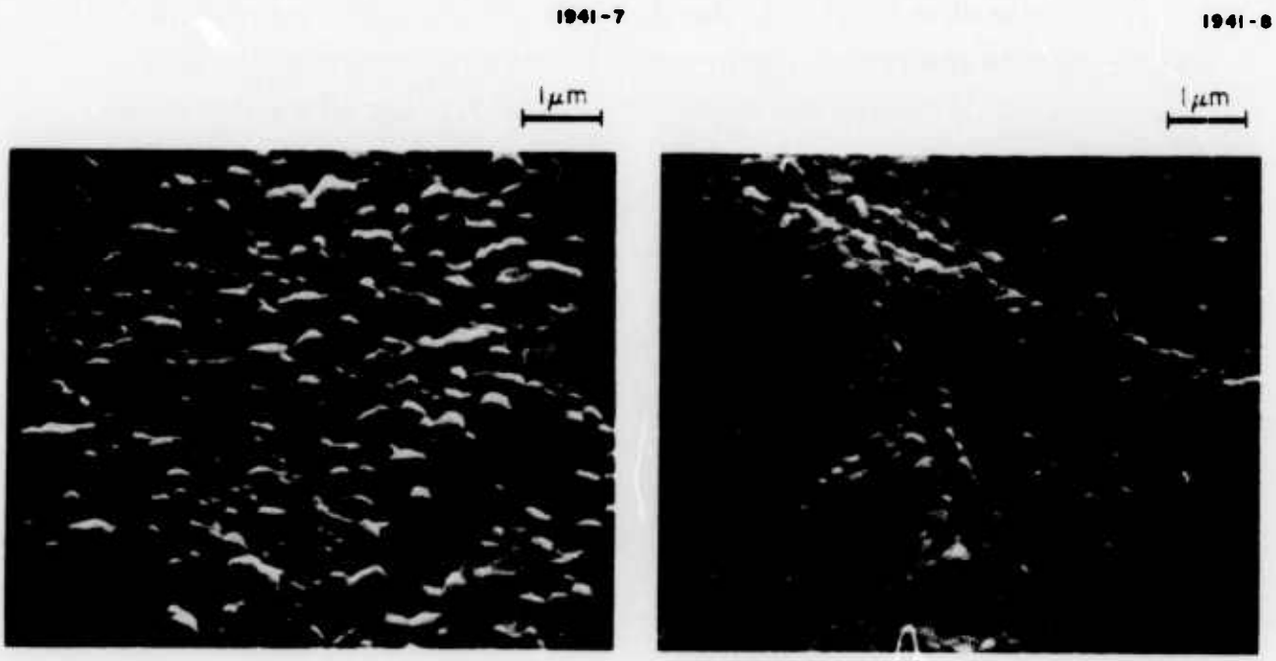

(a) Polished with Linde A (b) Polished with Linde B

Fig. 32. Scanning Electron Micrographs of Window Finished KCl Surfaces.

SECTION III

CONCLUSIONS AND RECOMMENDATIONS

A. WINDOW MATERIALS

As stated in Section I, the object in the study of window materials was to upgrade the technology of metal halides for their use for high-power lasers. Although the metal fluoride technology was given some attention, the emphasis in the study was on alkali metal chlorides (in particular, KCl and NaCl) for high-power laser windows at 10μm. Consequently, the conclusion and recommendations which follow deal with the study of alkali metal halide technology. Although the study centered on KCl, the technology is just as applicable to NaCl.

The main thesis of the materials study was that the characterization measurements by earlier workers for high-power laser window applications; e.g., optical absorption at 10.6 μm (β), mechanical strength (yield, Y, and ultimate, S), surface stability, etc., were not intrinsic to the halide materials but reflected the status of materials technology at the time. The measured quantities were parameters and not properties of the materials as to be shown by their dependence on the history of the material, (i.e., processing). We conclude from the study that the proposition has been demonstrated.

At the start of the study, window grade commercial KCl showed $\beta = 0.007\ cm^{-1}$. The development of a one-step RAP technology now produces reproducible KCl crystals up to 10-cm diameter with $\beta \leq 0.0005\ cm^{-1}$. The inequality sign is to draw attention to the limitation arising from the technology of optical finishing rather than of materials purification.

Also, at the beginning of the study, the mechanical parameters characterizing the measurements on the current KCl crystals were: Y = 300 psi and S = 640 psi (Ref. 1). The one-step RAP technology, applied to purification and crystal growth as well as annealing, have led

to an increase in Y by more than 100% and in S by as much as 500%. A similar improvement is indicated in the application of a parallel technology to metal fluorides (see Appendix VI).

The (Y, S) of the single crystal are considerably higher than those of the large-grain polycrystalline aggregate (Polytran) but low, especially in Y, compared to the very fine-grain aggregate obtained by hot pressing or the press-forged form. Although water etching shows the feasibility of achieving in single-crystal KCl, a more than one order-of-magnitude increase over the old value of S, it also shows that a value of $Y \lesssim 10^3$ psi appears to be an intrinsic limitation of the undoped material. However, the single-crystal approach based on congruently melting solid solutions of mixed halides, demonstrates the feasibility of achieving $Y \approx 6 \times 10^3$ psi or values of the yield point comparable to the press-forged metal halide.

Solution-growth procedures did not produce crystals that served to provide the standards for the melt-grown crystal. The study showed that the procedures given in the literature for the solution growth of high-crystal quality alkali metal halides fell far short of meeting the performance requirements for high-power laser windows. Continuing the study of solution growth for laser window applications is not recommended.

One can say that adequate control of anion purity, especially the exclusion of $OH^-(s)$, has been established in the study. RAP recipes for materials purification, crystal growth and annealing have been developed. Although the study treated the measurement of $[OH^-(s)]$ in the last quarter, a satisfactory procedure remains to be developed and tested for reliability. The importance of such a procedure lies in its use as a control of, and a monitor for, materials processing of metal halides.

The study also demonstrated the need for a greater depth in the investigation of the physico-chemical aspects of surface fabrication and finishing. The achievements of the one-step RAP served to emphasize the inadequacy of the current technology of surface fabrication. We regard the study of the latter as one of the frontiers in the upgrading of halide materials technology to meet the rigid requirements for high-power laser window applications.

The upgrading of halide materials technology must, of necessity, proceed by a series of approximations. It has been the good fortune of this study to have established early a recipe for the reproducible achievement of $\beta < 10^{-3}$ cm^{-1} (KCl single crystal). Subsequently, upgrading of (Y, S) became possible without exacting an exorbitant degradation in β. Of these two mechanical parameters, the primary one is Y. The upgrading in S is required in the sense that S > Y to the extent that the material is far from being brittle.

The one-component single-crystal approach upgraded S to a far greater extent than Y, maintaining $\beta < 10^{-3}$ cm^{-1}. The plastic region widened but Y fell far short of the minimum bound, 6×10^{3} psi. Our recommendation for further study, based on the single-crystal approach, is the investigation of single-crystal solid-solution mixed halides. This appears to be the most promising approach which can meet the homogeneity requirement in scale-up. An early feasibility study of the growth of large crystals should be undertaken.

For the approach based on the use of polycrystalline aggregates as laser windows, press fabrication appears to be the most practical. Press forging should start with crystals grown by the one-step RAP. This investment in the quality of the starting material is a necessity and will avoid complicating the process further. It is inherent in this process that the problems of homogeneity, (e.g., grain size distribution) will gain prominence with scale-up. For this reason, it is also recommended that the study of hot pressing, a process capable of a high degree of uniformity, be continued. This asset, which stems from the use of a powder with very small grain size, is at the moment also a drawback. The high specific surface of the material and the problems of interfaces are no doubt the causes of the degradation in β. The study demonstrated very significant improvements, indicating the necessity of developing a one-step RAP for the process.

B. WINDOW COATINGS

The major effort on the window coating task was directed toward the development of technology for producing passivation/antireflection coatings on laser windows that would have absorption at 10.6 μm of 0.1% (or less) per coated surface. This goal was attained for coatings on KCl and on CdTe substrates. The KCl coating consisted of a two-layer coating of ZnTe and ZnS, and resulted in an absorption of 0.05% per surface. The CdTe antireflection coating consists of two film layers of BaF_2 and ZnS, and resulted in an absorption of 0.06% per surface. Another coating design which was investigated for KCl, was a two-layer combination of As_2S_3 and ThF_4 which gave a best value of absorption of 0.19% per surface, (somewhat higher than the program goal requirement). The absorption in the ThF_4 film was the limiting factor in this latter case.

The performance of the coatings on KCl, in terms of their optical absorption and mechanical and surface passivation qualities, are strongly dependent on the techniques used for KCl surface finishing and the various process steps used for fabrication of the KCl window from the starting KCl powder to the final window blank. Optimum performance of the finished and coated window depends on stringent and careful quality control of all procedures and processing steps used. The level of performance we have achieved to date is a result of our focusing attention on the following procedures:

(1) Reactive atmosphere processing of the KCl crystals in a one-step RAP from powder to final crystal boule

(2) KCl boules are saw-cut to approximate window blank thickness with a wire diamond saw using Convoil fluid as a lubricant.

(3) The rough surface grinding operation is performed on a cast iron lap with SiC emery paper (No. 600) to remove gross surface roughness

(4) The final surfaces are finished dry on cloth using Linde A (Al_2O_3) abrasive and a small amount of ethyl alcohol, until the required level of flatness and parallelism is achieved. (These window finish samples are flat within a few fringes of visible light, with no attempt to achieve optimum parallelism.)

(5) Directly after polishing, the window blanks are heated up to 50°C and placed in a vacuum deposition chamber for application of the optical coatings or potted in carbofilm plastic for future use

(6) The optical coating thicknesses during coating deposition are carefully controlled using optical monitoring. Spectrophotometric transmission curves are taken of the coated windows to insure that coating thickness are accurate and to enable corrections to be made to the process if transmission of the coatings is not peaked at the 10.6 μm design wavelength.

Continued effort is required to develop surface finishing and coating technology for halide and semiconductor laser windows for use in high power infrared laser systems. The ultimate achievement that is required is to provide a technology for window surfaces and coatings with high-power laser damage thresholds as close as possible to the intrinsic threshold of the bulk window materials. The results achieved in window coating technology to date are still limited by the present coating state of the art and by the substrate finish quality prior to application of the optical coating. Further improvements in surface finishing technology should be continued with the use of polishing agents with small grain size (10^{-3} μm or less) along with investigation of surface cleaning procedures to be used prior to the application of the optical coatings. The improvements in the surface finishing techniques should result in less surface damage, smoother surfaces and minimum optical absorption at 10.6 μm. The important aspect of future finishing work should be to develop a technology which will also permit the achievement of the window flatness and parallelism needed for operational laser systems. In our work to date we have not been able to meet the latter requirements without suffering some increase in absorption in the KCl window over the intrinsic material property.

APPENDIX I

REACTIVE ATMOSPHERE PROCESSING OF ALKALI HALIDES

If one considers what mechanisms may be responsible for excess 10-μm optical absorption in alkali halides, the hydroxyl ion (OH^-) coupled to a lattice metal ion looms as a major possibility. Since OH^- has its source in water, a ubiquitous material, it is likely to be present in relatively large amounts unless it is stringently controlled. Achievement of such control was, therefore, a major initial effort in early phases of the high power laser window programs at Hughes Research Laboratories.

Contamination with OH^- occurs through hydrolysis in the presence of water vapor at the elevated temperatures necessary for crystal growth. This process is summarized in the simple reaction equation, written here for chlorides,

$$Cl(c) + H_2O(g) \rightleftharpoons OH^-(c) + HCl(g) \qquad (14)$$

which tells us that in the presence of water in the gas phase (g) a chloride ion in the condensed phase (c) is replaced by a hydroxyl ion with the production of HCl. From the equilibrium relation for this reaction, we find that the ratio C, of hydroxyl ion to chloride ion in the solid is given by:

$$C = \frac{[OH^-(c)]}{[Cl^-(c)]} = K_1 \frac{p_{H_2O}}{p_{HCl}} \qquad (15)$$

where K_1 is the equilibrium constant and the p's are partial pressures.

Since the objective is to achieve a low value of C, one must remove the H_2O and provide HCl. The use of vacuum or an inert gas is not wholly effective in achieving a small C because P_{H_2O} is never zero, while P_{HCl} is essentially zero in those circumstances.

The first alternative that suggests itself is to use an HCl atmosphere, a procedure which has been effective in the analogous problem with fluorides. However, the halogen acids are corrosive and in a flowing system, corrosion of the ducts by HCl provides a means for contamination. This disadvantage is overcome in a closed system. But, if such a system were to remain compact and held to ordinary pressures, the amount of HCl available for exchange is very limited.

The use of a noncorrosive and a condensed system, which can act as an exchange agent, overcomes these drawbacks. Since H_2O is a component that cannot be easily excluded, it is best to adopt a reaction that converts $H_2O(g)$ to HCl to favor a low value of C in eq. (15). Examples are

$$\left.\begin{aligned} SOCl_2 + H_2O &= SO_2 + 2HCl \\ COCl_2 + H_2O &= CO_2 + 2HCl \\ CCl_4 + 2H_2O &= CO_2 + 4HCl \end{aligned}\right\} \qquad (16)$$

Each of these compounds exhibits a corresponding exchange reaction with OH^- in the crystal. With CCl_4, the exchange cycle per molecule of CCl_4 consumed is

$$2OH^-(c) + CCl_4(g) = 2Cl^-(c) + CO_2(g) + 2HCl(g) \qquad (17)$$

There is an advantage to the use of CCl_4 in that thermal dissociation occurs at $\leq 300^{\circ}C$, yielding two reactive species,

$$CC\ell_4 \rightarrow CC\ell_3 + C\ell \tag{18}$$

There are five possible reaction paths for the products of this dissociation. One obvious path is the reverse of eq. (18). Two paths are accounted for by

$$2CC\ell_3 \rightarrow C_2C\ell_6 \tag{19}$$

and

$$2C\ell \rightarrow C\ell_2 \tag{20}$$

Both products in eq. (19) and eq. (20) serve as indicators of the progress of the reaction. The C_2Cl_6 deposits as fine needles on the colder parts of the apparatus, and Cl_2 imparts a yellow color to the source (liquid CCl_4).

The remaining two paths are the scrubbing reactions of CCl_3 and Cl on the crystal's surface layer. Quite likely, the deepest penetration is effected by Cl. The atomic radius of Cl is $\sim$0.94 Å, while Cl^- is 1.81 Å. In RAP applied to the crystal, its diffusion into the bulk may also be greatly enhanced by a resonance-type electron transfer, $Cl + Cl^-(s) \rightarrow Cl^- + Cl(s)$, etc. In such a case one does not have to rely on OH^- diffusing out all the way to the surface for the exchange reaction.

Among the halogens, chlorine has the largest electron affinity (unit: eV): F, 3.58; Cl, 3.81; Br, 3.54; I, 3.29; and OH, 1.73. This feature provides the drive for the electron transfer process,

$$C\ell(c) + OH^-(c) \rightleftharpoons C\ell^-(c) + OH(c) \tag{21}$$

The formation of molecular chlorine from the atomic form, eq. (20) preserves the potential for exchange:

$$Cl_2(g) + OH^-(c) \rightleftharpoons Cl^-(c) + HCl(g) + 1/2\ O_2(g) \qquad (22)$$

It should be noted that the use of Cl_2 in RAP includes the advantage derived from the use of HCl, as shown in eq. (14). The reason for this is seen in eq. (22) which shows that HCl is a product of the action of Cl_2 on OH^-. By the same token aside from the corrosion factor, the use of CCl_4 is an optimum because of the benefits derived from the generation of nascent (atomic) chlorine which in turn can produce molecular Cl_2.

Equations (14) and (22) are not independent. They are related through a well known reaction (the Deacon process):

$$C\ell_2(g) + H_2O(g) \rightleftharpoons 2HC\ell(g) + 1/2O_2(g) \qquad (23)$$

It follows that a form like eq. (15) can be derived with

$$K_1 = K_{25}/K_{22} \qquad (24)$$

where the subscripts of the equilibrium constants at the right hand side identify the respective reactions.

The second degradation which shows further advantage in the use of CCl_4, is the formation of phosgene by a scavenging action on H_2O from outgassing of the apparatus,

$$CCl_4(g) + H_2O(g) \rightleftharpoons COCl_2(g) + 2HCl(g) \qquad (25)$$

Phosgene, in turn, hydrolyzes readily to form more HCl:

$$COCl_2(g) + H_2O(g) \rightleftharpoons CO_2(g) + 2HCl(g) \qquad (26)$$

The parameter P_{H_2O}/P_{HCl}, the decisive factor in eq. (15), is sensitively dependent on either eq. (25) or eq. (26), because 2 moles of HCl are formed at the expense of 1 mole of H_2O.

The reactive atmosphere is effective at all stages of crystal preparation, purification, crystal growth, and anneal. The use of reactive atmosphere processing (RAP) adds another component to the system. Naturally, the equilibrium behavior (e.g., solid-melt) deviates from the thermodynamic behavior reported in the literature. For instance, (a) the melting points are observed to be higher, (b) solid-solid transitions in one-component systems disappear, (c) incongruent behavior reported for certain binary compounds (two-component halides) is lifted, (d) composition is shifted for congruent behavior of solid solutions of mixed halides, etc. These changes in physical behavior are accompanied by changes in the measured physical "properties" of RAP crystals. For example, optical absorption at the 3-μm and 10-μm regions, thermal conductivity, electrical conductivity, mechanical hardness, yield strength, ultimate strength, etc., effects important for high-power laser windows.

The process parameters of KCl and NaCl allow the merger of purification and crystal growth into a one-step RAP (refer to Section III. A). The study demonstrated that a fairly cheap starting material (less than a dollar a pound), 99.9% pure or mole fraction of metal ion impurities $x \approx 10^{-3}$, can be employed. Most likely, the process can utilize a lower grade starting material, but this is not an advantage. The longer processing time incurred by the use of lower purity starting materials provides the limiting factor. The case just considered is dynamic RAP (flowing system).

For purposes of scale-up, compact configurations are desired. Hence, it is of interest to determine the order-of-magnitude upper bound in x which renders feasible a closed-system RAP crystal growth. With no sacrifice in generality, let MO be an oxide impurity (say, in a KCl melt) and consider the following scavenging action,

$$MO(c) + CC\ell_4(g) \rightleftharpoons MC\ell_2(c) + COC\ell_2(g) \qquad (27)$$

Again, it is instructive to write the equilibrium constant, K_{27}, as follows,

$$\frac{[MO(c)]}{[MC\ell_2(c)]} = \frac{1}{K_{27}} \cdot \frac{P_{COC\ell_2}}{P_{CC\ell_4}} \qquad (28)$$

Obviously, to achieve a very small value of the ratio on the left-hand side of eq. (28), a large value of P_{CCl_4} should be applied. In a large scale operation, this choice is not too practical in a closed system. In a sealed-off quartz apparatus, $P_{CCl_4} \approx 150$-mm Hg at room temperature, or a vapor-phase concentration of $c = 8 \times 10^{-6}$ mole cm^{-3}.

The other alternative to displacing reaction (27) forward is: Moles CCl_4 >> Moles MO, i.e.,

$$cV >> nx \ , \qquad (29)$$

where V is the volume of the vapor phase, c is as defined in the preceding paragraph, n is the moles of KCl, and x is the mole fraction of the impurity MO.

It follows from equation (29) that,

$$x << c\left(\frac{V}{v}\right)\Big/\left(\frac{n}{v}\right) \ , \qquad (30)$$

where v is the volume of the melt. For KCl, $n/v = 2.5 \times 10^{-2}$ mole cm^{-3}. For compact operation in a closed system, $V/v \approx 3$, which approximates the volume ratio of the powder charge to the melt. Therefore, from eq. (30), the tradeoff to a closed-system RAP crystal growth operation is that: $x << 10^{-3}$, i.e., the starting material should be at least four-nines pure.

APPENDIX II

OPTICAL ABSORPTION OF POTASSIUM CHLORIDE AT TEN MICRONS

The calorimetric absorption coefficient at 10.6 μm, α, has been measured in NaCl, KCl, and KBr (Harshaw optical crystals).[1] A linear fit of fractional power absorbed by the sample, P_a/P_o, against sample thickness, L, extrapolated to L = 0, indicated a large surface absorption 2σ, in each case.[1] The behavior was attributed to the hygroscopic character of the crystals.[1,22] We report here an assessment in KCl of the effect of surface hydrolysis and hygroscopic behaviors on α, and a study of the dependence of P_a/P_o on L. The effects on α of bulk purification, annealing, reworking the surface and the polishing vehicles used, are also presented.

Single crystals of KCl, 1- to 2-cm diameter, were pulled from the melt using a vitreous carbon crucible (Beckwith Corp.). The starting powders were Matheson, Coleman, and Bell (MCB) 99.9% pure and Johnson Matthey (JM) 99.999%. In one of the runs the starting material was a zone refined ingot from the MCB source.[23] The steady-state growth rate was ≤ 1 cm hr^{-1}. Only the steady state sections of the crystals were employed for the measurements described below. Sections of various thicknesses were obtained by cleaving at (100). The surfaces were polished using a suspension of Linde A in ethanol.

The optical absorption of the material was measured using the optical calorimeter technique.[24] The technique is shown schematically in Fig. 33. The sample is irradiated with power P_i from a CO_2 laser, and the resulting temperature rise with time $\Delta T/\Delta t$ is measured. The optical power absorbed by the sample P_a is given by

$$P_a = \frac{(1 - R)(1 - e^{-\alpha L})}{(1 - Re^{-\alpha L})} P_i \qquad (31)$$

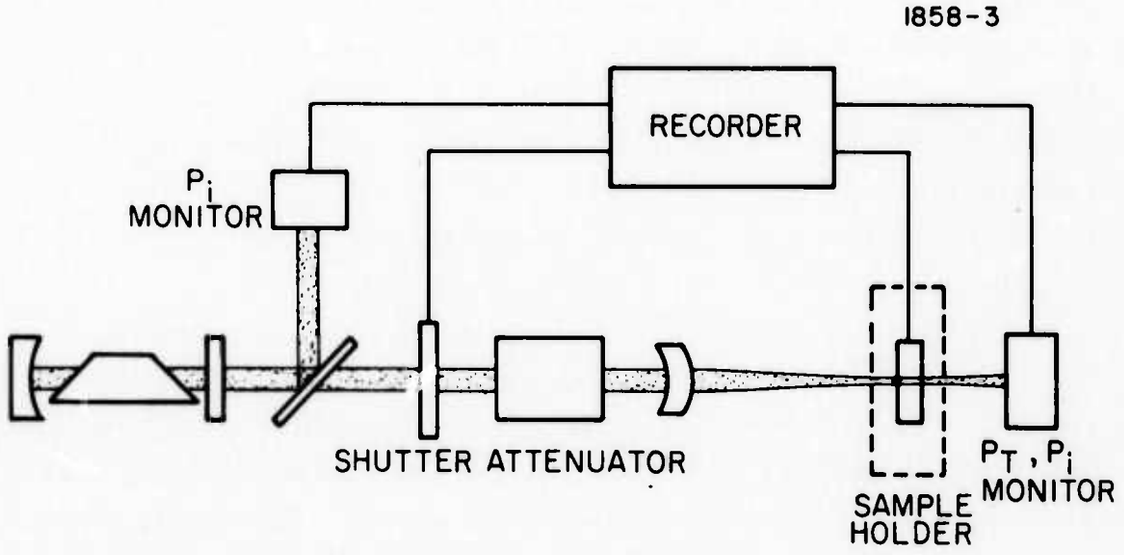

Fig. 33. Laser Calorimeter Schematic.

which is the expression for the power absorbed by a sample of thickness L, absorption α and surface reflectance R where $R = (n-1/n+1)^2$. The expression is derived by assuming multiple surface reflections and summing for multiple passes through the sample.

If this expression is then expanded in a Taylor's series, the result is

$$\frac{P_a}{P_i} = \alpha L \left[1 - \left(\frac{1 + R}{1 - R}\right) \frac{\alpha L}{2} + \ldots.\right] \tag{32}$$

For

$$\left(\frac{1 + R}{1 - R}\right) \frac{\alpha L}{2} << 1 \tag{33}$$

the absorbed power can be approximated by

$$P_a \approx \alpha L P_i \tag{34}$$

This treatment assumes no interference effects; i. e., the sample is non-resonant.

For the case of a sample with parallel faces and normally incident beam; that is, when the reflected beams interfere, the expression used for the absorbed power P_a is

$$P_a = \alpha L \left(\frac{n^2 + 1}{2n}\right) P_T \tag{35}$$

where P_T is the power transmitted through the sample. This equation is derived in Ref. 24. From the calorimeter data, the absorbed power is

$$P_a = mC \frac{\Delta T}{\Delta t} \quad , \tag{36}$$

where m and C are the sample mass and specific heat. The absorption coefficient is obtained from the calorimeter working equation, where

$$\alpha = \frac{mC}{LP_o} \cdot \frac{\Delta T}{\Delta t} \tag{37}$$

$$P_o = P_i \text{ or } \left(\frac{n^2 + 1}{2n}\right) P_T \quad . \tag{38}$$

For the study of the effect of surface hydrolysis on surface absorption at 10.6 μm, KCl random cuts (Harshaw Chemical Co., Cleveland, Ohio) were used. The equilibrium constant, K, of hydrolysis,

$$Cl^-(s) + H_2O(g) \rightleftharpoons OH^-(s) = HCl(g) \quad , \tag{39}$$

is given as follows,

$$\frac{[OH^-(s)]}{[Cl^-(s)]} = K \frac{P_{H_2O}}{P_{HCl}} \tag{40}$$

The symbols (s) refer to the surface layer where the anion concentrations are represented in brackets and (g) to the vapor phase where the concentrations of molecular species are given as partial pressures. To favor the displacement of reaction (39) from right to left, the crystals were subjected to the halide gas (flowing system with He as the carrier gas) at 500°C for 16 hours and cooled to room temperature under the same atmosphere. The crystal specimens for the measurements were generated by cleaving at (100) and polished initially with Linde A in ethanol. For the first specimen, L = 0.68 cm, P_a/P_o before and after the treatment was 21.8×10^{-4} and 22.4×10^{-4}, respectively. Similarly, for the second specimen, L = 1.01 cm, the respective values were

24.2×10^{-4} and 21.2×10^{-4}. It is concluded that under ambient conditions surface hydrolysis provides a negligible contribution to surface absorption at 10.6 μm.

For the study of crystal surface corrosion by water vapor, define P_{H_2O} as the ambient vapor pressure at a given temperature, and $P^{*}_{H_2O}$ and $P^{o}_{H_2O}$ as the vapor pressures of the saturated solution and the solvent, respectively, at the same temperature. The three regions of interest are:

(A) Dewpoint or Precipitation Region, where $P_{H_2O} \geq P^{o}_{H_2O}$

(B) Deliquescence Region, where $P^{*}_{H_2O} < P_{H_2O} < P^{o}_{H_2O}$

(C) Efflorescence Region, where $P_{H_2O} \leq P^{*}_{H_2O}$.

The consequence of a short residence time in (A) will be taken up in a separate publication. In (B), a deliquescent behavior of KCl or NaCl can be conditioned by impurities, although the pure crystals are not even hygroscopic at ordinary pressures and temperatures.[22] In (C), the KCl surface should remain stable indefinitely if its surface free energy equals that of the material employed to saturate the solution. In general, this equality is not realized and the inequality can go either way. Consequently, the study of hygroscopic behavior in (C) was chosen and is described in the following.

A large bell jar housed the optical calorimeter (crystal and reference). Then temperatures of the vapor phase and the humidostat were monitored and heat lamps were positioned outside the bell jar. Although a dynamic measurement of α by eq. (37) was not possible in this setup, resetting the calorimeter in the optical bench and starting a measurement could be realized within 5 min. A saturated aqueous

solution with excess KCl powder was used as the humidostat. Vapor pressure data show that saturated KCl solution maintains an 80% humidity from 20 to 90°C (75% for saturated NaCl solution); i.e., essentially, the same heat of vaporization as in pure water.

The deviation in the values of α shown in Table XVI is ±10%; the steps are listed in chronological order. During heatup, incipient clouding was observed in ~10 min, at which time the gas-phase temperature was 40°C. This condition never progressed further, even with a 3-hour exposure at 65°C and P_{H_2O} = 110 mm. Such surface condition persisted for the duration of the steps that followed. If it affected α, the effect is small enough to be beyond the given precision and, as the data suggest, possibly reversible. These results rule out hygroscopic behavior as the cause for surface absorption in the KCl specimens under study.

The results of absorption measurements at 25°C for three samples of KCl given in the sequence (L in cm, $10^4 P_a/P_o$, N) are listed below; N stands for the cumulative number of cleavages at (100) for the preparation of the specimen.

Sample 1 (2.05, 32.8, 2), (1.10, 15.4, 3), (0.95, 14.3, 3), (0.56, 8.96, 4), (0.51, 9.69, 4), and (0.27, 4.05, 5).

Sample 2 (2.10, 10.5, 2), (1.15, 8.05, 3), (0.89, 8.01, 3), (0.66, 8.58, 4), and (0.49, 7.35, 4).

Sample 3 (2.52, 23.9, 2), (1.90, 22.8, 3), (1.26, 11.5, 3), (1.22, 14.6, 3), (0.61, 9.15, 4), and (0.57, 8.55, 4).

The value of α, calculated from eq. (37), is derived from P_a/P_o, the total power absorbed with the contributions broken down as follows:

$$\left(\frac{P_a}{P_o}\right)_i - \frac{y_o}{L_o} L_i = 2\sigma + N_i A + \ldots , \qquad (41)$$

TABLE XVI

Absorption Coefficient at 10.6 μm Versus Humidity and Temperature Exposures

Sample: HRL Czochralski Grown KCl Crystal; Cleaved, Scrubbed, and Polished in CH_3OH-Linde A			
Cumulative Time, hr	Vapor Phase Temperature,* °C	P_{H_2O}, mm	α, cm^{-1}
0	25	10	0.0044
+ 2.5	25	19	0.0044
+60.0	25	19	0.0046
+ 3.0	65	110**	0.0046†
+ 3.0	25	10	0.0048
+15.0	25	10	0.0042

*Assumed to be the equilibrium temperature of the crystal.

**Temperature of the humidostat (saturated KCl solution) was 58°C.

†After a 1 hour cooling to match crystal and reference temperature to ambient (25°C).

T566

where i runs through all the specimens of each sample. The subscript o refers to the thickest specimen with $N_o = 2$; Y_o is the bulk absorption optimized for the given sample; i. e., $2\sigma = 0$ and $A = 0$. Surface absorption; treated as a constant of the sample, is given by 2σ. From the preceding studies, surface hydrolysis and hygroscopic behavior, 2σ is assumed to be negligible.

After cleaving at (100), subsurface damage, in the form of slips at (110) propagated into the bulk, are seen in the specimen observed between crossed polaroids. Using a given cleaving procedure, it is assumed that the contribution to bulk absorption per cleaving may be characterized in eq. (41) by a constant A for each sample. A thick cleaving tool was used for Sample 1, and a thin single edge razor blade for Samples 2 and 3.

Other contributions to the right-hand side of eq. (41) can come from surface reworking and the chemicals used in polishing. In the present case, these contributions were held down to values beyond the precision of the measurements in order that one may examine eq. (41) for the case $A = 0$ (Model I) and the case of $2\sigma = 0$ (Model II).

Were $A = 0$ and $2\sigma = 0$, $(P_a/P_o)_i$ versus L_i would yield a zero intercept. The bulk absorption coefficient is given by the slope, y_o/L_o. Each sample has essentially a constant geometrical cross section. Therefore, y_o/L_o will contain contributions to the absorption arising from sources distributed homogeneously in the bulk; e. g., dissolved impurities, scattering centers, etc.

In Model I ($A = 0$), the least-square treatment of the data $(P_a/P_o)_i$ and L_i, yields 2σ and y_o/L_o. In Model II, the least-square treatment of the data, $(P_a/P_o)_i$, L_i, and N_i, yields A and y_o/L_o. Using A one obtains $(P_a/P_o)_i'$, the power absorbed corrected for the cumulative contribution of damage by cleaving:

$$(P_a/P_o)_i' = (P_a/P_o)_i - N_i A \quad . \tag{42}$$

The least-square treatment of a linear dependence of $(P_a/P_o)_i'$ on L_i serves to test the assumption that $2\sigma = 0$. The slope corresponds to α_c, which for consistency should be close to the value of y_o/L_o. The plots of $(P_a/P_o)_i$ versus L_i (Model I), and $(P_a/P_o)_i'$ versus L_i (Model II) are shown in Figs. 34 and 35 for Samples 1 and 2 which typify two extremes in behavior by Model I. A comparison of the two models for the three samples is given in Table XVII.

Sample 1 shows the lowest damage parameter A; consequently, a good linear fit results with both models (see Fig. 34). Still, there is an improvement from Model I to II of a one order-of-magnitude reduction in 2σ. Compared to Sample 1, Samples 2 and 3 show an increase of about two orders of magnitude in A. Consequently, a large 2σ results in Model I (see Fig. 35). A value of 2σ of $\pm 0.3 \times 10^{-4}$ may be taken as zero within the accuracy of the measurements. The entries are given one digit beyond the significant figure merely for comparisons between the two models. Note in Sample 2 that a large 2σ is accompanied by a fictitiously low y_o/L_o in Model I. It is seen that y_o/L_o increases from Model I to II; the latter approaching from the low side of the experimental value $(P_a/P_o)_o/L_o$. For $L_i = L_o$, cleaving damage contributes the least because $N_o = 2$.

The improvement in the value of the bulk absorption coefficient, y_o/L_o, with purification of the starting material in crystal growth is seen in a comparison of Samples 1 and 2 (Table XVII). Good agreement is seen between y_o/L_o and α_c in Model II (Table XVII). The correlation coefficient to a linear fit improves from Model I to II (Table XVII). In summary, the results support the two assumptions of Model II, 2σ is negligible and A can be treated as a constant of the sample.

The results of annealing (50 hour treatment at 700°C) Sample 3 specimens also support Model II: KCl fabricated specimen (cleaved and polished) with $L = 1.90$ cm gave from eqs. (33) and (37) $\alpha = 0.0012\ \text{cm}^{-1}$ before anneal and $\alpha = 0.00063\ \text{cm}^{-1}$ after anneal; another piece with $L = 1.22$ cm gave $\alpha = 0.0012\ \text{cm}^{-1}$ before and $\alpha = 0.00053\ \text{cm}^{-1}$ after anneal. The values after anneal are almost a

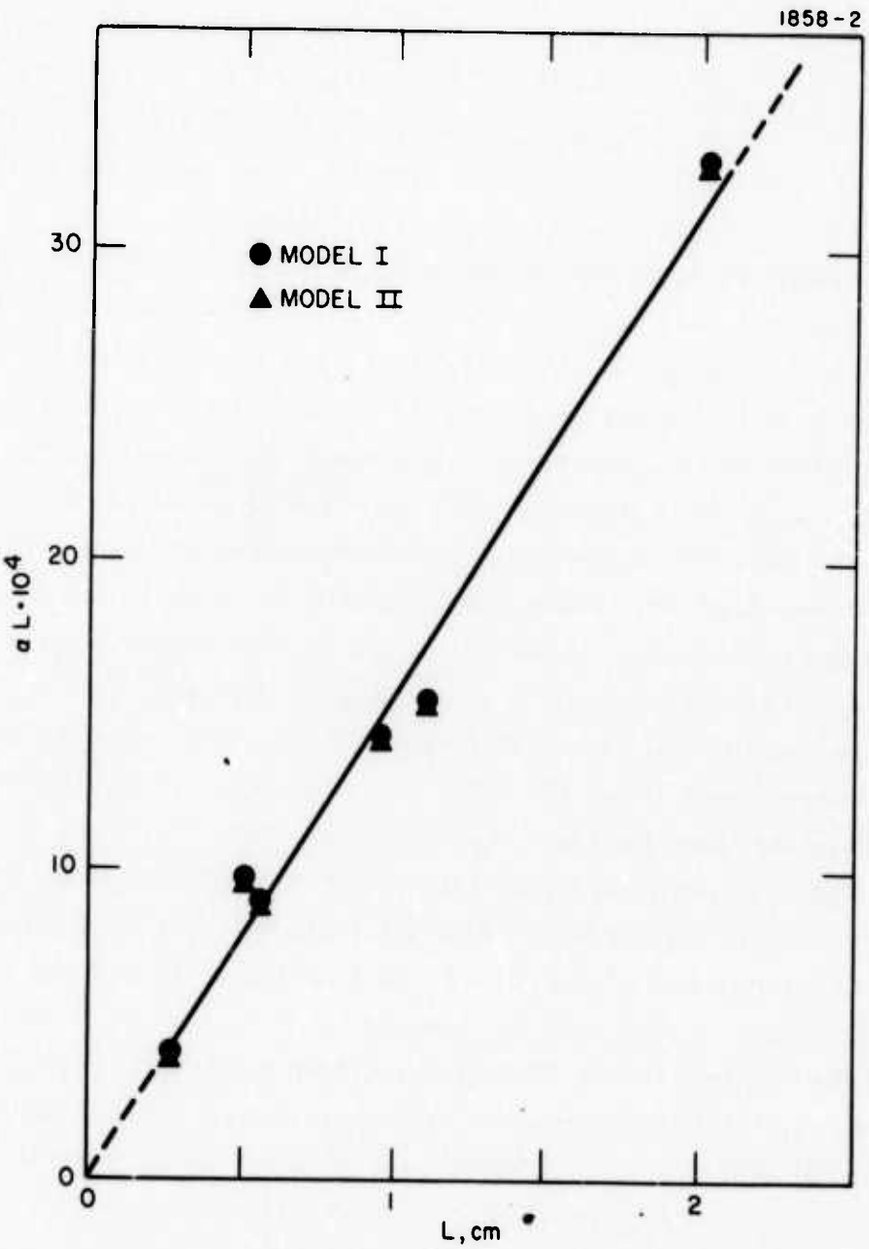

Fig. 34. Optical Absorption of KCl (Sample 1) at 10.6 μm Versus Thickness: ● Model I. ▲ Model II.

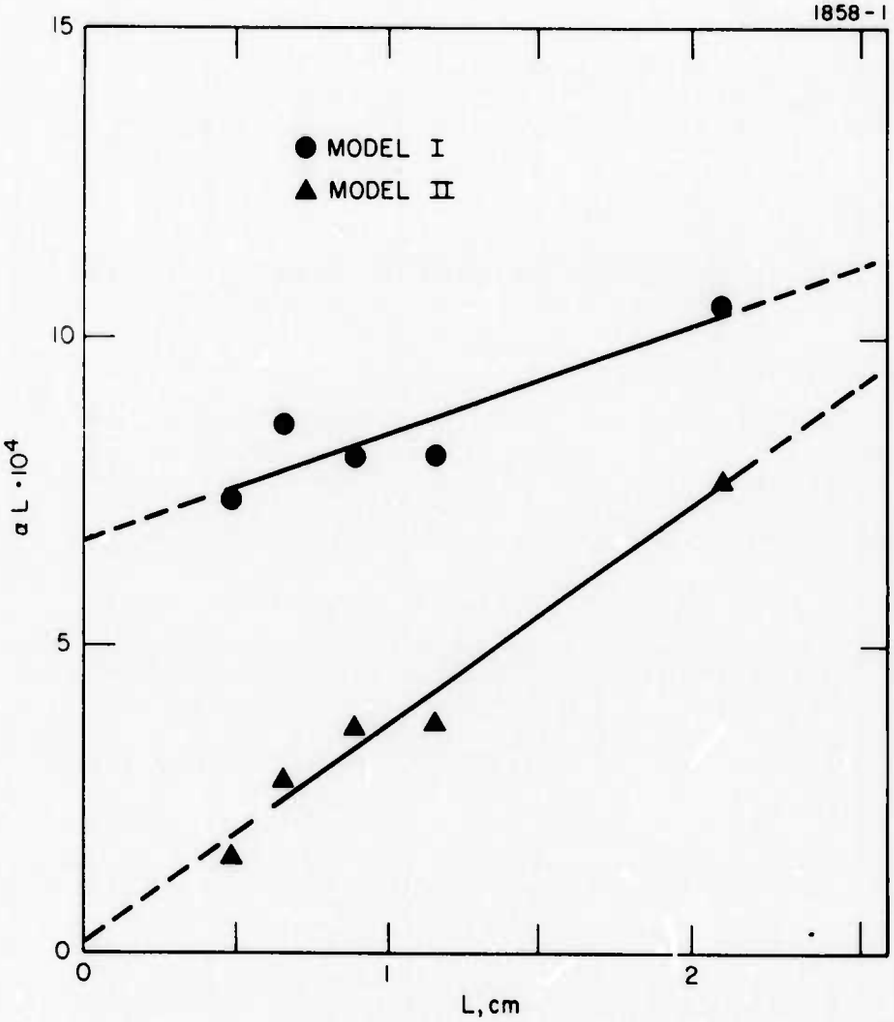

Fig. 35. Optical Absorption of KCl (Sample 2) at 10.6 μm Versus Thickness: ● Model I. ▲ Model II.

TABLE XVII

Comparison of Models I and II in KCl

Measurement	Model I	Model II
$2\sigma \cdot 10^4$	0.09	0.01
$(y_o/L_o) \cdot 10^4$, cm^{-1}	—	15.7
$\alpha_c \cdot 10^4$, cm^{-1}	15.6	15.6
$A \cdot 10^4$ cm^{-1} $cleave^{-1}$	—	0.01
Correlation Coefficient	0.993	0.993
Sample 2[a]		
$2\sigma \cdot 10^4$	6.69	0.19
$(y_o/L_o) \cdot 10^4$, cm^{-1}	—	3.73
$\alpha_c \cdot 10^4$, cm^{-1}	1.71	3.51
$A \cdot 10^4$, cm^{-1} $cleave^{-1}$	—	1.44
Correlation Coefficient	0.903	0.985
Sample 3[a]		
$2\sigma \cdot 10^4$	3.53	-0.23
$(y_o/L_o) \cdot 10^4$, cm^{-1}	—	9.16
$\alpha_c \cdot 10^4$, cm^{-1}	8.58	9.38
$A \cdot 10^4$, cm^{-1} $cleave^{-1}$	—	0.85
Correlation Coefficient	0.957	0.969

[a]Sample 1 grown directly from MCB (99.9%) KCl powder. Sample 2 was grown from the ingot obtained by a three-pass zone refining of MCB (99.9%). Sample 3 was grown from JM (99.999%) KCl powder.

T675

factor of two lower than the value of α_c for Sample 3 (Table XVII) and are in line with the results of Sample 2.

The effect on α of surface reworking, as shown in Table XVIII, indicates that the measure value may still have been affected by damage introduced by the polishing operation. Such damage is easily observed using polarized light on an annealed specimen, before and after polishing. Thus, it is very likely that with improved techniques in polishing, a value of α_c for KCl $\leq 3.5 \times 10^{-4}$ cm^{-1} can be obtained.

A genuine surface absorption effect can arise from the type of liquid vehicle employed in the polishing operation. This effect was demonstrated in a cleaved KCl as follows:

Step 1 — Faces were smoothed with 3/0 emery paper and polished with Linde A in ethanol: $\alpha = 0.0016 \pm 0.0002$ cm^{-1} and L = 0.92 cm.

Step 2 — Faces again were roughened with 3/0 emery paper and polished with Linde A in glycerine-H_2O (1:1) saturated with KCl at pH $\leq$ 1 (using HCl): $\alpha = 0.0060 \pm 0.0002$ cm^{-1} and L = 0.90 cm.

Step 3 — Faces roughened with 3/0 emery paper and polished with Linde A in ethanol: $\alpha = 0.0016 \pm 0.0001$ cm^{-1} and L = 0.90 cm.

The source of the surface absorption, which accounts for three times the uncorrected value for the bulk, is shown in a comparison of the IR transmission (Beckman IR-12 spectrophotometer) of the specimen after Steps 1 and 2 (see Fig. 36). The absorption in the 3-μm region (curve 2 for Step 2) can be due to O-H and C-H. In view of the low pH employed, such species of OH is not OH^- as resulting from hydrolysis, but the functional group of the polyhydric alcohol (glycerine). The C-O and C-C vibrations would account for the absorption envelope at the 9.5-μm region which is seen to extend past 10.6 μm. The pertinent difference

TABLE XVIII

The Value of α in A_1' (m = 0.67 g, L = 0.27 cm) Versus Surface Treatment*

Chronological Order	Surface Treatment	α, cm^{-1}
Step 1	After cleaving	0.0043
Step 2	Polished	0.0067
Step 3	Repolished	0.013
Step 4	Repolished	0.015
Step 5	Annealed	0.0020
Step 6	Polished	0.0015

*The beam was positioned at the geometric center. Polishing was carried out with Linde A in ethanol.

T570

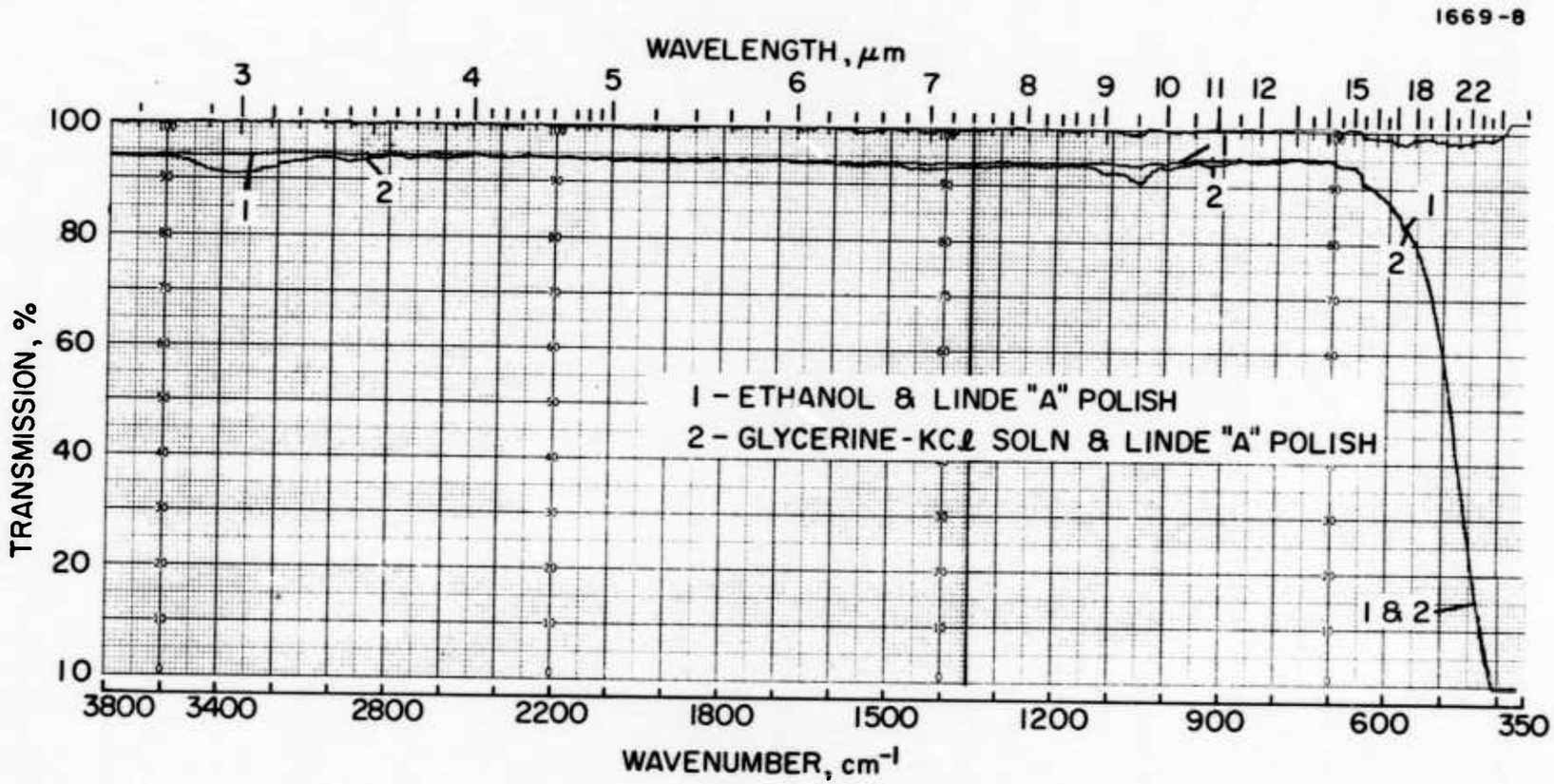

Fig. 36. Transmission of a KCl Crystal Specimen Polished with Linde A in Ethanol (Curve 1) and Then Polished with Linde A in a Glycerine H_2O Solution Saturated in KCl and pH $\lesssim$ 1 (Curve 2).

in the polishing procedures for Steps 1 and 2 resides in the volatility of the alcohols: At 25°C, the vapor pressure of C_2H_5OH is 56 mm, while $C_3H_5(OH)_3$ is 4.5×10^{-4} mm. This result shows the importance of avoiding incorporation in the surface (Beilby) layer of materials that provide an M-O linkage (M = C or some other element); e.g., the abrasive (Al_2O_3) or even the wax coating of the lap.[25]

We have shown that surface hydrolysis and hygroscopic behaviors are negligible causes for surface absorption. However, the contribution of fabrication damage to the measurement of α is not negligible. If such effect is not taken into consideration, the extrapolation of total absorption to L = 0 can be misinterpreted as a contribution from the surface. A contribution to surface absorption can come from the type of chemicals employed in the polishing operation.

An improvement in the bulk absorption coefficient from $\alpha = 1.6 \times 10^{-3}$ cm^{-1} to $\alpha = 3.5 \times 10^{-4}$ cm^{-1} was shown to result from purification. The results of annealing and polishing studies indicate that improved techniques in surface preparation are necessary to achieve reproducibly $\alpha < 10^{-3}$ cm^{-1}.

APPENDIX III

ABSORPTION SPECTROPHOTOMETRY IN THE CRYSTAL

The object is to derive a figure of merit for the method in terms of C_{min}, the lower limit in the mole fraction of OH^- in the crystal. The optical absorption is described by,

$$I = I_o e^{-\alpha L} \tag{43}$$

where L = thickness and α in cm^{-1} the absorption coefficient at the peak wavelength in question and is given by,

$$\alpha = N\sigma \ . \tag{44}$$

Now, N in cm^{-3} is the density of absorbers and σ in cm^2 is the absorption cross-section. The density of absorbers, N, is related to C, the mole fraction of OH^-(s),

$$N = \left(\frac{N_o \rho}{[MX]}\right) C \tag{45}$$

where the proportionality factor refers to the ion density of the host; N_o = Avogadro number, ρ = crystal density, and [MX] = the molecular or formula weight of the metal halide.

In absorption spectrophotometry, D, the experimentally measured optical density is given by

$$D = \alpha L \ . \tag{46}$$

It follows from eqs. (44) to (46) inclusive that,

$$C = \frac{[MX] \cdot D}{N_o \rho \sigma L} \qquad (47)$$

As a figure of merit for the method we calculate C_{min}. Realistic values are $D_{min} = 0.01$ and $L = 1$ cm. Now, $N_o = 6.023 \times 10^{23}$. For NaCl, $[MX] = 58.44$ and $\rho = 2.165$ g cm^{-3}; for KCl, $[MX] = 74.56$ and $\rho = 1.984$ g cm^{-3}. Therefore, from eq. (47),

$$C_{min} = 4.48 \times 10^{-25}/\sigma \text{ for NaCl}$$

$$C_{min} = 6.24 \times 10^{-25}/\sigma \text{ for KCl.}$$

APPENDIX IV

SOLUTION ACIDIMETRY OF ALKALI HALIDE CRYSTALS

The interpretation of acidimetric procedures considered below is based on the assumption that when the alkali halide crystal is dissolved in water, the $[OH^-(s)]$, expressed as a mole fraction, C, is solely responsible for the shift in acidity.

Consider first the procedure based on a pH-shift measurement. The fundamental constraint in the solvent (H_2O) is,

$$[H^+]\,[OH^-] = K_w \quad . \tag{48}$$

The ionization constant of the solvent, K_w, is assumed to be invariant over the electrolyte concentration range employed, ≤ 1 M (M = molar). Using the least hydrolyzed case as our C = 0; i.e., the reference, $[H^+] = 10^{-pH_o}$ and $[OH^-] = 10^{-(pK_w - pH_o)}$. For the hydrolyzed case, eq. (48) yields,

$$[10^{-pH_o} - y]\,[10^{-(pK_w - pH_o)} + 10^{pC} - y] = 10^{-pK_w}\,, \tag{49}$$

where y is the concentration reacted to attain equilibrium. As a matter of convenience, we have adopted a 1-M concentration of the halide crystal so that C, the mole fraction of $OH^-(s)$ in the solid, is also the molarity of OH^- in solution.

In the case of KCl, preliminary observations suggest a reference value of $pH_o = 5.6$ at 1 M in KCl. Since $pK_w = 14.0$, it follows that,

$$10^{-pH_o} >> 10^{-(pK_w - pH_o)} \quad . \tag{50}$$

From eqs. (49) and (50),

$$y \approx \frac{(10^{-pH_o} + 10^{-pC})}{2} \left\{ 1 - \left[1 - \frac{10^{-(pH_o+pC-0.602)}}{(10^{-pH_o} + 10^{-pC})^2} \right]^{1/2} \right\}. \qquad (51)$$

Note that the value of y is independent of pK_w. Calculations using eq. (51) with $pH_o = 5.6$ yield the working range in C:

Case 1. $C = 10^{-5}$ yields $y = 10^{-5.6028}$, pH = 7.8 and pH-shift = +2.2.

Case 2. $C = 10^{-7}$ yields $y = 10^{-7.00}$, pH = 5.618 and pH-shift = +0.02.

Hence, the measurement is applicable to the range, $10^{-7} \leq C \leq 10^{-5}$, using a pH meter with a precision of ±0.01. Of course, this implies that the measurement is carried out in a closed system which manifests commensurate stability in the pH reading; i.e., negligible drift with time.

Next, consider the use of an acid-base dye indicator, H.$\mathscr{I}$, where the ionization is given by,

$$\begin{array}{ccccc} H.\mathscr{I} & \rightleftharpoons & H^+ & + & \mathscr{I}^- \\ c(1-\alpha) & & c\alpha + [H^+]_o & & c\alpha \end{array} \qquad (52)$$

where c is the molarity concentration of the dye, α is the degree of ionization, and $[H^+]_o$ characterizes the hydrogen-ion concentration of the electrolyte solution. The equilibrium constant of eq. (52) and the total hydrogen-ion concentration, $[H^+]$, are related as follows,

$$\frac{K}{[H^+]} = \frac{[\mathscr{I}^-]}{[H\mathscr{I}]} \qquad (53)$$

where,

$$\text{(a)}\quad [H^+] = c\alpha + [H^+]_o$$

$$\text{(b)}\quad [\mathcal{I}^-] = c\alpha\text{, and} \tag{54}$$

$$\text{(c)}\quad [H\mathcal{I}] = c(1-\alpha)$$

The equilibrium constant can also be expressed as follows,

$$K = c\,\frac{\alpha^2}{1-\alpha} + \frac{\alpha}{1-\alpha}\,[H^+]_o \tag{55}$$

which is useful for determining K and $[H^+]_o$. For $c\alpha >> [H^+]_o$, $K = K_o$, where

$$K_o = \frac{c\alpha^2}{1-\alpha}\text{ ,} \tag{56}$$

the intrinsic case; i. e., the dye determines the hydrogen-ion concentration.

The two bands of the optical absorption in solution are due to $H\mathcal{I}$, the species favored by decreasing pH, and $\mathcal{I}^-$, the species favored by increasing pH. Note the following conservation in terms of the concentrations shown in eqs. (54)(b) and (54)(c),

$$[H\mathcal{I}] + [\mathcal{I}^-] = c\text{ .} \tag{57}$$

For simplicity, assume that the absorption bands are fairly resolved. Assign to $H\mathcal{I}$ the extinction coefficient ϵ_1 at peak wavelength absorption λ_1 and, similarly, to $\mathcal{I}^-$, ϵ_2 and λ_2.

The absorbance of $\mathcal{I}^-$ is,

$$y_2 = \epsilon_2 L [\mathcal{I}^-] \tag{58}$$

where L is the cell thickness. A similar expression holds between y_1 and $H\mathcal{I}$. Since eqs. (53) and (57) yield,

$$\frac{K}{[H^+]} = \frac{[\mathcal{I}^-]}{c - [\mathcal{I}^-]} , \tag{59}$$

it can be shown that,

$$\frac{dy_2}{dpH} = 2.303\, \epsilon_2 Lc\alpha(1 - \alpha) . \tag{60}$$

Thus, the change in y_2 with pH is most sensitive at $\alpha = 1/2$.

Equation (60) also serves as a figure of merit for the method. It was shown above that a pH-shift corresponding to dpH = 0.01 accommodates a working range in OH^-(s) of, $10^{-7} \leq C \leq 10^{-5}$. A comparable value of dy_2 is easily obtained. If the choice of the dye is such that $\alpha \approx 1/2$, then dy_2 = dpH implies according to eq. (60), $\epsilon_2 Lc \lesssim 2$, and from eqs. (54)(b) and (58), the absorbance is, $y_2 \approx 1$. These operating conditions are easily realized.

According to eq. (53), the measurement of $[\mathcal{I}^-]/[H\mathcal{I}]$, which is also $\alpha/(1 - \alpha)$ by eqs. (54)(b) and (54)(c), yields $[H^+]$ in terms of K. The measurement can be carried out using the two or just one of the absorption bands. From eq. (58) and the analogous expression for $[H\mathcal{I}]$, it follows from eq. (53) that,

$$\frac{K}{[H^+]} = \frac{\alpha}{1 - \alpha} = \frac{\epsilon_1}{\epsilon_2} \cdot \frac{y_2}{y_1} . \tag{61}$$

All the quantities at the right hand side of the equality are experimentally determined.

The one-absorption band method makes use of eqs. (58) and (59),

$$\frac{K}{[H^+]} = \frac{1}{\frac{\epsilon_2 Lc}{y_2} - 1} \tag{62}$$

Or, in terms of the λ_1-band,

$$\frac{K}{[H^+]} = \frac{\epsilon_1 Lc}{y_1} - 1 \tag{63}$$

Determining α for various concentrations of the dye, c, for the KCl concentration employed (say, 1 M) yields K. From the $K/[H^+]$ value, $[H^+]$ is obtained and from eq. (54)(a), $[H^+]_o$. The value of K has to be determined only once by eq. (55) for a given dye and concentration of KCl. However, it can also be used to obtain $[H^+]_o$ directly, but this will involve a series of measurements with c as the variable.

APPENDIX V

PLASTIC DEFORMATION OF IONIC FCC CRYSTAL

Given a face-center cubic (fcc) ionic crystal, the problem is to determine the orientation that will best resist plastic deformation.

Figure 37 illustrates the primary slip planes in such a crystal at room temperature; the shading lines on each plane indicate the slip direction in that plane. These slip systems are a Type (110) $<\bar{1}10>$ classification, of which there are six. Burgers vectors b in these slip systems will meet at angles of $\pi/3$, $\pi/2$, or $2\pi/3$. Since $b_1^2 \leq b_2^2 + b_3^2$ for $\cos^{-1}(\vec{b_2} \cdot \vec{b_3}/b_2 b_3) \geq \pi/2$, and the energy of a dislocation is proportional to b^2, only one of these angles leads to association and locking of dislocations, viz. $\pi/3$.

One of the criteria for optimization of resistance to plastic deformation is that $\cos^2\phi$ be minimum, ϕ being the angle between the direction of applied stress and the closest slip direction. The other optimization criterion is that as many interferent slip systems as possible be simultaneously active. The latter criterion implies that the direction of applied stress must be a principal axis of symmetry of the crystal; this confines the selection to only low index directions, of which there are few, even in a cubic crystal.

Consider the two-fold, three-fold, and four-fold symmetric directions. With the applied stress in the <110> direction, although one of the slip systems has a cos ϕ of zero, another slip system has a slip direction parallel with the direction of applied stress, and the crystal is free to slip in that direction without interruption. Note in this case that there are four other slip systems with a favorable cos ϕ of one-half, and are interferent, but they assume a role secondary to that of the <110> slip direction.

With the applied stress in the <111> direction, three of the slip systems have a cos ϕ of zero, while the other three have a cos ϕ of $\sqrt{2/3}$. The latter three systems also are interferent.

With the applied stress in the <100> direction, two slip systems have a cos $\phi = 0$, while the other four have cos $\phi = \sqrt{2}/2$. Among the latter four slip systems, however, each one is interferent with only two of the other three and is cooperative with the remaining slip system. This condition is similar to that where only two interferent slip systems exist.

From these considerations it may be concluded, therefore, that the best direction for resistance to plastic deformation in an fcc ionic crystal is the <111> direction. It should be pointed out, however, that such secondary factors as dislocation pinning by impurity ions and reduction of dislocation mobility by the formation of jogs have been disregarded; it is a possibility that these factors may predominate in real crystals.

1881-2

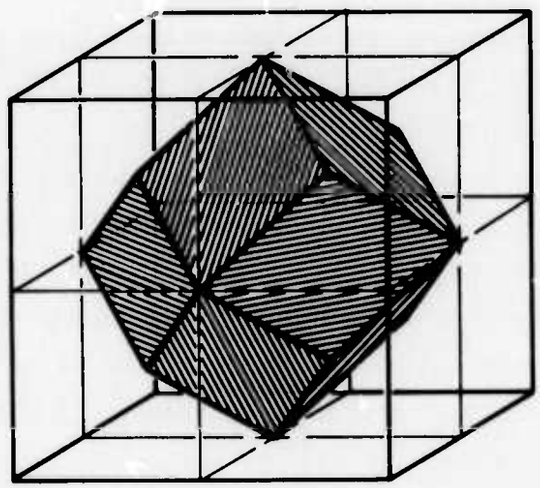

Fig. 37. Slip Planes in an Ionic fcc Crystal.

APPENDIX VI

CRYSTAL GROWTH AND EVALUATION OF METAL FLUORIDES

Because of their low solubility, only the refractory metal fluorides were considered for use as windows in the 3- to 5-μm region, and only those materials which were potentially capable of achieving an absorption coefficient $\leq 10^{-3}$ cm^{-1}. Czochralski growth from the melt was carried out under a reactive atmosphere processing (RAP) of He + HF with a dewpoint parameter corresponding to a pressure ratio of $P_{H_2O}/P_{HF} \approx 10^{-6}$.

Since no apparatus was available to measure calorimetrically the absorption at 3 to 5 μm, the measurement of β, the optical absorption coefficient at 10.6 μm, determined by adiabatic calorimetry (App. II), was used as the index to the OH^- content of the solid. This index to anion purification through crystal growth was based on the activity of the metal-to-oxygen vibration at the 10-μm region, which, in turn, was a measure of the absorption at the 3-μm region arising from the oxygen-to-hydrogen vibration.

Hydrolysis can readily occur at temperatures well below the melting point, even in a refractory crystal such as CaF_2.[26] A significant lowering in mechanical strength is associated with hydrolysis, a result which may be deduced in the comparison between LiF crystal that is air-grown and that grown in vacuum.[27] The latter growth method yields a specimen that is less hydrolyzed, but still not completely free in OH^- (Appendix I).

For convenience, we adopted the measurement of surface microhardness (Knoop) as a qualitative indicator to the effect of RAP on the mechanical properties. However, more direct evidence was obtained after the contract ended.*

---

* The maximum strength reported in the literature for CaF_2 is 8000 psi at Raytheon (Quarterly Report December 1970, ARPA Order 1180). Our RAP grown CaF_2 gave a modulus of rupture of 12,000 psi.

The results of optical and mechanical evaluations are collected in Table XIX. The standard deviations shown were derived from at least four determinations. The crystals employed as starting materials came from Harshaw (Cleveland, Ohio). Except in the case of SrF_2, the value of β was obtained by means of the adiabatic calorimeter. The Knoop values of PbF_2 show that the reported value of 200 kg/mm^2 in the 1967 Catalog of Harshaw Optical Crystals (Refer to Table 2, page 13) is in error.

Both β and the Knoop hardness are useful indices to RAP. Larger changes in the optical absorption could have resulted at the 3-μm region where the absorption cross section is larger. The results show that the advantages of RAP are best realized if the procedure is applied right at the beginning; i.e., the conversion of the oxide or carbonate powder to the fluoride. This also points to the importance of maintaining the specific surface of the material to reverse hydrolysis prior to operating at the melting point (crystal growth). Consequently, a one-step materials handling would be the preferred approach to RAP.

It is seen that, among the metal fluorides, BaF_2 has the lowest β.[28] We considered the possibility that the tail of the absorption at 18 μm contributed to β.[29] Consequently, we investigated two approaches.

Czochralski growth of BaF_2 containing one mole percent $BaCl_2$ was carried out. The resulting specimens have large scattering losses (precipitate ?). Atmosphere control was a problem since the correct ratio of HF:HCl to maintain over the melt was not known. Crystal growth at a point of congruency was more desirable.

The phase diagram shows such a point, i.e., BaFCl.[30] Czochralski boules were grown from a molten equimolar mixture. DTA characterization of the crystal with a DuPont Thermalyzer gave a melting point of 1000 °C (under He) in good agreement with the phase diagram. X-ray powder patterns showed the crystal to have a tetragonal structure as reported; the lattice constants agreed with the literature.

TABLE XIX

Comparison of Metal Fluoride Crystals

Metal Fluoride	Starting Material		RAP-Grown Crystal	
	Form	Knoop, kg/mm^2	β, cm^{-1}	Knoop, kg/mm^2 [a]
LaF_3	Powder[b]	–	1.17 ± 0.03	272 ± 10, 269 ± 6 277 ± 5, 282 ± 10
PbF_2	Crystal	19 ± [illegible] 21 ± 1	– [c]	24 ± 1, 30 ± 0 26 ± 1, 31 ± 1
SrF_2	Crystal	134 ± 0, 137 ± 1	0.46[d]	135 ± 2, 136 ± 2
BaF_2	Crystal	80.1 ± 3.5	0.20	81 ± 5
	Powder[e]	–	0.22	91 ± 2
	Powder[f]	–	0.172 ± 0.003	85 ± 2

[a] The pair of values in the first row refer to indentations oriented perpendicular to each other on the polished surface. The similar pair on the next row refer to the measurements on the cleaved surface of the same material.

[b] From dry conversion of La_2O_3 (Shinetsu, 99.99%)

[c] For the starting material, $\beta = 0.30 \pm 0.02\ cm^{-1}$. RAP-grown material suffered a slight chemical reduction.

[d] From transmission data.

[e] From dry conversion of J.T. Baker 99.9% $BaCO_3$

[f] From dry conversion of Johnson Mathey 99.999% $BaCO_3$

T886

A polished crystal of BaFCl gave $\beta = 0.030\ cm^{-1}$ which degraded to $0.110\ cm^{-1}$ after an overnight exposure to the atmosphere. The deterioration was not due to a surface layer change because after repolishing, $\beta = 0.105\ cm^{-1}$. The microscope revealed the occurrence of numerous cleavages in the bulk. The Knoop indentations were poorly defined even at loads as low as 15 g. Edges of the indentations crumbled badly and the hardness values covered a large spread, 120 to 210 kg/mm^2. In summary, the value of β was reduced by a factor of six from BaF_2 to BaFCl and although the material (BaFCl) was also considerably harder, it was ultra brittle.

REFERENCES

1. "Windows for High-Power Lasers," by F. Horrigan, C. Klein, R. Rudko, and D. Wilson, Microwaves, pp. 68-76 (January 1969).

2. "Strain Ageing in $CdCl_2$-Doped Rock Salt," by L.M. Brown and P. L. Pratt, Phil. Mag. 8, 717 (1963).

3. "Impurity-Induced Infrared Absorption in Alkali Halide CO_2 Laser Windows," by F.W. Patten, R.M. Garvey, and M. Hass, Mat. Res. Bull. 6, 1321 (1971).

4. "Der Einflusz von OH^--Ionen and Absorptions Spektrum und Ionenleitfahigkeit von KCl-Einkristallen," by B. Fritz, F. Luty, and F. Anger, Z. Phys. 174, 240 (1963).

5. "Influence of OH^- Ions on Infrared Absorption and Ionic Conductivity in Lithium Fluoride Crystals," by T.G. Stoebe, J. Phys. Chem. Solids 28, 1375 (1967).

6. "U.V. and I.R. Absorption in OH^--Doped NaF," by M.L. Meistrich, J. Phys. Chem. Solids 29, 1119 (1968).

7. "Distribution of Hydroxide Ions in Doped Alkali Halide Crystals," by T.G. Stoebe, J. Phys. Chem. Solids 31, 1291 (1970).

8. "Environmental Effects on the Mechanical Properties of Ionic Solids with Particular Reference to the Joffe Effect," by R.J. Stokes, T.L. Johnston, and C.H. Li, AIME Trans. 218, 655 (1960).

9. "Effect of Atmosphere Conditions on the Brittleness of NaCl," by E.S. Machlin and G.T. Murray, J. App. Phys. 30 (No. 11), 1731 (1959).

10. "Influence of Room Temperature Atmospheric Reaction Products on the Ductility of Sodium Chloride Crystals," by D. Otterson, J. Chem. Phys. 38 (No. 7), 1481 (1963).

11. "Optical Properties of Alkali Halides Containing Hydroxyl Ions," by H.W. Etzel and D.A. Patterson, Phys. Rev. 112 (No. 4), 1112 (1958).

12. "A Method for Purification and Growth of KCl Single Crystals," by C. T. Butler, J. R. Russell, R. B. Quincy, Jr., and D. E. LaValle, Report No. ORNL-3906 (February 1966), Oak Ridge National Laboratory (Oak Ridge, Tennessee), operated by Union Carbide Corp., for the U.S. Atomic Energy Commission, Contract No. W-7405-eng-26. See also references cited.

13. "Preparation of Ultrapure Alkali Halide Single Crystals," by F. Rosenberger, from Crystal Growth (Proceedings of 1966 ICCG Conference), edited by H.S. Peiser, see B20, p. 141 (Pergamon Press, 1967).

14. "Infrared and Ultraviolet OH Bands in Hydroxide-Doped KCl, KBr, NaCl and NaBr," by T. I. Gie and M. V. Klein, Bull. Amer. Phys. Soc. Ser. II, 8, 230 (1963).

15. "Handbook of Analytical Chemistry," edited by L. Meites, First Edition, page 1-25 (McGraw-Hill 1963).

16. "On the Presence of NaOH in Crystalline NaCl," by D. Otterson, J. Chem. Phys. 33 (No. 1), 227 (1960).

17. "Growth of Large Sodium Chloride Crystals from Solution for Color-Center Studies," by P. M. Gruzensky, J. Chem. Phys. 43 (No. 11), 3807 (1965).

18. "Growth Poisoning of Lithium Fluoride from Aqueous Solutions."

19. Cox, J. Thomas, and Hass George (1964), "Antireflection coatings for optical and infrafed optical materials, "Physics of Thin Films 2 (Academic Press).

20. Macleod, H.A., (1969) Thin Film Optical Filters, American Elsevier Publishing Company, Inc., New York.

21. Smith, S.O. and Seeley J.S. (1968) "Multilayer filters for the region 0.8 to 100 microns, "Final Scientific Report, Contract AF61(052)-833.

22. Pure NaCl powder is not hygroscopic. See H. Remy, Treatise on Inorganic Chemistry, Vol. I, (Elsevier Publishing Co., 1956) p. 188. However, in the single crystal, surface damage can be effected with a very small weight change ($<10^{-6}$ g/cm^2).

23. Details of the materials preparation will be given in a separate publication.

24. R. Weil, J. Appl. Phys. 41 (7), 3012 (1970).

25. With vegetable waxes, the C-O linkage is present in the free fatty acids as well as in their esters with the higher alcohols.

26. W. Bontinck, "The Hydrolysis of Solid CaF_2" Physica, XXIV, 650 (1958).

27. L.S. Combes, S.S. Ballard, and K.A. McCarthy, "Mechanical and Thermal Properties of Certain Optical Crystalline Materials," J. Opt. Soc. 41 (No. 4), 215 (1951).

28. The value is in good agreement with the Raytheon determination reported in their Final Technical Report (Sept 1971), Contract DAAHO1-70-C-1251, U.S. Army Missile Command, ARPA Order 1180 (cf. Fig. 15 on page 64).

29. W. Kaiser, W.G. Spitzer, R.H. Kaiser, and L.E. Howarth, "Infrared Properties of CaF_2, SrF_2 and BaF_2," Phys. Rev. 127 (No. 6), 1950 (1962).

30. E.M. Levin, C.R. Robbins, and H.F. McMurdie, "Phase Diagrams for Ceramists," The American Ceramic Society (1964), see Fig. 1621.